PHILOSOPHICAL TRANSACTIONS OF THE ROYAL SOCIETY A MATHEMATICAL, PHYSICAL & ENGINEERING SCIENCES

Circular Dichroism as a Measure of Superhelix Density: A Theoretical Study

Alexandra J. MacDermott

Phil. Trans. R. Soc. Lond. A 1985 **313**, 453-505
doi: 10.1098/rsta.1985.0001

Phil. Trans. R. Soc. Lond. A **313**, 453–505 (1985) [453]
Printed in Great Britain

CIRCULAR DICHROISM AS A MEASURE OF SUPERHELIX DENSITY: A THEORETICAL STUDY

By ALEXANDRA J. MacDERMOTT
Physical Chemistry Laboratory, South Parks Road, Oxford OX1 3QZ, U.K.

(*Communicated by S. F. Mason, F.R.S.* – *Received* 13 *April* 1984)

CONTENTS

In chromatin, the DNA helix is itself helically coiled to form a superhelix, the tightness of which affects the transcription accessibility. Elucidation of the possible role of supercoiling in the control of gene expression requires an accurate and non-destructive method to measure superhelix density, and in this paper we show how the sensitivity of circular dichroism (c.d.) to supercoiling can be exploited. The chromatin c.d. at 270 nm shows a reduction to 45–70% of that of straight, non-supercoiled B-DNA. This has been attributed variously to secondary structural changes or tertiary interactions between adjacent superhelical turns. We investigate this effect by calculating the ratio of the c.d. of supercoiled and of straight DNA as a function of

superhelix density with the use of the Tinoco model, but introducing a novel metric technique to relate c.d. to curvature. Tertiary interactions are shown to cancel one another, leaving the c.d. of chromatin unchanged, so the observed depression must arise from secondary structural effects. We investigate c.d. as a function of secondary structure, and find that base-twisting affects the c.d. much more than base-tilting, and can produce a strong depression. We therefore introduce a model of supercoiled DNA with base-twisting in proportion to the local Riemann curvature of the bent helix, and this reduces the chromatin c.d. to 70% of that of non-supercoiled DNA. Further reduction to 45% is achieved if chromatin forms a left-hand supersuperhelix. These results suggest that c.d. has considerable potential as a quantitative measure of supercoiling.

1. Introduction

In the genetic material chromatin, the DNA double helix is itself helically coiled to form a left-handed superhelix. This is further coiled to give a supersuperhelix or solenoid (Bram *et al.* 1975; Finch & Klug 1976; Bradbury 1978; Campbell *et al.* 1978; Georgiev *et al.* 1978; Miller *et al.* 1978; Thoma *et al.* 1979), which itself has a higher order structure, being arranged in loops (Cook 1974; Campbell 1978; Nicolini 1979; Cook *et al.* 1980) that are grouped into chromosomes. This hierarchy of coils is not just a convenient device to pack the DNA into the cell nucleus, but is now known to have important effects on DNA function. In particular, the superhelical tertiary structure is believed to play a central role in the control of gene expression (Cook 1974; Campbell 1978; Mirkin *et al.* 1979; Luchnik 1980; Luchnik & Glaser 1981; Smith 1981; MacDermott 1982; Lilley 1983), acting as a genetic switch through its effect on transcription. Supercoiled DNA circles are transcribed much faster than their γ-irradiated (nicked) counterparts (Colman & Cook 1977), because the free energy of supercoiling assists the local unwinding of the duplex necessary to expose the bases for initiation of transcription. (In a closed circle, unwinding of the right-handed double helix involves simultaneous unwinding of the left-handed superhelix (Bauer & Vinograd 1968) and this is favoured by release of superhelical strain.) It has also been shown (Akrigg & Cook 1980) that the exact degree of supercoiling, not just its mere presence or absence, affects the rate of transcription and, moreover, that RNA polymerases from different types of cell prefer different superhelix densities for optimal operation. It has therefore been suggested (Cook 1974; Denhardt 1979) that genes relevant to a particular cell are supercoiled to just the required degree to enable the particular polymerase to expose the bases for transcription by local duplex unwinding, while the rest of the genome is supercoiled to the wrong degree and thus repressed. Nuclear DNA is constrained by molecular splices to a series of independent, quasi-circular loops (Cook 1974; Nicolini 1979; Cook *et al.* 1980; Cook & Brazell 1980), each of which could have a different superhelix density. Such differential supercoiling of different genes could be created by twisting and untwisting enzymes such as DNA gyrase and topoisomerase and could be preserved during replication (Cook 1974) thus providing a heritable genetic switch. Genes would thus be switched on or off only once, at the moment of cell differentiation, the daughter cells then inheriting the appropriate differential supercoiling and requiring no further regulation.

Unusually high superhelix densities have been observed in cancer cells (Hartwig & Matthes 1979; Hartwig 1980; Luchnik & Glaser 1981; Luchnik *et al.* 1982), reflecting their characteristic undifferentiated state with too many genes switched on, and this could find application in clinical diagnosis (Preumont *et al.* 1981; Luchnik *et al.* 1982). Hypomethylation has also been observed in cancer cells (Ehrlich & Wang 1981; Feinberg & Vogelstein 1983*a*; Lu *et al.* 1983).

PHILOSOPHICAL TRANSACTIONS OF THE ROYAL SOCIETY A MATHEMATICAL, PHYSICAL & ENGINEERING SCIENCES

Methylation of the cytosine bases in DNA is correlated with gene inactivity (Razin & Riggs 1980; Lindahl 1981; Gama-Soza *et al.* 1983) and it has been suggested that it causes B→Z transitions in alternating CGCG sequences, so reducing the density of left-handed superhelical turns and switching genes off (Nordheim *et al.* 1981; MacDermott 1982). Carcinogens may interfere with methylation (Lu *et al.* 1983), thereby converting left-handed turns stored in the Z-sections to superturns, resulting in the tightly supercoiled, hypomethylated cancerous state. The switching on of oncogenes has been implicated in carcinogenesis, and *ras* oncogenes have recently been shown (Feinberg & Vogelstein 1983*b*) to be hypomethylated in human tumour cells, which could indicate that these genes are switched on by excessive supercoiling.

Further elucidation of the role of the superhelix in the control of gene expression and carcinogenesis requires an accurate and non-destructive means of measuring superhelix density. A major problem is the extreme fragility of the superhelix; most extraction, sample preparation, and observation techniques are liable to nick the DNA, thus releasing the supercoiling. A new gentle lysis method (Cook & Brazell 1975, 1976) has been developed to extract supercoiled 'nucleoid' DNA intact from cells, but techniques to measure superhelix density still leave much to be desired. Sedimentation has limited accuracy and can be destructive, X-ray and electron diffraction are still more destructive, and neutron scattering is expensive and complex. The most striking feature of the superhelix is the additional chirality it confers on the already chiral DNA helix, so optical activity immediately suggests itself as a simple, non-destructive, and inexpensive means of detecting supercoiling. Circular dichroism (c.d.) has the advantage of providing a direct window onto the DNA, whose bases absorb in a separate spectral region (260–280 nm), whereas in neutron scattering, special D_2O techniques are needed to make the DNA show up against the histones around which it is wrapped in chromatin.

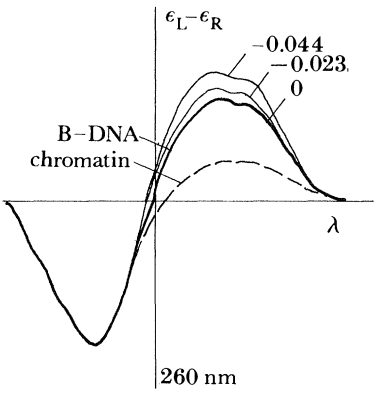

FIGURE 1. Experimental c.d. spectra of pure B-DNA in solution at zero superhelix density σ, supercoiled DNA in solution with $\sigma = -0.023$, -0.044, and chromatin.

The few available c.d. spectra of supercoiled DNA do indicate a strong dependence on superhelix density, but there is disagreement as to its cause, and theoretical understanding has hitherto been insufficient to exploit the effect as a quantitative measure of superhelix density. The experimental spectra, summarized schematically in figure 1, fall into two categories; first those of pure DNA in solution at low superhelix density, and second, those of chromatin, in which the DNA is wrapped around the histones at a much higher superhelix density. Maestre & Wang (1971) and Gray *et al.* (1978) examined the 280 nm c.d. of bacteriophage DNA circles

and observed increases compared with the corresponding nicked (and therefore unsupercoiled) circles of approximately 10–15% at superhelix density $\sigma \approx -0.023$ superhelix (s.h.) turns per base pair, and about 25% for $\sigma \approx -0.044$. These authors attribute the increase to a change in secondary structure, perhaps towards a more A-like form, with increased base-tilt. At the higher superhelix densities ($\sigma \approx -0.13$) found in chromatin, substantial reductions in c.d., to between 45% (Shih & Fasman 1970) and 70% (Henson & Walker 1970; Simpson & Sober 1970) of that of straight B-DNA, have been observed. These have also been attributed to secondary structural change, this time towards the C-form (Permogorov *et al.* 1970; Matsuyama *et al.* 1971; Hanlon *et al.* 1972). More recently, however, it has been suggested that tertiary effects, involving interactions between adjacent turns of the superhelix, are responsible for the reduction (Cowman & Fasman 1978; Fasman & Cowman 1978). Furthermore, the c.d. of chromatin varies during the cell cycle (Nicolini *et al.* 1975), and the extra large c.d. reductions seen during the non-replicative G_1- and M-phases have been attributed to quaternary interactions in the supersuperhelix, which is believed to uncoil for the replicative S-phase, giving a less depressed c.d. (Nicolini 1979, 1980).

The first objective of this study is therefore to determine whether secondary or tertiary effects are responsible for the c.d. of the superhelix. It is important to establish the correct secondary structure, because it is conceivable that supercoiling could influence DNA function not only topologically, but through any effect it may have on the secondary structure (Luchnik 1980). The second objective is to provide a theoretical explanation of the experimental spectra, with a view to developing c.d. as a useful quantitative measure of supercoiling.

Non-c.d. evidence, such as X-ray scattering (Bram 1971; Bram & Ris 1971), infrared dichroism (Taillandier *et al.* 1979), nuclease digestion (Noll 1974; Kornberg 1977), and energy calculations (Levitt 1978) all points to chromatin having a B-type secondary structure, apparently suggesting that tertiary effects are more likely to be responsible for the depressed chromatin c.d., especially in view of the close proximity of adjacent turns of the superhelix, which are only 0.6 nm apart in the latest models (Finch *et al.* 1977; Bradbury 1978). Our initial calculation of the c.d. as a function of superhelix density in §4 therefore assumes a standard B-form secondary structure.

In addition to secondary and tertiary effects, one should also consider the effect of curvature. When the cylindrical DNA molecule is coiled into a superhelix, the cylinder becomes curved, and the metric and Riemann curvature of its surface are analysed in Appendix 3. We have calculated elsewhere (MacDermott 1985) the rotational strength of a superhelix using the free electron model, which is independent of secondary structure and does not admit interturn interactions. The results show that curvature by itself may have a strong influence on the c.d. of DNA.

We do not calculate the absolute magnitude of the c.d., but simply examine the effect of changing geometry, and especially increasing curvature, by calculating the ratio, $\Delta\epsilon(x)/\Delta\epsilon(0)$, of the superhelix to straight helix c.d. maxima as a function of superhelix density. This ratio is readily obtained experimentally by examining supercoiled circles before and after nicking by γ-irradiation.

2. The exciton model of polymer c.d.

We calculate the DNA c.d. on the basis of the widely used Tinoco (1962) exciton model (an alternative approach, not considered here, involves linear response theory (Rhodes & Redmann 1977; Redmann & Rhodes 1979)).

The circular dichroism,

$$\Delta\epsilon \propto \left\{R_{\mathrm{OA}} f(u) - \left(\frac{1}{\sigma_\nu}\sum_K R_{\mathrm{OA}K}(\nu_{\mathrm{OA}K} - \nu_{\mathrm{OA}})\right) f'(u)\right\}, \tag{1}$$

due to a polymer transition O→A has two parts (Bloomfield *et al.* 1971). The non-conservative contribution has the shape of the absorption spectrum, regarded as a Gaussian,

$$f(u) = (1/2\pi)^{\frac{1}{2}}\, \mathrm{e}^{-\frac{1}{2}u^2}, \tag{2}$$

where $u = (\nu - \nu_{\mathrm{OA}})/\sigma_\nu$ is the frequency in units of standard deviations, σ_ν, from the absorption frequency ν_{OA}. The conservative contribution has the shape of the derivative $f'(u)$, and arises from the splitting of the excited state A into exciton levels A_K corresponding to frequencies $\nu_{\mathrm{OA}K}$.

The coefficient of the non-conservative contribution is the rotational strength, given (for magnetically forbidden transitions, and neglecting static field terms (Tinoco 1962; Bloomfield *et al.* 1971)) by

$$R_{\mathrm{OA}} = -\left(\frac{2\pi\nu_{\mathrm{a}}}{c}\right)\sum_{i=1}^{N}\sum_{j}'\sum_{\mathrm{b}}'\frac{V_{i\mathrm{oa};j\mathrm{ob}}\,\nu_{\mathrm{b}}}{h(\nu_{\mathrm{b}}^2 - \nu_{\mathrm{a}}^2)}\boldsymbol{R}^{ij}\cdot\boldsymbol{\mu}_{j\mathrm{ob}}\wedge\boldsymbol{\mu}_{i\mathrm{oa}}, \tag{3}$$

in terms of interactions $V_{i\mathrm{oa};j\mathrm{ob}}$ between electric dipole transition moments $\boldsymbol{\mu}_{i\mathrm{oa}}$ and $\boldsymbol{\mu}_{j\mathrm{ob}}$ for different transitions o→a and o→b on monomers i and j, separated by distance vector $\boldsymbol{R}^{ij}$ within a polymer of N units.

The coefficient of the conservative contribution (Bloomfield *et al.* 1971),

$$\sum_K R_{\mathrm{OA}K}(\nu_{\mathrm{OA}K} - \nu_{\mathrm{OA}}) = \left(\frac{\pi\nu_{\mathrm{a}}}{c}\right)\sum_{i=1}^{N}\sum_{j\neq i}^{N}\frac{V_{i\mathrm{oa};j\mathrm{oa}}}{h}\boldsymbol{R}^{ij}\cdot\boldsymbol{\mu}_{j\mathrm{oa}}\wedge\boldsymbol{\mu}_{i\mathrm{oa}}, \tag{4}$$

is of similar form, but arises from interactions between identical transitions on monomers i and j.

In both cases, absorption of a photon by the ith group can be regarded as inducing virtual transitions in the other group j, corresponding to exciton jump between groups. We shall see later that the helicity of exciton jump between chirally disposed groups can provide a physical picture of the differing optical activities of the DNA helix, superhelix, and supersuperhelix.

If the monomers are far enough apart, the interaction $V_{i\mathrm{oa};j\mathrm{ob}}$ can be approximated by a multipole expansion, retaining only the dipole–dipole term to give

$$V_{i\mathrm{oa};j\mathrm{ob}} = (1/4\pi\epsilon_{\mathrm{o}})\,\boldsymbol{\mu}_{i\mathrm{oa}}\cdot\boldsymbol{T}^{ij}\cdot\boldsymbol{\mu}_{j\mathrm{ob}}, \tag{5}$$

where

$$\boldsymbol{T}^{ij} = \{1 - 3\hat{\boldsymbol{R}}^{ij}\hat{\boldsymbol{R}}^{ij}\}\,(R^{ij})^{-3} \tag{6}$$

and $\hat{\boldsymbol{R}}^{ij}$ is the unit vector along $\boldsymbol{R}^{ij}$. Expression (1) therefore becomes

$$\Delta\epsilon \propto \{O^{\mathrm{nc}} f(u) - O^{\mathrm{c}} f'(u)\}, \tag{7}$$

with the coefficients given by

$$\left.\begin{matrix} O^{\mathrm{nc}} \\ O^{\mathrm{c}} \end{matrix}\right\} = \mp\frac{\pi\nu_{\mathrm{a}}}{c}\sum_i\sum_j{}' \boldsymbol{\mu}_{i\mathrm{oa}}\cdot\boldsymbol{T}^{ij}\cdot\boldsymbol{B}^j\wedge\boldsymbol{\mu}_{j\mathrm{oa}}\cdot\boldsymbol{R}^{ij}, \tag{8}$$

where, in the conservative case,

$$(\boldsymbol{B}^j)^{\mathrm{c}} = \boldsymbol{\mu}_{j\mathrm{oa}}\boldsymbol{\mu}_{j\mathrm{oa}}/4\pi\epsilon_{\mathrm{o}}h\sigma_\nu \tag{9}$$

and in the non-conservative case,

$$(\boldsymbol{B}^j)^{\mathrm{nc}} = \boldsymbol{\alpha}^j(\nu_{\mathrm{a}}) = (2/4\pi\epsilon_{\mathrm{o}})\sum_{\mathrm{b}}{}'\frac{\boldsymbol{\mu}_{j\mathrm{ob}}\boldsymbol{\mu}_{j\mathrm{ob}}\nu_{\mathrm{b}}}{h(\nu_{\mathrm{b}}^2-\nu_{\mathrm{a}}^2)} \tag{10}$$

is the polarizability at frequency ν_{a}, which can be approximated by the frequency-independent polarizability

$$(\boldsymbol{B}^j)^{\mathrm{nc}} \approx \boldsymbol{\alpha}^j = (2/4\pi\epsilon_{\mathrm{o}})\sum_{\mathrm{b}}{}'\boldsymbol{\mu}_{j\mathrm{ob}}\boldsymbol{\mu}_{j\mathrm{ob}}/h\nu_{\mathrm{b}} \tag{11}$$

if $\nu_{\mathrm{b}} \gg \nu_{\mathrm{a}}$.

Experimental c.d. spectra are commonly measured as a function of wavelength, and if the bandwidth is not too large, then in (7) we can write $f(u) = \mathrm{e}^{-\frac{1}{2}u^2} \approx \mathrm{e}^{-\frac{1}{2}w^2} = f(w)$, where $w = (\lambda-\lambda_{\mathrm{oa}})/\sigma_\lambda$ is the wavelength in units of standard deviations, and $f'(u) = -f'(w)$, giving

$$\Delta\epsilon \propto \{O^{\mathrm{nc}}f(w) + O^{\mathrm{c}}f'(w)\}. \tag{12}$$

3. Application of the exciton model to supercoiled DNA

In specializing the above theory to DNA, we take as chromophores the purine and pyrimidine bases and consider the c.d. arising from their $\pi^*\leftarrow\pi$ transitions in the 260 nm region. This system conforms to the basic assumptions of the Tinoco (1962) model; the chromophores are electronically isolated, and the wavelength of the exciting radiation is large compared with the distance between interacting chromophores. But the other two approximations in §2, namely retention of only the dipole–dipole term of the interaction, followed by the so-called polarizability approximation, requiring $\nu_{\mathrm{b}} \gg \nu_{\mathrm{a}}$, are somewhat more problematic. The nearest-neighbour separation of 0.34 nm along the helix axis may be too close for the dipole approximation to apply; and because there are four different DNA bases absorbing at similar frequencies, some of the non-conservative contribution represents interactions with ν_{b} and ν_{a} nearly equal. Different authors have adopted various compromises; for example, Moffitt (1956) used the more complicated monopole approximation for nearest-neighbour interactions, retaining the simpler dipole approximation for the rest, while Bush & Brahms (1967) used the monopole approximation for interaction with near-u.v. transitions, and the polarizability theory for far-u.v. transitions. Because we are interested here in calculating only the ratio $\Delta\epsilon(x)/\Delta\epsilon(0)$, rather than accurate c.d. magnitudes, we retain the polarizability theory for all interactions, in the interests of simplicity. We overcome the problem of non-conservative interactions with $\nu_{\mathrm{a}} \approx \nu_{\mathrm{b}}$ by introducing the 'average base', whose $\pi^*\leftarrow\pi$ transition moment is a vector average of those of the bases A, T, G, C, weighted according to their abundance in the DNA. All bases are then identical, so there is effectively only one 'average' transition $\mathrm{o}\rightarrow\mathrm{a}$ in the 260 nm region, and interaction between transitions of this type on different chromophores is now covered by the conservative contribution (that must, however, be

weighted by a statistical factor (described later) because there are in reality four different bases). The non-conservative contribution now arises solely from interaction with transitions o→b in the far-u.v., for which the polarizability approximation is valid.

To calculate $\Delta\epsilon(x)/\Delta\epsilon(0)$, we consider the optical activity of just one turn of the helix and take at first just one strand, extending later to the double helix. The summation over all groups i in (8) then reduces, for a straight, non-supercoiled, helix, to multiplication by k, the number of bases per turn (10 for B-DNA). We rename the ith group the zeroth group, and examine the optical activity $\boldsymbol{\Omega}^j$ due to the interaction of the transition moment $\boldsymbol{\mu}_{i\mathrm{oa}} = \mu\hat{\boldsymbol{a}}(0)$ (where $\hat{\boldsymbol{a}}(0)$ is a unit vector in the direction of the zeroth group's transition moment, which has magnitude μ) with all transitions, represented by $\boldsymbol{B}^j$, on all other groups j. Note that if $(\boldsymbol{B}^j)^{\mathrm{nc}}$ is expressed in the 'proper' frame of the jth chromophore (see Appendix 1), it is diagonal, having non-zero components B^{nc}_{qq}, corresponding to the components α_{11}, α_{22}, α_{33} of the polarizability tensor. Turning to $(\boldsymbol{B}^j)^{\mathrm{c}}$, we see that because $\boldsymbol{\mu}_{j\mathrm{oa}}$ in (9) is directed along the x-axis in the proper frame, the tensor has only one non-zero component,

$$B^{\mathrm{c}}_{11} = \boldsymbol{\mu}_{j\mathrm{oa}} \cdot \boldsymbol{\mu}_{j\mathrm{oa}}/4\pi\epsilon_{\mathrm{o}}\, h\sigma_\nu. \tag{13}$$

A matrix $\boldsymbol{P}^j$ is required to relate the proper frame of the jth group to that of the zeroth group; so (8) becomes

$$\left.\begin{matrix} O^{\mathrm{nc}} \\ O^{\mathrm{c}} \end{matrix}\right\}_{1\,\mathrm{turn}} = \mp\,(\pi\nu_{\mathrm{a}}\,\mu^2 k/c) \sum_j{}' \boldsymbol{\Omega}^j, \tag{14}$$

where

$$\boldsymbol{\Omega}^j = \hat{\boldsymbol{a}}(0) \cdot \boldsymbol{T}^j \cdot \boldsymbol{P}^j \boldsymbol{B} (\boldsymbol{P}^j)^{-1} \wedge \hat{\boldsymbol{a}}(0) \cdot \boldsymbol{R}^j. \tag{15}$$

We term the two strands of DNA the T- and V-helices (cf. Rhodes 1961); the zeroth chromophore of the T-helix is hydrogen-bonded to the zeroth chromophore of the V-helix, the nth group n_{T} of the T-helix to the nth group n_{V} of the V-helix, etc. as shown in figure 2. The T- and V-helices are antiparallel, in the sense of the local orientation of their chromophores being opposite (see Appendix 1). They are therefore identical and equivalent, but we choose to number the groups with n increasing in the z-direction of the T-helix, and survey the molecular geometry from the viewpoint of the 0_{T} group, so that (14) becomes

$$\left.\begin{matrix} O^{\mathrm{nc}} \\ O^{\mathrm{c}} \end{matrix}\right\}_{1\,\mathrm{turn}} = \mp\,(2\pi\nu_{\mathrm{a}}\,\mu^2 k/c) \left\{ \sum_{n=-\infty}^{\infty}{}' \boldsymbol{\Omega}(0_{\mathrm{T}} \rightarrow n_{\mathrm{T}}) + \sum_{n=-\infty}^{\infty} \boldsymbol{\Omega}(0_{\mathrm{T}} \rightarrow n_{\mathrm{V}}) \right\}, \tag{16}$$

where $\boldsymbol{\Omega}(0_{\mathrm{T}} \rightarrow n_{\mathrm{T}})$ and $\boldsymbol{\Omega}(0_{\mathrm{T}} \rightarrow n_{\mathrm{V}})$ represent the intra- and inter-strand interactions respectively.

The position of each chromophore is defined by its angular coordinate ϕ round the helix; because all chromophores are equivalent in the straight helix, we may define the phase $\phi(0_{\mathrm{T}})$ of the 0_{T} group to be zero, so that of the 0_{V} group becomes $\phi(0_{\mathrm{V}}) = -|\phi_{\mathrm{bp}}|$, where $|\phi_{\mathrm{bp}}|$ is the phase difference between the helices (the angle between paired bases, see figure 2), and we take the V-helix to lag behind the T-helix. The phase separations of any two chromophores 0_{T} and n_{T} or n_{V} are therefore

$$\begin{aligned} \Delta\phi(0_{\mathrm{T}} \rightarrow n_{\mathrm{T}}) &= n2\pi/k, \\ \Delta\phi(0_{\mathrm{T}} \rightarrow n_{\mathrm{V}}) &= n2\pi/k - |\phi_{\mathrm{bp}}|, \end{aligned} \tag{17}$$

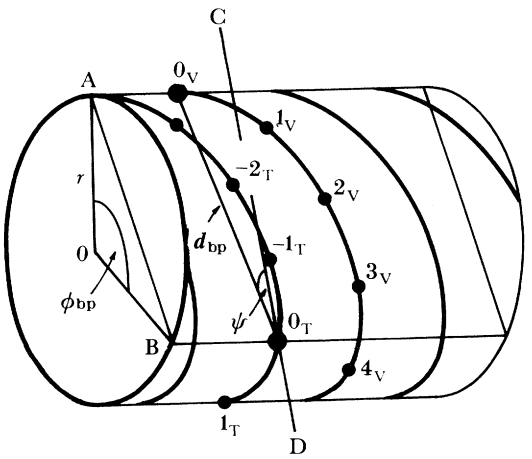

FIGURE 2. The T- and V-helices. The line $0_V 0_T$ lies in the plane ABCD.

and their longitudinal separations parallel to the helix axis are

$$\Delta z(0_T \to n_T) = np/k,$$
$$\Delta z(0_T \to n_V) = np/k + d_{bp} \sin\psi, \tag{18}$$

where p is the pitch of the helix, d_{bp} is the distance between paired bases, and ψ is the angle at which $\boldsymbol{d}_{bp}$ is tilted (figure 2).

In the superhelix, the equivalence of the chromophores is lost; those on the inside of the bent helix cylinder have different environments from those on the outside, and in fact a helix with 10 groups per turn has 10 inequivalent types of chromophore site. We distinguish these sites by the label m, which takes the values -4 to $+5$, so that the optical activity of one turn of a supercoiled double helix becomes

$$\left.\begin{matrix} O^{nc} \\ O^{c} \end{matrix}\right\}_{1\text{ turn}} = \mp (2\pi\nu_a \mu^2/c) \sum_{m=-4}^{+5} \left\{ \sum_{n=-\infty}^{\infty}{}' \Omega(0_T^m \to n_T) + \sum_{n=-\infty}^{\infty} \Omega(0_T^m \to n_V) \right\}, \tag{19}$$

where $\Omega(0_T^m \to n_T)$ represents the interaction between a 0_T group of the m-type, and the group n_T that differs from it in phase by $n2\pi/k$. But what is the phase $\phi(0_T^m)$ of the group 0_T^m? The simplest assumption would be to take $\phi = 0$ for an $m = 0$ group, so that an m-type group has phase $m2\pi/k$. But the true phase might actually be $(m2\pi/k + \alpha)$, where α is the phase of the $m = 0$ group, its value depending on the orientation of the helix cylinder on the surface of the superhelix cylinder. This orientation may be random, in which case, for an ensemble of superhelices, α will be positive as often as it is negative, giving an average of 0. Alternatively, α may assume a preferred value which maximizes the neutralization of the inside phosphate groups, or other favourable interactions with the histones. But as there is no experimental evidence available, we choose here the most convenient value of α, namely that which preserves the equivalence of the T- and V-helices, $\alpha = \frac{1}{2}|\phi_{bp}|$ (this may in fact be the 'preferred' phase, as it would not be possible for both helices to assume any other 'preferred' phase). The phase of a zeroth group of m-type is thus defined (see figure 4) as

$$\phi(0_T^m) = m2\pi/k + \tfrac{1}{2}|\phi_{bp}|, \tag{20}$$

but the phase differences and vertical separations remain the same as in the straight helix, given by (17) and (18).

We choose to evaluate $\Omega(0_{\mathrm{T}}^{m} \rightarrow n_{\mathrm{T}})$ and $\Omega(0_{\mathrm{T}}^{m} \rightarrow n_{\mathrm{V}})$ in the 'transition' frame $\{\hat{\boldsymbol{\imath}}^{t}[0, \phi(0_{\mathrm{T}}^{m})]\}$ of the zeroth chromophore (see Appendix 1) as $\hat{\boldsymbol{a}}(0_{\mathrm{T}}^{m})$ then only has one component, the x-component, which is unity. Equation (15) therefore becomes

$$\Omega = a_1 \, T_{1b} \, P_{bc} \, B_{cc} \, P_{cd}^{-1} \, \epsilon_{fd1} \, a_1 \, R_f, \tag{21}$$

where summation over repeated subscripts is implied. ϵ_{abc} is the Levi–Civita tensor density, $\boldsymbol{B}$ is diagonal in its proper frame $\{\hat{\boldsymbol{\imath}}^{t}[0, \phi(n)]\}$, and for simplicity we have dropped superscripts. Noting that $a_1 = 1$, and expanding, we obtain

$$\Omega = \sum_{q=1}^{3} B_{qq} \, \Omega_q, \tag{22}$$

where

$$\Omega_q = (T_{11} \, P_{1q} + T_{12} \, P_{2q} + T_{13} \, P_{3q}) \, (P_{3q} \, R_2 - P_{2q} \, R_3). \tag{23}$$

The planar DNA bases can be regarded as cylindrically symmetrical, so the non-conservative optical activity becomes

$$\Omega^{\mathrm{nc}} = \alpha_{\perp}\{\Omega_1 + \Omega_2\} + \alpha_{\parallel} \, \Omega_3, \tag{24}$$

where $\alpha_{\perp}$ and $\alpha_{\parallel}$ are the in-plane and out-of-plane polarizabilities. Now clearly the optical activity is zero for spherically symmetric chromophores ($\alpha_{\perp} = \alpha_{\parallel}$), so it is generally true that

$$\Omega_1 + \Omega_2 = -\Omega_3. \tag{25}$$

Therefore the non-conservative optical activity becomes

$$\Omega^{\mathrm{nc}} = -(\alpha_{\perp} - \alpha_{\parallel}) \, \Omega_3, \tag{26}$$

while its conservative counterpart is

$$\Omega^{\mathrm{c}} = B_{11}^{\mathrm{c}} \, \Omega_1. \tag{27}$$

$\boldsymbol{P}$ is the matrix which transforms the proper frame $\{\hat{\boldsymbol{\imath}}^{t}[0, \phi(n_{\mathrm{T}})]\}$ or $\{\hat{\boldsymbol{\imath}}^{t}[0, \phi(n_{\mathrm{V}})]\}$ of the nth group back into that of the zeroth, $\{\hat{\boldsymbol{\imath}}^{t}[0, \phi(0_{\mathrm{T}}^{m})]\}$. In the straight helix it is simply (see Appendix 1)

$$\boldsymbol{P} = \boldsymbol{A}^{-1} \boldsymbol{M}^{-1}(\Delta\phi) \, \boldsymbol{S} \boldsymbol{A}, \tag{28}$$

where

$$\boldsymbol{A} = \boldsymbol{L} \boldsymbol{t} \tag{29}$$

rotates the proper frame of a chromophore transition moment into axes radial, tangential and longitudinal to the helix cylinder, and

$$\left.\begin{matrix} \boldsymbol{S}^{\mathrm{T}} \\ \\ \boldsymbol{S}^{\mathrm{V}} \end{matrix}\right\} = \begin{bmatrix} 1 & 0 & 0 \\ 0 & \pm 1 & 0 \\ 0 & 0 & \pm 1 \end{bmatrix} \tag{30}$$

reverses these axes if a chromophore on the antiparallel V-helix is involved; also

$$\boldsymbol{M}^{-1}(\Delta\phi) = \begin{bmatrix} \cos\Delta\phi & -\sin\Delta\phi & 0 \\ \sin\Delta\phi & \cos\Delta\phi & 0 \\ 0 & 0 & 1 \end{bmatrix} \tag{31}$$

takes account of the phase separation $\Delta\phi(0_{\mathrm{T}} \rightarrow n_{\mathrm{T}})$ or $\Delta\phi(0_{\mathrm{T}} \rightarrow n_{\mathrm{V}})$ of the chromophores.

PHILOSOPHICAL TRANSACTIONS OF THE ROYAL SOCIETY A MATHEMATICAL, PHYSICAL & ENGINEERING SCIENCES

In the superhelix, the sequence of transformations must take account of the non-zero phases ϕ_0 and $\phi_0+\Delta\phi$ of the zeroth and nth groups respectively, and also of their phase difference around the superhelix,

$$\Delta\Phi = \Delta z C/R, \tag{32}$$

where

$$C = \cos\alpha_{sh} = 2\pi Rx/p, \tag{33}$$

α_{sh} is the superhelix angle, R the radius of the superhelix cylinder, and x the superhelix density in superhelix turns per turn of the helix. (It is convenient to use here the geometrical superhelix density x = s.h. turns per h. turn; for B-DNA, there are 10 b.p. per turn, and so x is in fact equal to the conventional superhelix density σ = s.h. turns per 10 b.p.). We therefore have

$$\boldsymbol{P} = \boldsymbol{A}^{-1}\boldsymbol{W}^{-1}(0_T^m \to n)\,\boldsymbol{SA}, \tag{34}$$

where

$$\boldsymbol{W} = \boldsymbol{M}(\phi_0+\Delta\phi)\,\boldsymbol{h}^{-1}\boldsymbol{M}(\Delta\Phi)\,\boldsymbol{h}\boldsymbol{M}^{-1}(\phi_0); \tag{35}$$

and

$$\boldsymbol{h} = \begin{bmatrix} 1 & 0 & 0 \\ 0 & \sin\alpha_{sh} & \cos\alpha_{sh} \\ 0 & -\cos\alpha_{sh} & \sin\alpha_{sh} \end{bmatrix} \tag{36}$$

rotates the helix frame into the superhelix frame (see Appendix 1).

The distance vector $\boldsymbol{R}$ between chromophores (Appendix 2) is given in the helix frame at $\phi = 0$ by

$$\{\boldsymbol{R}\}^h[0] = \hat{\boldsymbol{i}}^h[0]\,r(\cos\Delta\phi - 1) + \hat{\boldsymbol{j}}^h[0]\,r\sin\Delta\phi + \hat{\boldsymbol{k}}^h[0]\,\Delta z \tag{37}$$

for the straight helix, and

$$\left.\begin{aligned} \{\boldsymbol{R}\}^h[0,0] = \hat{\boldsymbol{i}}^h[0,0]\,\{&R[\cos\Delta\phi - 1] - r\cos\phi_0 + r\cos(\phi_0+\Delta\phi)\cos\Delta\Phi \\ &- r\sin(\phi_0+\Delta\phi)\,S\sin\Delta\Phi\} \\ +\hat{\boldsymbol{j}}^h[0,0]\,\{&RS\sin\Delta\Phi - \Delta zSC - r\sin\phi_0 \\ &+ r\cos(\phi_0+\Delta\phi)\,S\sin\Delta\Phi \\ &+ r\sin(\phi_0+\Delta\phi)\,[S^2\cos\Delta\Phi + C^2]\} \\ +\hat{\boldsymbol{k}}^h[0,0]\,\{&RC\sin\Delta\Phi + \Delta zS^2 + r\cos(\phi_0+\Delta\phi)\,C\sin\Delta\Phi \\ &+ r\sin(\phi_0+\Delta\phi)\,[\cos\Delta\Phi - 1]\,SC\} \end{aligned}\right\} \tag{38}$$

for the superhelix, where $C = \cos\alpha_{sh}$, $S = \sin\alpha_{sh}$, and R, r are the radii of the superhelix and helix cylinders. We require $\boldsymbol{R}$ in the transition frame at $\Phi = 0$, $\phi = \phi_0$, and so incorporate the transformation

$$\{\boldsymbol{R}\}^t\,[0,\phi_0] = \boldsymbol{A}^{-1}\boldsymbol{M}(\phi_0)\,\{\boldsymbol{R}\}^h[0,0]. \tag{39}$$

The elements of $\boldsymbol{T}$ are found from the components of $\boldsymbol{R}$ by using (6).

All that remains to be done before Ω_q, and hence Ω^{nc} and Ω^c, can be evaluated from equations (22), (26) and (27), is to assign numerical values to the various geometrical parameters of the DNA molecule. Of these, we consider first the local orientation of the chromophores. The interacting transition moments are taken as point dipoles (whose directions define the x-axis of the 'transition' frame $\{\hat{\boldsymbol{i}}^t\}$ (see Appendix 1)) at the centre, M, of the bases; their orientation θ is normally defined (Bloomfield *et al.* 1971) with respect to the C_5–C_4 bond for purines, and

PHILOSOPHICAL TRANSACTIONS OF THE ROYAL SOCIETY A MATHEMATICAL, PHYSICAL & ENGINEERING SCIENCES

the C_6–N_3 axis for pyrimidines, as shown in figure A 1.3; so we take these bonds as defining the x-axis $\hat{\boldsymbol{i}}^{\mathrm{loc}}$ of the 'local' frame, with $\hat{\boldsymbol{k}}^{\mathrm{loc}}$ pointing in the $3' \rightarrow 5'$ direction of the sugar backbone. Figure A 1.2 indicates how the local frame is related to the helix frame by the matrix

$$\boldsymbol{L} = \boldsymbol{M}_z^{-1}(\alpha)\, \boldsymbol{M}_y^{-1}(\beta)\, \boldsymbol{M}_z^{-1}(\gamma), \tag{40}$$

where α, β, γ are the Euler angles. By using the atomic coordinates of Arnott *et al.* (1969) for B-DNA from X-ray data, we deduced (MacDermott 1981) the orientation of the local axes for purine and pyrimidine; and because DNA contains equal numbers of purine and pyrimidine bases, a straight vector average gave the orientation of the local axes of the 'average base' and hence the Euler angles $\alpha = -102.79°$, $\beta = -6.26°$, $\gamma = 44.93°$. By calculating the coordinates of the centre M of the average base, it was possible to deduce (MacDermott 1981) the phase $\phi_{\mathrm{bp}} = -171.52°$ of the V-helix relative to that of the T-helix, and also the average radius $r = 324.88$ pm, and the length $d_{\mathrm{bp}} = 648.32$ pm of a line joining the centres of paired bases. This line is tilted (MacDermott 1981) at an angle

$$\psi = \cos^{-1}\{\cos\beta[\cos^2\beta + \sin^2\beta\, \sin^2(\alpha - \tfrac{1}{2}\phi_{\mathrm{bp}})]^{-\frac{1}{2}}\}, \tag{41}$$

where the positive (negative) square root is taken for positive (negative) β, and $\psi = -1.84°$ for B-DNA from the data of Arnott *et al.* (1969).

We now consider the magnitudes of the polarizability and of B_{11}^{c}, so that the relative weighting of the non-conservative and conservative contributions to the c.d. can be assessed. For the polarizability volume of the average base, we adopt the value $(\alpha_\perp - \alpha_\parallel) = 0.56 \times 10^{-29}$ m^3 used by Bush & Brahms (1967) and originally obtained from Kerr effect measurements (Lefevre & Lefevre 1955). B_{11}^{c} is given by (13), in which $\boldsymbol{\mu}_{j\mathrm{oa}} \cdot \boldsymbol{\mu}_{j\mathrm{oa}}$ can be related through the oscillator strength to the extinction coefficient, giving (MacDermott 1981)

$$\begin{aligned} B_{11}^{\mathrm{c}} &= (3 \ln 10 \sqrt{(2\pi)}/8\pi^3 L)\, \epsilon_{\max}\, \lambda_a \\ &= (\epsilon_{\max}/\mathrm{m^2\ mol^{-1}})\, (\lambda_a/\mathrm{m}) \times 1.16 \times 10^{-25}\ \mathrm{m^3}. \end{aligned} \tag{42}$$

Although all chromophores are treated as identical 'average bases', there are in reality four different types; thus pairwise interactions giving a conservative c.d. (i.e. interactions between identical bases) are much rarer than non-conservative interactions (which can occur between any two bases). The relative weighting of the non-conservative and conservative contributions must therefore reflect not only the polymer geometry in the form $-\Omega_3/\Omega_1$, and the intrinsic electronic properties of the chromophores in the form $(\alpha_\perp - \alpha_\parallel)/B_{11}^{\mathrm{c}}$, but also the relative probability $P(\mathrm{nc})/P(\mathrm{c})$ of a pairwise interaction producing a non-conservative or a conservative effect:

$$\Omega^{\mathrm{nc}}/\Omega^{\mathrm{c}} = P(\mathrm{nc})\, (\alpha_\perp - \alpha_\parallel)\, (-\Omega_3)/P(\mathrm{c})\, B_{11}^{\mathrm{c}}\, \Omega_1. \tag{43}$$

$P(\mathrm{nc})$ is clearly unity, as all pairwise interactions produce a non-conservative effect, but since only identical pairs give a conservative contribution, $P(\mathrm{c})$ is the sum of the probabilities of a pair constituting either both adenine or both thymine bases, etc., thus,

$$P(\mathrm{c}) = [p(\mathrm{A})]^2 + [p(\mathrm{T})]^2 + [p(G)]^2 + [p(\mathrm{C})]^2, \tag{44}$$

where $p(\mathrm{A})$, $p(\mathrm{T})$, etc., are the fractions of adenine, thymine, etc., in the DNA. The conservative contribution is therefore large for artificial DNAs containing all A–T, or all G–C, base pairs, for which $P(\mathrm{c}) = \frac{1}{2}$, but is a minimum for the most mixed DNAs (50 % A–T), for which $P(\mathrm{c}) = \frac{1}{4}$.

The statistical factor $P(\mathrm{nc})/P(\mathrm{c})$ thus has an important effect on $\Omega^{\mathrm{nc}}/\Omega^{\mathrm{c}}$ and so the overall shape of the c.d. spectrum varies with A–T content.

The relative rarity of conservative interactions also affects the averaging process used to obtain $\epsilon_{\max}$ and λ_{a}, and hence B^{c}_{11}, from (42); their effective average values for conservative interactions will be biased more towards those of the most common base than their average values for non-conservative interactions. Thus, the conservative average is

$$\bar{\epsilon}^{\mathrm{c}}_{\max} = \sum_{\mathrm{B}} [p(\mathrm{B})]^2 \epsilon^{\mathrm{B}} / \sum_{\mathrm{B}} [p(\mathrm{B})]^2 \tag{45}$$

(where ϵ^{B} is the extinction coefficient for one of the four bases B, and $p(\mathrm{B})$ the fraction of this base in the DNA), in contrast to

$$\bar{\epsilon}^{\mathrm{nc}}_{\max} = \sum_{\mathrm{B}} p(\mathrm{B})\, \epsilon^{\mathrm{B}} / \sum_{\mathrm{B}} p(\mathrm{B}) \tag{46}$$

for non-conservative interactions.

These different averaging processes also affect the factor $\mu^2 \nu_{\mathrm{a}}$ in (19): since $\mu^2 \propto \overline{\epsilon_{\max} \lambda}$, we have $\mu^2 \nu_{\mathrm{a}} \propto \bar{\epsilon}_{\max}$, so the ratio of the non-conservative and conservative coefficients becomes

$$O^{\mathrm{nc}}/O^{\mathrm{c}} = F^{\mathrm{nc}} \sum \Omega_3 / \sum \Omega_1, \tag{47}$$

where the summation is over all interacting groups and

$$F^{\mathrm{nc}} = \bar{\epsilon}^{\mathrm{nc}}_{\max} P(\mathrm{nc})\, (\alpha_{\perp} - \alpha_{\parallel}) / \bar{\epsilon}^{\mathrm{c}}_{\max} P(\mathrm{c})\, B^{\mathrm{c}}_{11}. \tag{48}$$

Finally, we consider the orientation of the transition moment with respect to the local frame. For a given base, this is defined by the angle θ it makes with $\hat{\boldsymbol{i}}^{\mathrm{loc}}$, so the matrix $\boldsymbol{t} = \boldsymbol{M}^{-1}(\theta)$ takes the transition frame into the local frame (see Appendix 1). The average value of θ is given by

$$\bar{\theta} = \tan^{-1} (\bar{\mu}_y / \bar{\mu}_x), \tag{49}$$

and since the magnitude of the average transition moment is proportional to $(\overline{\epsilon_{\max} \lambda})^{\frac{1}{2}}$, its x-component is given by

$$\bar{\mu}^{\mathrm{nc}}_x \propto \sum_{\mathrm{B}} (\epsilon^{\mathrm{B}} \lambda^{\mathrm{B}})^{\frac{1}{2}} \cos\theta^{\mathrm{B}}\, p(\mathrm{B}) / \sum_{\mathrm{B}} p(\mathrm{B}) \tag{50}$$

in the non-conservative case and by a process analogous to (45) for the conservative case; the average y-components $\bar{\mu}_y$ are obtained similarly so $\bar{\theta}^{\mathrm{nc}}$ and $\bar{\theta}^{\mathrm{c}}$ can thus be determined.

From data (table 1) on the $\pi^* \leftarrow \pi$ transitions of individual bases (Bloomfield *et al.* 1971)

Table 1. Characteristics of $\pi^* \leftarrow \pi$ transitions in DNA bases

base	λ/nm	$\epsilon_{\max}$/(dm^3 mol^{-1} cm^{-1})	θ/deg
adenine	260	14900	−3
thymine	270	9700	−19
guanine	275	9000	−6
cytosine	267	9100	12

we calculated F^{nc} and $\bar{\theta}$ for various percentages of A–T, and found that F^{nc} varied widely, from 0.2974 at 100% A–T, to 0.7091 at 40% A–T, while $\bar{\theta}$ varied from 2.96° at 100% G–C to −10.21° at 100% A–T, with 1–2° difference between $\bar{\theta}^{\mathrm{c}}$ and $\bar{\theta}^{\mathrm{nc}}$ at intermediate compositions. The DNAs used to produce the experimental superhelix c.d. described earlier

ranged from 47 to 54% A–T. We therefore assume an average value of 50% A–T in our calculations, because $\bar{\theta}^{c}$ and $\bar{\theta}^{nc}$, and also $\bar{\lambda}^{c}$ and $\bar{\lambda}^{nc}$, are then conveniently equal, with $\bar{\theta} = -4.08°$, and $F^{nc} = 0.6777$. For accurate comparison of theory with experiment, one could of course take account of the exact A–T content of a particular DNA, by using the methods outlined above. (For simplicity, we have used only one transition on each of the four bases, namely that in the important 260–275 nm region. To include other transitions, such as those on A and G in the nearby 240–250 nm region (Arnott & Selsing 1975), at $\theta \approx 90°$, would raise complicated problems concerning the weighting given to them in constructing the average transition moment. However, the likely effect on the c.d. of a different $\bar{\theta}$ is examined in Appendix 4, and we show that inclusion of other transitions would probably have little effect where only relative c.d. values for different structures are required.)

The non-conservative and conservative contributions to the c.d. can now be evaluated by using

$$\left.\begin{aligned} O^{c}_{1\,\mathrm{turn}} &\propto \sum_{m=-4}^{+5} \left\{ \sum_{n=-\infty}^{\infty\prime} \Omega_1(0^{m}_{T} \to n_{T}) + \sum_{n=-\infty}^{\infty} \Omega_1(0^{m}_{T} \to n_{V}) \right\}, \\ O^{nc}_{1\,\mathrm{turn}} &\propto F^{nc} \sum_{m=-4}^{+5} \left\{ \sum_{n=-\infty}^{\infty\prime} \Omega_3(0^{m}_{T} \to n_{T}) + \sum_{n=-\infty}^{\infty} \Omega_3(0^{m}_{T} \to n_{V}) \right\}. \end{aligned}\right\} \tag{51}$$

We evaluated the geometric factors Ω_1 and Ω_3 for each m-value, for a given n, by using (23), in which the components of $\boldsymbol{R}$ and hence $\boldsymbol{T}$ are given by (38), (39) and (6), and those of $\boldsymbol{P}$ by (34), (35) and (29). The process was repeated for all n, with the summations terminated at $n = 20$ for the straight helix; for the superhelix, n values up to several hundred must be included to encompass interactions between turns. The computed summation over geometric factors is multiplied by the electronic structure factor F^{nc} in the non-conservative case, giving O^{nc} and O^{c}, which are then multiplied by the shape functions $f(w)$ and $f'(w)$ to give the total c.d. spectrum, from (12), as a function of wavelength.

Before applying this theory to supercoiled DNA, we tested it on straight DNA (for which the summation over m in (51) is replaced by multiplication by the number of groups per turn) and obtained the theoretical spectra shown in figure A 4.2 for A- and B-forms and some intermediate structures. The shapes of the calculated A and B spectra agree well with those of experimental spectra (Johnson & Tinoco 1969; Ivanov *et al.* 1973), confirming the validity (at least for purposes of comparing different DNA geometries) of our approximations, namely retention of the dipole and polarizability approximations even for nearest neighbours, and use of the 'average base' concept.

4. C.D. of a superhelix with standard B secondary structure

Although some authors have attributed the decreased c.d. spectrum of chromatin to deviations from B-type geometry, X-ray scattering (Bram 1971; Bram & Ris 1971) and infrared dichroism (Taillandier *et al.* 1979) both indicate a B-form secondary structure; furthermore, computer energy calculations (Levitt 1978) show that a superhelix should be most stable in the B-form with 10 b.p. per turn of the helix, in agreement with nuclease digestion studies (Noll 1974; Kornberg 1977). These calculations also show that the strain energy of smooth supercoiling is rather small (in agreement with variable temperature studies showing that the free energy of supercoiling is largely entropic in origin (Pulleyblank *et al.* 1975)) and that the

sugar backbone of DNA has sufficient conformational flexibility to allow smooth, as opposed to kinked, supercoiling (Levitt & Warshel 1978). Furthermore, ^{31}P n.m.r. studies (Kallenbach *et al.* 1978; Klevan *et al.* 1979; Shindo & McGhee 1980) favour a smooth superhelix over the alternative kinked models (Crick & Klug 1975; Sobell *et al.* 1976; Sobell *et al.* 1978).

We therefore assume smooth supercoiling and standard B geometry for the initial c.d. calculation. Estimates of the radius of the chromatin superhelix vary from 4.5 to 5.5 nm, and recent neutron, X-ray, and electron microscopy measurements (Finch *et al.* 1977; Bradbury 1978) indicate a superhelix pitch of 2.7–2.8 nm. We therefore assume $P = 2.75$ nm and $R = 4.0$ nm for the radius of the superhelix cylinder (obtained by subtracting the helix radius, $r = 1.0$ nm, from the average measured external radius of 5.0 nm), corresponding to a superhelix density

$$x = p(4\pi^2R^2 + P^2)^{-\frac{1}{2}} = pC/2\pi R = -0.1337 \text{ s.h. turns/h. turn}, \tag{52}$$

where $p = 3.38$ nm is the pitch of the helix, and C the cosine of the superhelix angle α_{sh}. We computed O^{nc} and O^{c} for a range of superhelix densities from zero to ± 0.1337, assuming $R = 4.0$ nm, and the results are presented in figure 3 in the form of the ratio $\{\Delta\epsilon(x)/\Delta\epsilon(0)\}[w_{max}]$, of the positive c.d. maxima for the superhelix and helix, where

$$\Delta\epsilon[w] = O^{nc}\, e^{-\frac{1}{2}w^2} - O^{c} w\, e^{-\frac{1}{2}w^2}. \tag{53}$$

The wavelength of maximum c.d. is given by

$$w_{max} = \tfrac{1}{2}\{O^{nc} - [(O^{nc})^2 + 4(O^{c})^2]^{\frac{1}{2}}\}/O^{c} \tag{54}$$

(from $\mathrm{d}/\mathrm{d}w\ \Delta\epsilon[w] = 0$, with $O^{c} < 0$), which corresponds to a w_{max} of about one standard deviation if O^{nc} is small compared to O^{c}, but the maximum shifts if O^{nc} becomes larger. In fact, O^{c} is typically 10–20 times larger in magnitude than O^{nc}, so although O^{nc} varies greatly with x, the variation of the total c.d. can be explained entirely by changes in the conservative contribution.

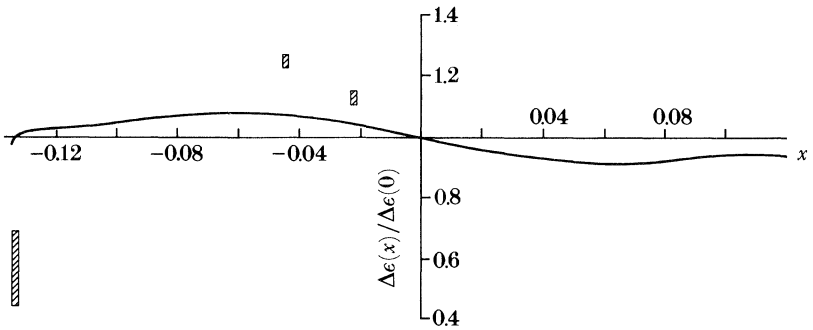

FIGURE 3. The computed ratio $\Delta\epsilon(x)/\Delta\epsilon(0)$ as a function of superhelix density x for superhelix radius $R = 4$ nm; the bars indicate the range of earlier experimental results.

The computed $\Delta\epsilon(x)/\Delta\epsilon(0)$ ratio is roughly in line with observation, showing an increase at small negative x, followed by a reversal at large negative x (and the opposite for positive x). However, the experimental increase at small negative x is seen to be severely underestimated, and there is almost no reduction in c.d. at high x ($\Delta\epsilon(x)/\Delta\epsilon(0) = 0.996$ at $x = -0.1337$). An

optimistic first interpretation might be that the wrong superhelix radius has been used. However, although $R = 3.5$ nm gave a greater increase at moderate superhelix densities, and $R = 4.5$ nm gave a smaller increase, neither produced the required reduction at high x.

Before considering improvements in the model to remedy these discrepancies, we examine the physical reasons for the present result.

The chirality of a straight, non-supercoiled, helix arises from the $\hat{\boldsymbol{j}}^{\mathrm{h}}[0]$ component of the distance vector, $R_2 = r \sin \Delta\phi$, which changes sign on going from a right to a left-hand helix (whereas the components $R_1 = r(\cos \Delta\phi - 1)$ and $R_3 = \Delta z$ are unchanged). Any increase (decrease) in the magnitude of this antisymmetric component should therefore increase (decrease) the optical activity. The relative size of R_2 and R_3 is also important; thus the straight helix has maximum chirality, or helicity, for a helix angle $\alpha_{\mathrm{h}} = 45°$. Similar considerations apply to the superhelix angle α_{sh}, with the maximum difference between the optical activity of left and right-hand superhelices occurring at medium values of x, while at very high x, corresponding to $\alpha_{\mathrm{sh}} \approx 0$, these differences disappear as the tight superhelix increasingly resembles an (achiral) circle. R_1 also has a role; a helix must go well 'down' (large negative R_1) as well as to the right or left (large $|R_2|$) and well forward (R_3 comparable to $|R_2|$), otherwise it is not a helix, but simply an (achiral) straight line that happens to be pointing to the right or left.

Calculation of the components of the distance vector $\boldsymbol{R}(0_{\mathrm{T}}^m \to 1_{\mathrm{T}})$ between nearest neighbours (evaluated in the proper helix frame $\{\hat{\boldsymbol{i}}^{\mathrm{h}}[0, \phi(0_{\mathrm{T}}^m)]\}$ of the zeroth chromophore) shows that both R_2 and $|R_1|$ are increased, compared with the straight helix values, for right-hand supercoiling, and decreased for left supercoiling, while R_3 is increased on the outside of the superhelix $(-\frac{1}{2}\pi < \phi(0_{\mathrm{T}}^m) < \frac{1}{2}\pi,\ m = -4,\ -3,\ -2)$, and decreased on the inside $(\frac{1}{2}\pi < \phi(0_{\mathrm{T}}^m) < \frac{3}{2}\pi, m = 1, 2, 3)$. This effect on R_3 is expected, because the helix is stretched by the positive curvature of the outside, and compressed by the negative curvature of the inside, leading to larger contributions to the optical activity from bases on the outside (see table 2, which shows the conservative nearest-neighbour interaction $\Omega_1(0_{\mathrm{T}}^m \to 1_{\mathrm{T}})$ for chromophores of different m-values, whose positions are shown in figure 4). The effects on R_2 and $|R_1|$ appear surprising, since they imply that right (left) supercoiling makes the helix more (less) chiral, although it decreases (increases) the c.d. But in the exciton model, it is not the chirality of a structure itself that determines the optical activity, but the chirality of the relative orientation of transition dipoles located on this structure. We should therefore examine the effect of supercoiling on the chromophore orientation as well as on the helix itself.

Consider the proper frame of the 'top' of the helix cylinder ($\phi = 0$). This is $\{\hat{\boldsymbol{i}}^{\mathrm{h}}[0, 0]\}$ and for zero superhelix density it remains unchanged all along the helix, but in the superhelix it evolves with superhelical phase $\boldsymbol{\Phi}$ according to

$$\begin{aligned}\{\hat{\boldsymbol{i}}^{\mathrm{h}}[\boldsymbol{\Phi}, 0]\} &= \boldsymbol{h}^{-1}\boldsymbol{M}(\boldsymbol{\Phi})\,\boldsymbol{h}\{\hat{\boldsymbol{i}}^{\mathrm{h}}[0, 0]\} \\ &= \begin{bmatrix} \cos\boldsymbol{\Phi} & S\sin\boldsymbol{\Phi} & C\sin\boldsymbol{\Phi} \\ -S\sin\boldsymbol{\Phi} & S^2\cos\boldsymbol{\Phi} + C^2 & SC(\cos\boldsymbol{\Phi} - 1) \\ -C\sin\boldsymbol{\Phi} & SC(\cos\boldsymbol{\Phi} - 1) & C^2\cos\boldsymbol{\Phi} + S^2 \end{bmatrix} \{\hat{\boldsymbol{i}}^{\mathrm{h}}[0, 0]\} \end{aligned} \tag{55}$$

At very high superhelix density, $S \approx 0$ and $C \approx 1$ ($\alpha_{\mathrm{sh}} \approx 0$), so, for small $\boldsymbol{\Phi}$,

$$\{\hat{\boldsymbol{i}}^{\mathrm{h}}[\boldsymbol{\Phi}, 0]\} \approx \begin{bmatrix} 1 & 0 & +\epsilon \\ 0 & 1 & 0 \\ -\epsilon & 0 & 1 \end{bmatrix} \{\hat{\boldsymbol{i}}^{\mathrm{h}}[0, 0]\} \tag{56}$$

Table 2. Conservative interstrand interactions between an m-type chromophore and its nearest neighbour at different superhelix density†

m	$x = -0.05$ $\Omega_1(0_T^m \to 1_T)$	$+0.05$ $\Omega_1(0_T^m \to 1_T)$
−4	−0.01659	−0.01403
−3	−0.01658	−0.01405
−2	−0.01653	−0.01399
−1	−0.01646	−0.01388
0	−0.01640	−0.01376
1	−0.01636	−0.01366
2	−0.01637	−0.01364
3	−0.01643	−0.01370
4	−0.01650	−0.01382
5	−0.01657	−0.01395

m	$x = -0.1337$ $\Omega_1(0_T^m \to 1_T)$	$+0.1337$ $\Omega_1(0_T^m \to 1_T)$
−4	−0.01638	−0.01572
−3	−0.01623	−0.01562
−2	−0.01597	−0.01535
−1	−0.01559	−0.01488
0	−0.01499	−0.01414
1	−0.01433	−0.01334
2	−0.01413	−0.01306
3	−0.01469	−0.01364
4	−0.01562	−0.01469
5	−0.01625	−0.01546

† For the straight helix ($x = 0$) $\Omega_1(0_T \to 1_T) = -0.01520$ for all m.

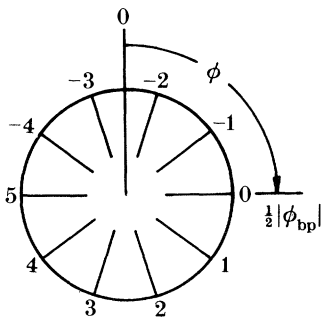

Figure 4. Positions of chromophores with different m values; the $m = 0$ chromophore has angular coordinate $\phi = \frac{1}{2}|\phi_{bp}|$.

(where ϵ is a small quantity, and we note that $C, \Phi > 0$ for $x > 0$, $C, \Phi < 0$ for $x < 0$, and $S > 0$ always), showing, predictably, that the $\hat{\boldsymbol{i}}^h$ and $\hat{\boldsymbol{k}}^h$ axes at superhelix phase Φ tip slightly forward (with respect to those at $\Phi = 0$) as the helix cylinder bends downwards. But, more interestingly, at low to medium superhelix density ($S \approx 1, C \approx 0$) we obtain, for small Φ,

$$\{\hat{\boldsymbol{i}}^h[\Phi, 0]\} \approx \begin{bmatrix} 1 & \pm\delta & 0 \\ \mp\delta & 1 & 0 \\ 0 & 0 & 1 \end{bmatrix} \{\hat{\boldsymbol{i}}^h[0, 0]\}, \tag{57}$$

showing that the $\hat{\boldsymbol{i}}^h$ and $\hat{\boldsymbol{j}}^h$ axes turn slightly to the right (left) for right (left) supercoiling. In other words, the helix cylinder not only bends downwards and points to the right (left), but

also rolls over to the right (left). (Strictly, one should consider the proper helix frame $\{\hat{\boldsymbol{i}}^{\mathrm{h}}[\Phi, \phi]\}$ of a chromophore of arbitrary phase ϕ; a similar right or left turning of $\hat{\boldsymbol{i}}$ and $\hat{\boldsymbol{j}}$ is found for all ϕ, although $\hat{\boldsymbol{i}}$ and $\hat{\boldsymbol{k}}$ of course tip forward on top of the cylinder, and backward underneath.)

The chiral rolling, or torsion, about the cylinder axis, explains both the increased (decreased) R_2 and $|R_1|$, and the decreased (increased) c.d., for right (left) supercoiling. The effect on the distance vector can be appreciated from figure A 2.2, where the chiral rotation of $\hat{\boldsymbol{i}}^{\mathrm{h}}[\Phi, 0]$ with respect to $\hat{\boldsymbol{i}}^{\mathrm{h}}[0, 0]$ is clearly seen. The displacement $\omega\omega'$ of the centre of the helix cylinder is $\Delta z\hat{\boldsymbol{k}}^{\mathrm{h}}$ in the straight helix, but in a superhelix ω' also drops downwards, making R_1 more negative by $R(\cos\Delta\Phi - 1)$. This effect, however, is dominated by the chiral torsion of the cylinder; for $x > 0$, $\omega' Q'$ twists to the right, adding to the $\hat{\boldsymbol{j}}^{\mathrm{h}}[0, 0]$ component, R_2, of $\boldsymbol{R}$, and reducing the $\hat{\boldsymbol{i}}^{\mathrm{h}}[0, 0]$ component, to give a larger negative R_1; for $x < 0$, $\omega' Q'$ twists to the left, reducing R_2 and making R_1 less negative. Therefore the helicity of a helix is indeed increased by positive supercoiling, and decreased by negative supercoiling.

TABLE 3. TOTAL CONSERVATIVE AND NON-CONSERVATIVE CONTRIBUTIONS AS A FUNCTION OF SUPERHELIX DENSITY FOR STANDARD B-DNA SECONDARY STRUCTURE AND $R = 4.0$ nm

x	$O^{\mathrm{c}} = \sum_n \Omega_1$ (conservative)	$O^{\mathrm{nc}} = F^{\mathrm{nc}} \sum_n \Omega_3$ (non-conservative)
0	−0.4117	0.0288
−0.02	−0.4276	0.0304
−0.04	−0.4411	0.0302
−0.06	−0.4499	0.0266
−0.08	−0.4525	0.0198
−0.10	−0.4485	0.0127
−0.12	−0.4389	0.0142
−0.1337	−0.4145	0.0242
0	−0.4117	0.0288
0.02	−0.3959	0.0271
0.04	−0.3826	0.0272
0.06	−0.3736	0.0303
0.08	−0.3698	0.0359
0.10	−0.3707	0.0406
0.12	−0.3745	0.0354
0.1337	−0.3926	0.0240

The c.d. (from (3) and (4)) is proportional to the product of the 'helicity factor', $\boldsymbol{\mu}^{(0)} \wedge \boldsymbol{\mu}^{(n)} \cdot \boldsymbol{R}$, which roughly mirrors the helicity of the helix, and the interaction V between $\boldsymbol{\mu}^{(0)}$ and $\boldsymbol{\mu}^{(n)}$, which more closely reflects the mutual orientation of the dipoles than the helicity of the helix. From (51) and (21) to (27), we see that conservative interactions are between $\boldsymbol{\mu}^{(0)}$, along $\hat{\boldsymbol{i}}^{t}[0, \phi_0]$, and $\boldsymbol{\mu}^{(n)}$, along $\hat{\boldsymbol{i}}^{t}[\Phi, \phi_0 + \Delta\phi]$, while non-conservative interactions can be regarded as between $\boldsymbol{\mu}^{(0)}$ and a vector along $\hat{\boldsymbol{k}}^{t}[\Phi, \phi_0 + \Delta\phi]$. Because $\hat{\boldsymbol{i}}$ and $\hat{\boldsymbol{k}}$ are affected differently by supercoiling, the conservative and non-conservative optical activities show very different x-dependences (table 3). Consider first the helicity factor. In the conservative case $\boldsymbol{\mu}^{(0)} \wedge \boldsymbol{\mu}^{(n)}$ is roughly proportional to $\sin\Delta\phi$ (we neglect any $\hat{\boldsymbol{k}}$ component of $\boldsymbol{\mu}$ as this is small for B-DNA), but the effective angle between the dipoles is slightly larger (smaller) than $\Delta\phi$ for right (left) supercoiling as $\boldsymbol{\mu}^{(n)}$ twists to the right (left) with the $\{\hat{\boldsymbol{i}}^{\mathrm{h}}[\Phi, 0]\}$ frame, so the helicity factor

increases (decreases); in the non-conservative case, $\boldsymbol{\mu}^{(0)} \wedge \hat{\boldsymbol{k}}$ points along $\hat{\boldsymbol{\jmath}}$ or $-\hat{\boldsymbol{\imath}}$ according to whether $\boldsymbol{\mu}^{(0)}$ is radial or tangential, and since R_2 and $|R_1|$ increase (decrease) for right (left) supercoiling, $\boldsymbol{\mu}^{(0)} \wedge \boldsymbol{\mu}^{(n)}$. $\boldsymbol{R}$ will also increase (decrease). Consider next the interaction V, given by (5) and (6). In the conservative case the dominant term is $\boldsymbol{\mu}^{(0)} \cdot \boldsymbol{\mu}^{(n)}$ (roughly proportional to $\cos \Delta\phi$), and this decreases (increases) for right (left) supercoiling as $\boldsymbol{\mu}^{(n)}$ twists away from (back towards) $\boldsymbol{\mu}^{(0)}$; this is reinforced by the $|R|^{-3}$ dependence of V (because increased (decreased) R_2 and R_1 means increased (decreased) $|R|$ for right (left) supercoiling). The result is that because the transition dipoles are brought closer together and into a more parallel arrangement by left supercoiling, they interact to a greater extent, leading to a stronger conservative c.d. despite the decreased helicity factor; and for right supercoiling, the dipoles move apart and interact less, giving a weaker conservative c.d. despite the increased helicity of the helix itself. In the non-conservative case the dominant term in V is $-3(\boldsymbol{\mu}^{(0)} \cdot \hat{\boldsymbol{R}})\,(\hat{\boldsymbol{R}} \cdot \hat{\boldsymbol{k}})$ and, whether $\boldsymbol{\mu}^{(0)}$ is radial or tangential, $\boldsymbol{\mu}^{(0)} \cdot \boldsymbol{R}$ will increase (decrease) for right (left) supercoiling because of the increased (decreased) R_2 and $|R_1|$; $(\hat{\boldsymbol{R}} \cdot \hat{\boldsymbol{k}})$ shows little dependence on superhelix handedness, but becomes larger as $|x|$ increases ($\hat{\boldsymbol{k}}^{\mathrm{h}}[\Phi, 0]$ points increasingly downward, towards $\boldsymbol{R}$) and so amplifies any chiral effect on $(\boldsymbol{\mu}^{(0)} \cdot \hat{\boldsymbol{R}})$. The non-conservative interaction and helicity factor are thus affected in the same direction by supercoiling, giving a much stronger x-dependence than in the conservative case (where the two factors are opposed, the interaction dominating). However, the $|R|^{-3}$ dependence acts in opposition, and just dominates at very low $|x|$ to give a slight decrease (increase) before, at higher superhelix densities, the increased tipping of $\hat{\boldsymbol{k}}$ amplifies the chiral effect on the interaction and helicity factor to give a strongly increased (decreased) non-conservative contribution for right (left) supercoiling.

Because the helicity of a structure and the chirality of the mutual orientation of dipoles on the structure may be affected oppositely by supercoiling, it is natural to ask whether the x-dependence of the c.d. shown in figure 3 is general, or a special feature of the particular dipolar orientation in B-DNA, and also how sensitive the x-dependence is to slight changes in secondary structure. In Appendix 4 we show $\Delta\epsilon(x)/\Delta\epsilon(0)$ as a function of x for various secondary structures (some planar ($\beta = 0$) structures with dipoles more radial (A-like) than in B-DNA, and some B-like structures with differing out-of-plane tipping, β). The different dipolar orientations produce x-dependences that simply follow a more conservative pattern (increased c.d. for left supercoiling, decreased for right), or a more non-conservative pattern (for left supercoiling a slight increase at low x, followed by a reversal and strong decrease, and for right supercoiling a slight decrease followed by a sharp increase) according to whether the c.d. of the straight helix is conservative or non-conservative at that orientation. The calculated x-dependence in figure 3 is thus unique to B-DNA only in the sense that B geometry is very unusual (as described in Appendix 4) in giving a largely conservative spectrum and hence the conservative pattern of x-dependence.

Chiral interactions in supercoiled DNA can be classified as short range (within one turn of the helix), medium range (between turns of the helix) and long range (between turns of the superhelix). One might expect to relate the c.d. from short range interactions to changes in the local helix angle $\alpha_{\mathrm{h}}^{\mathrm{loc}}$, arising from curvature of the surface of the helix cylinder as it is coiled into a superhelix. However, x appears squared in the expression for $\tan \alpha_{\mathrm{h}}^{\mathrm{loc}}$ (Appendix 3), so the local curvature is the same for either handedness. This is because the metric of the cylinder surface is identical for left and right-hand superhelices, and the difference between them lies

PHILOSOPHICAL TRANSACTIONS OF THE ROYAL SOCIETY A MATHEMATICAL, PHYSICAL & ENGINEERING SCIENCES

in the way the two-dimensional surface is embedded into three-dimensional space, as reflected in the distance vector $\boldsymbol{R}$ and in the chiral torsion of the helix frame. But α_h^{loc} does affect the c.d., albeit achirally. Table 2 shows that the nearest-neighbour contribution from chromophores on the inside of the superhelix is decreased because of reduction of the local helix angle (Appendix 3) as the helix is compressed, while chromophores on the outside, where the helix is stretched to give an increased α_h^{loc}, show increased optical activity. But because the metric is achiral, these local curvature effects produce little difference in overall c.d. between left and right hand superhelices at $x = \pm 0.1337$; both show a slightly decreased c.d. compared to the straight helix because the curvature is strongest on the inside, so the decreased contribution from inside chromophores dominates the increased contribution from outside chromophores. However, at $x = \pm 0.05$, these achiral local curvature effects are swamped by the 'global' curvature effects of the chiral embedding of the two-dimensional curved cylinder surface into three-dimensional Euclidean space, as reflected in the distance vector (which increases the helicity of the helix for right supercoiling, and decreases it for left supercoiling), and in the chiral torsion of the cylinder (which brings the dipoles closer together, for left supercoiling, to give a larger conservative c.d., despite the reduced helicity of the helix itself, for all m-values at $x = -0.05$, table 2).

In medium range interactions, excitons jump between turns of the helix, so the helicity of the helix itself is irrelevant. Although, for small Φ, R_2 increases (decreases) for right (left) supercoiling, because of the term $r\cos(\phi_0 + \Delta\phi)\, S \sin \Delta\Phi$ in (A 2.7), at larger Φ the term $-\Delta z SC$ becomes more important (as the helix cylinder turns left (right) on moving forward along, as well as merely around, the superhelix cylinder) and R_2 starts to decrease (increase), so that the helicity of the path of exciton jump is decreased (increased) for right (left) supercoiling. The c.d. from medium range interactions, although small, thus reinforces the decrease (increase) for right (left) supercoiling from short range interactions.

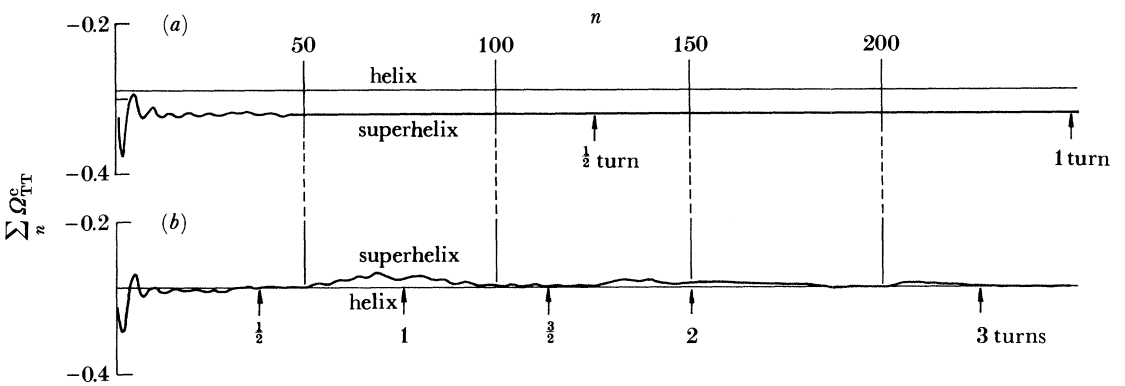

FIGURE 5. The conservative intrastrand contribution as a function of the number of contributing chromophores (n) for (a) $x = -0.04$, (b) $x = -0.1337$ (chromatin), with superhelix radius $R = 4$ nm.

Turning now to long range interactions, we see that the c.d. from nearest-neighbour interactions ($n = 1$) is in fact a good indicator of the final result (figure 3, obtained by summing over interactions to $n = \pm 1000$), which must therefore reflect mainly local effects, i.e. chiral embedding at low $|x|$, and achiral curvature effects at high $|x|$. So why is the c.d. not affected by longer range interactions between adjacent superhelical turns? Analysis of running totals

for summation over n chromophores shows that such interactions are quite strong, but the effect of interaction with the second half-turn is cancelled by that of interaction with the third half-turn. Figure 5*a* shows oscillations, corresponding to each helical turn, which at $x = -0.04$ converge rapidly to a value larger in magnitude than that of the straight helix; for $x = -0.1377$ (figure 5*b*), there are in addition oscillations corresponding to each turn of the superhelix, which die out after about three such turns, giving a total very close to the straight helix value. Thus, if the summation is terminated at $n = 70$, one does indeed obtain a c.d. spectrum that is strongly depressed owing to interaction with the adjacent superhelical turn, as predicted by Fasman & Cowman (1978); but if the summation is continued to $n = 1000$, this effect is cancelled, giving a spectrum virtually identical with that of the straight helix. The physical reason for this cancellation is illustrated in figure 6, which shows the general direction of exciton jump between turns. We see that interactions with groups between $\frac{3}{4}$ and 1 superhelical turn away have left helicity, which reduces the c.d. of the right-handed DNA helix; interactions with groups 1–$1\frac{1}{4}$ turns away have right helicity, which increases the c.d., cancelling the earlier decrease.

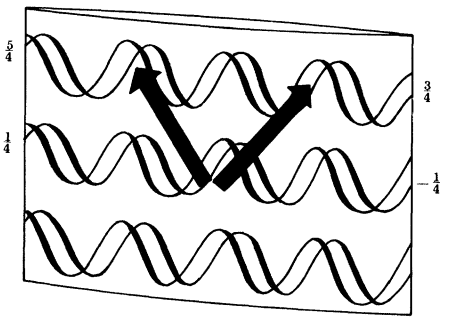

FIGURE 6. The cancellation of tertiary interaction contributions to the c.d.

We have thus shown that although Fasman & Cowman were correct in predicting tertiary interactions between turns, these have no net effect on the c.d. spectrum. We have also shown that although curvature strongly affects the c.d. of individual chromophores by increasing that of those on the positively curved outside, and decreasing that of those on the negatively, and more strongly, curved inside, the net effect of differential curvature of the inside and outside is to produce only a marginal reduction in the chromatin c.d., to 99.6% of the straight helix value. We therefore conclude that secondary structural changes, perhaps involving the often suggested base-tilting, must be responsible for the reduction in the chromatin $\Delta\epsilon(x)/\Delta\epsilon(0)$ ratio to 0.7.

But even when the geometry of each base is locally standard B-form, the global curvature of the helix cylinder produces a mutual tipping of the base-normals of neighbouring bases, so why does this not affect the c.d. spectrum? We show in Appendix 4 that base-tipping may be resolved into twisting (rotation about the line $\boldsymbol{d}_{\mathrm{bp}}$ joining paired bases) and tilting (rotation about an axis perpendicular to $\boldsymbol{d}_{\mathrm{bp}}$ and to the helix axis); twisting changes the orientation of the transition moment much more than tilting, and so has more effect on the c.d. spectrum. Now the mutual tipping of neighbouring bases built into a superhelix corresponds to a rotation about a diameter of the helix cylinder at phase $\phi = \frac{1}{2}\pi$; for most base-pairs (except those with phase $\frac{1}{2}\pi$, for which any effect is minimal because the cylinder is almost Euclidean at this point),

this rotation has more of the character of mutual tilting than of twisting, and so this global base-tipping has little effect on the c.d. Some alteration in local base geometry is therefore needed to produce the required reduction in chromatin c.d. This might take the form of a curvature-induced distortion that could amplify the differential curvature effects already seen to produce a very slight c.d. reduction even with standard B geometry.

5. Introduction of curvature-induced base-twisting

Because non-c.d. evidence points to chromatin being B-form, we seek a secondary structural modification to 'standard' B-DNA that is sufficiently subtle to alter the c.d. while keeping the structure within the B family. A modification of precisely this kind is suggested by the results in Appendix 4 for the variation of the B spectrum with base-tipping (i.e. Euler angle β). From figure A 4.2 we see that strong forward tipping (e.g. $\beta = +6°$, compared with $\beta = -6.26°$ for standard B-DNA) depresses the c.d. maximum to give spectra remarkably like those observed for chromatin. This is confirmed by Levitt's (1978) computer energy calculations, which show not only that the chromatin superhelix is most stable with 10 b.p. per turn, i.e. an essentially B structure, but furthermore that minimum energy is attained if the base-normals acquire an increased tip relative to the helix axis. Levitt shows that this results in a greatly increased twist angle, τ, which is especially pronounced on the inside of the helix, enabling the bases to twist away from one another, thus avoiding any unfavourable interactions from being forced together by negative curvature while at the same time finding more favourable stacking configurations.

We therefore consider a model of supercoiled DNA in which the basic local geometry (i.e. the values of α, γ, ϕ_{bp}, k, r, etc.) is that of the standard B-DNA of Arnott *et al.* (1969), the only changed parameter being the tip angle β. A crucial feature of this model is that for B geometry, the tip angle β is almost entirely twist, to which the c.d. is highly sensitive, rather than tilt, to which the c.d. is very much less sensitive (see Appendix 4). We model the variation of β with superhelix density by an expression of the form

$$\beta_{sh} = \beta_h + (x/x_{max})^n \beta' \chi[\phi(0^m)], \tag{58}$$

where the tip angle β_{sh} in a superhelix is set equal to that in a standard B-form straight helix ($\beta_h = -6.26°$), plus an additional term which is proportional to the nth power of the superhelix density, rises to a maximum of β' at $x = x_{max}$ (where $x_{max} = p/2\pi R$ is the superhelix density of a maximally curved superhelix, i.e. a circle), and is weighted by a phase factor $\chi[\phi(0^m)]$, allowing bases with different m-values to tip by differing amounts. In the absence of experimental measurements of β in chromatin, we note that Levitt's computations suggest an average mutual twist of $2\tau \approx 30°$ between base-normals of paired bases in a superhelix, corresponding to $|\beta| \approx 15°$, because $\beta \approx \tau$ for B geometry. (This large twist need not weaken the hydrogen bond, which can in any case tolerate deviations of up to 12° from linearity (Pauling 1960), because Levitt suggests that small out-of-plane movements of the carbonyl and amino groups in fact compensate for much of the twisting strain on the hydrogen bonds, while leaving the aromatic rings still strongly mutually twisted). Levitt does not give the direction of the base-normal tipping, but figure A 4.2 clearly shows that a large positive β depresses the c.d., while a large negative β elevates it. We may therefore guess that the maximum additional tipping, β', is about $+15°$, but acknowledge that β' is really an empirical parameter that could be estimated by comparison of our computed results with experimental spectra (although its

accurate determination must await improved X-ray resolution). Because the additional base-normal tipping is regarded as a curvature-induced distortion, the phase factor $\chi[\phi(0^m)]$ should mirror the phase of the Riemann curvature scalar,

$$R^{\mathrm{curv}}(\phi) = (C^2/rR)\cos\phi\,[1+2(r/R)\,C^2\cos\phi]^{-1}, \tag{59}$$

of the curved helix cylinder (Appendix 3). We therefore write

$$\beta_{\mathrm{sh}} = \beta_{\mathrm{h}} - (x/x_{\max})^n\,\beta'\cos\phi(0^m)\,[1+2(r/R)\,C^2\cos\phi(0^m)]^{-1}, \tag{60}$$

where the negative sign ensures that groups on the positively curved outside ($|\phi(0^m)| < \frac{1}{2}\pi$) tip backwards (towards increasingly negative β and larger c.d.), while those on the negatively curved inside ($\frac{1}{2}\pi < |\phi(0^m)| < \pi$) tip towards increasingly positive β and smaller c.d., the deformation being greatest on the inside ($\cos\phi(0^m) < 0$) where the curvature is strongest, so that an overall reduction in c.d. can be expected. (It is fairly plausible that inside and outside bases might twist in opposite directions, because the inside ones must twist to avoid unfavourable interactions as they are forced together, while the outside ones must twist to recover favourable stacking interactions reduced by increased separation.) This model, in which local deformation in secondary structure is directly proportional to the curvature at a given point, provides the required amplification of the differential curvature effect seen in the standard B-form superhelix, where positive and negative curvature were found respectively to increase and decrease the c.d.

One might imagine that a sensible value of n to try would be 2. However, if curvature-induced base-twisting arises from nearest-neighbour steric effects, a higher value of n may be appropriate, because the curvature may not become felt, over such short range, until higher values of x are reached. We therefore use $n = 6$ in (60), but recognize that, like β', n needs to be confirmed by comparison with experiment.

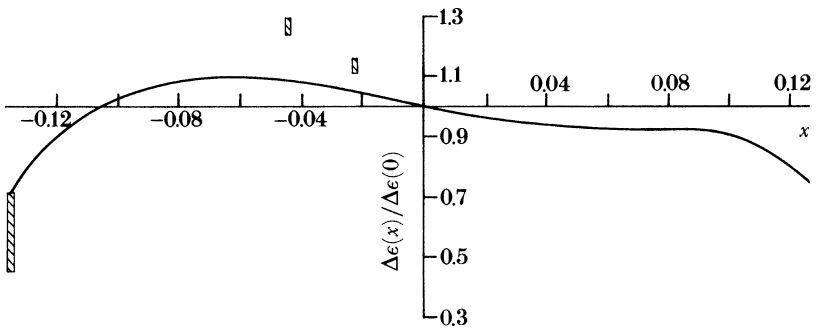

FIGURE 7. Computed $\Delta\epsilon(x)/\Delta\epsilon(0)$ ratio as a function of superhelix density x using tip angle $\beta_{\mathrm{sh}}(\phi)$ from (60), with $\beta' = 15°$, $n = 6$ and $R = 4$ nm.

Figure 7 shows the computed $\Delta\epsilon(x)/\Delta\epsilon(0)$ ratio as a function of x for an otherwise B-form superhelix having a modified tip angle given by (60) with $\beta' = 15°$ and $n = 6$. At low superhelix densities, the $\Delta\epsilon(x)/\Delta\epsilon(0)$ ratio remains as it was in figure 3 without curvature-induced base-tipping, but for chromatin it is reduced to about 0.7 in excellent agreement with most experiments. This seems to confirm the value $\beta' = +15°$ suggested by Levitt's work, but clearly the c.d. measurements on chromatin need to be repeated (in view of the wide range of

$\Delta\epsilon(x)/\Delta\epsilon(0)$, from 0.45 to 0.70, of results hitherto obtained) to find the best value of this parameter. The chromatin c.d. is much less sensitive to n (as $x/x_{\max} \approx 1$) than to β', but at more moderate superhelix densities (at which there is at present a total lack of experimental data) the x-dependence of the c.d. is quite sensitive to n, as shown in figure 8. New c.d. measurements over the whole range of x could test these predictions and determine the most

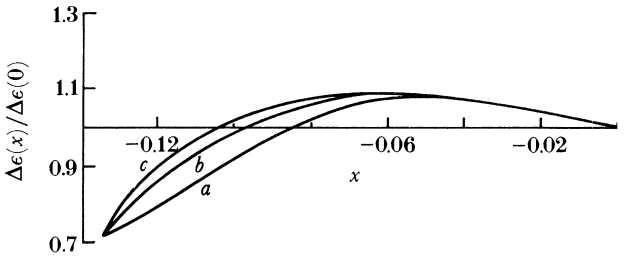

FIGURE 8. Computed dependence of $\Delta\epsilon(x)/\Delta\epsilon(0)$ on superhelix density x using the tip angle $\beta_{\mathrm{sh}}(\phi)$ from (60) with $\beta' = 15°$, $R = 4$ nm, and (*a*) $n = 2$, (*b*) $n = 4$, (*c*) $n = 6$.

appropriate values of n and β'. Despite the success of our base-tipping model in accounting for the reduced c.d. of chromatin, the exciton model, with or without extra base-tipping, fails to reproduce the observed 25% increase in c.d. at $x = -0.044$, predicting an increase of only about 8%. This may indeed prove to be a deficiency of the model, but we feel judgement should be reserved until the c.d. measurements have been repeated over the full range of superhelix density.

6. Extension to the supersuperhelix

Although secondary effects, in the form of increasing base-tipping with increasing curvature, can account well for the depressed c.d. of chromatin, quaternary effects should be considered as a possible alternative explanation, because there is established experimental evidence for supersupercoiling in chromatin, but only a theoretical indication of increased base-tipping. The major modifications required to encompass another order of coiling are in the transformation matrix $\boldsymbol{W}$ of (34), and in the distance vector, these being dealt with in Appendixes 1 and 2 respectively. We introduce an additional angular coordinate, the rotation Φ' round the supersuperhelix cylinder, which is related to the rotation round the superhelix cylinder by

$$\Delta\Phi' = X\Delta\Phi, \tag{61}$$

where

$$X = P(4\pi R'^2 + P'^2)^{-\frac{1}{2}}\{\text{s.s.h. turns/s.h. turn}\} \tag{62}$$

is the supersuperhelix density. Neutron scattering (Bradbury 1978) indicates a supersuperhelix pitch $P' \approx 10.5$ nm, and an outer radius of 13.7 nm, corresponding (with $R = 4.5$ nm and $r = 1.0$ nm) to a radius $R' = 8.25$ nm for the supersuperhelix cylinder, giving $|X| = 0.052$.

Just as a chromophore's phase $\phi(0^m)$ round the helix becomes significant when supercoiling breaks the cylindrical symmetry of the helix, so the phase $\Phi(0^M)$ round the superhelix must be considered when supersupercoiling is present. Chromatin ($x = -0.1337$) has 75 base-pairs per turn of the superhelix, i.e. 75 non-equivalent chromophore sites, distinguished by the index

M; we take the $M = 0$ group to be at $\Phi = 0$ ('on top' of the superhelix), so the Mth group has superhelical phase

$$\Phi(0^M) = Mx2\pi/k. \tag{63}$$

One should really compute the contribution to the c.d. of chromophores in each of the 75 different sites, and then take the average. Our purpose at this stage, however, is not to present a calculation of high accuracy, but simply to discover whether or not supersupercoiling can affect the c.d. spectrum. We therefore investigate the c.d. of only five sample types of chromophore (those at $\Phi(0^M) = 0, \frac{1}{4}\pi, \frac{1}{2}\pi, \frac{3}{4}\pi, \pi$, corresponding to $M = 0, 10, 19, 28, 37$) and average the results by using

$$\Omega[\text{average}] = \tfrac{1}{8}\{\Omega[0] + 2\Omega[\tfrac{1}{4}\pi] + 2\Omega[\tfrac{1}{2}\pi] + 2\Omega[\tfrac{3}{4}\pi] + \Omega[\pi]\}, \tag{64}$$

where $\Omega[\frac{1}{4}\pi]$, for example, represents the contribution from a chromophore in the $|\Phi| = \frac{1}{4}\pi$ region, and is multiplied by two because there are two such regions. This gives a rather crude average, but should indicate the general order of magnitude of quaternary effects on DNA c.d. Now $|X| = 0.052$ corresponds to 1442 chromophores, or about 19 turns of the superhelix, per turn of the supersuperhelix, so our computations sum to $n = \pm 2000$, to encompass interactions with groups in the first adjacent turn of the supersuperhelix.

Because the handedness of the supersuperhelix is uncertain (Thoma *et al.* 1979), one of the purposes of our rough calculation is to see if c.d. can resolve the matter. Our computations (MacDermott 1981) for chromatin ($x = -0.1337$) indicate a much greater depression in c.d. in the left-handed case ($\Delta\epsilon(x)/\Delta\epsilon(0) \approx 0.64$ for $X = -0.052$) than in the right-handed case ($\Delta\epsilon(x)/\Delta\epsilon(0) \approx 0.90$ for $X = +0.052$). The physical reasons for this can be analysed by plotting the running total of contributions from conservative intrastrand interactions (which are the predominant influence on the total c.d.) as a function of the number of interacting chromophores n, and in figure 9 this sum is plotted separately for chromophores at $\Phi = 0, \frac{1}{2}\pi, \pi$ in left and right-handed supersuperhelices.

Looking first at the very beginning of the curves, we see that even when the sum is terminated at low n ($n \approx 20$), before tertiary or quaternary interactions come into play, the supersuperhelix c.d. is already lower in magnitude than that of the superhelix. This can be explained by the greater curvature of the supersuperhelix. We recall that for a left-handed superhelix at high x, differential curvature effects tend to reverse the increase in c.d. observed at lower x; the stronger curvature of the supersuperhelix amplifies this effect, producing a more substantial reduction in c.d. For left-handed supersupercoiling, we have, at low n, $\Omega^{\mathrm{L}}[0] < \Omega^{\mathrm{L}}[\frac{1}{2}\pi] < \Omega^{\mathrm{L}}[\pi]$, while for right-handed supersupercoiling we have $\Omega^{\mathrm{R}}[0] > \Omega^{\mathrm{R}}[\frac{1}{2}\pi] > \Omega^{\mathrm{R}}[\pi]$. These opposite orderings represent a small chiral effect from the small non-zero value of α_{ssh}, superimposed on the large achiral reduction in c.d. magnitude caused by the extra-strong curvature at small α_{sh} and α_{ssh} (both x and X are close to their maximum possible values, corresponding to circles). We saw earlier that left (right) handed supercoiling increases (decreases) the c.d. arising from local interactions, because chiral torsion brings the dipoles closer together (takes them further apart), and it can be seen that supersupercoiling increases this torsion. The effects of left- and right-handed supersupercoiling are therefore respectively to lessen or enhance the general decrease in c.d. from the strong curvature; these effects will of course be greatest on the inside of the superhelix, where the curvature is greatest, so $\Omega^{\mathrm{R}}[\pi]$ is therefore the most reduced, and $\Omega^{\mathrm{L}}[\pi]$ the least reduced at $n \approx 20$.

PHILOSOPHICAL TRANSACTIONS OF THE ROYAL SOCIETY A MATHEMATICAL, PHYSICAL & ENGINEERING SCIENCES

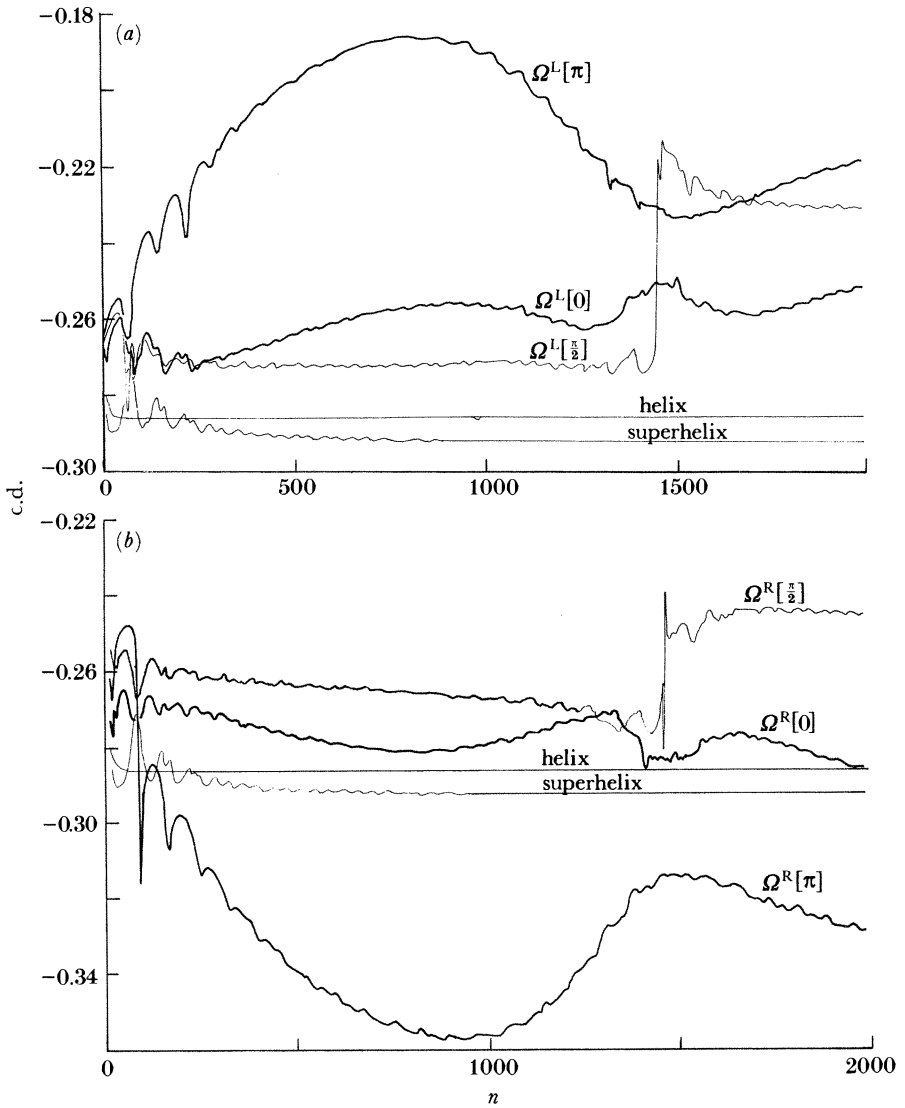

FIGURE 9. Computed running sum of conservative intra-strand interactions in supersuperhelix, for chromophores at superhelix phases $\Phi = 0, \frac{1}{2}\pi, \pi$, at supersuperhelix density (*a*) $X = -0.052$, (*b*) $X = +0.052$.

Turning now to higher n, a peak is seen at $n = 50$–100 arising from tertiary interactions with the first adjacent superhelical turn. This peak is sharpest for $\Omega[\pi]$ because adjacent turns are forced very close together on the inside of the superhelix. In the supersuperhelix, as in the superhelix, interaction with the second half-turn of the superhelix ($\pi < \Phi < 2\pi$), is cancelled by that with the third half-turn ($2\pi < \Phi < 3\pi$), so that tertiary interactions have no net effect on the c.d.

At still higher n, a series of similar peaks of diminishing size is seen, corresponding to interaction with more distant turns of the superhelix. But these oscillations are merely superimposed on a much larger one arising from the first turn of the supersuperhelix; for a left-handed supersuperhelix, interactions with the first half-turn ($0 < \Phi' < \pi$) have left helicity, so decreasing the magnitude of the c.d., while those with the second half-turn ($\pi < \Phi' < 2\pi$)

have right helicity, thus tending to increase the c.d. again; but because the second half-turn of a supersuperhelix is very much farther away than the first, cancellation is incomplete, so that at $\Phi' = 2\pi$ (or $n \approx 1450$), a net decrease over the value at much lower n has occurred; and exactly the opposite effect occurs for a right-handed supersuperhelix, producing a net increase. These quaternary oscillations are of much larger amplitude than the tertiary oscillations, because quaternary folding brings so many more chromophores close enough to interact significantly. The amplitude is especially large for $\Omega[\pi]$, as groups on the inside experience the maximum curvature and have the largest number of close neighbours, but is less pronounced for $\Omega[0]$, as the outside is less curved and fewer groups are within interactive range. The peak is almost absent for $\Phi(0^M) = \frac{1}{2}\pi$, where there is no quaternary curvature, but there is a sudden change at $\Phi' = 2\pi$, where adjacent turns come extremely close together.

It is interesting to note that although left-handed supercoiling and supersupercoiling both have an elevating effect on the c.d. from local interactions within about one turn of the helix, they have opposite effects on the c.d. from longer range interactions. Thus, for a straight ($X = 0$) left-handed superhelix, the running total c.d. reaches a minimum at $\Phi = 2\pi$. In contrast, left-handed supersupercoiling leads to a minimum at $\Phi' = \pi$, since exciton jump to groups with $\Phi' < \pi$ has left helicity, and a maximum at $\Phi' = 2\pi$. This is because α_{ssh} and α_{sh} are both small, so the helix axis is almost perpendicular to the superhelix axis in chromatin and the supersuperhelix axis is almost perpendicular to this, i.e. almost coincident with the helix axis. Helicity is of opposite sign when referred to perpendicular axes, so left-handed superhelicity and supersuperhelicity are equivalent respectively to right and left helicity about the helix axis, thus explaining the respective increase and decrease in c.d. from groups at $\Phi < \pi$ and $\Phi' < \pi$.

An apparently puzzling feature of the curves in figure 9 is that the tertiary peaks in the supersuperhelix ($|X| \neq 0$) curve are of opposite sign to those in the plain superhelix ($X = 0$, figure 5*b*), despite x being negative in both cases. This is resolved by returning to figure 6, where tertiary interactions with groups at $\pi < \Phi < 2\pi$ were depicted as having left helicity (about the helix axis) for the plain superhelix; when the superhelix cylinder is itself bent ($|X| \neq 0$), these interactions acquire in addition a right helicity that apparently dominates at high $|X|$, producing the inversion of tertiary peaks seen in figure 9.

In summary, our computation has shown that left-handed supersupercoiling reduces the c.d. much more than does right-handed supersupercoiling, the main reason being their large and opposite effects on the interactions $\Sigma\Omega[\pi]$ between groups on the highly curved and very crowded inside of the superhelix. Although we have clearly terminated the summation too soon (figure 9 shows that the c.d. is still changing at $n = 2000$), this quaternary effect is undoubtedly real unlike the tertiary effects, which give a depressed c.d. on summation to $n = 70$ but have cancelled by the time the series converges. The crucial difference between the superhelix and supersuperhelix is that in the latter the quaternary turns are so large that cancellation is incomplete (because the cancelling groups are so much further away than in the superhelix), thus leaving a non-zero effect. At $n = 2000$ the $\Omega[\pi]$ curves are about to embark on another oscillation, but the increasing distance will prevent them swinging all the way back, so the final result at $n = \infty$ should be a still greater difference between the c.d. of left and right-handed supersuperhelices.

We thus conclude that if the supersuperhelix is left-handed ($\Delta\epsilon(x)/\Delta\epsilon(0) \approx 0.64$), quaternary effects alone could account for the observed chromatin $\Delta\epsilon(x)/\Delta\epsilon(0)$ ratio of 0.45–0.70, without invoking secondary effects. However, if it is right-handed ($\Delta\epsilon(x)/\Delta\epsilon(0) \approx 0.90$), then secondary

effects must be present. But although either curvature-induced base-tipping (giving $\Delta\epsilon(x)/\Delta\epsilon(0) \approx 0.71$) or left-handed supersupercoiling ($\Delta\epsilon(x)/\Delta\epsilon(0) \approx 0.64$) could separately account for the most frequently observed ratio of 0.70 (figures 10*a*, *b*), the fact that much lower values have been observed, and that the reduction in c.d. varies systematically during the cell cycle (Nicolini *et al.* 1975), strongly suggests that both effects are contributing. We therefore computed the c.d. of a superhelix with both base-tipping (described by (60) with $n = 6$ and $\beta' = 15°$, as before) and left-handed supersupercoiling ($X = -0.052$), and obtained a $\Delta\epsilon(x)/\Delta\epsilon(0)$ ratio of about 0.48 (figure 10*c*) in striking agreement with the lowest experimental chromatin ratios. Because such a large additional reduction cannot be obtained with right-handed supersupercoiling, our results suggest that the supersuperhelix is more likely to be left-handed. This seems reasonable biologically. Right-handed supersupercoiling would destablize the left-handed superhelix, because removal of positive supersuperturns, with concomitant removal of negative superturns, would clearly be energetically favoured; negative supersuperturns, however, would help keep the negative superturns locked in for future use in facilitating transcription.

It is therefore likely that the most frequently observed experimental $\Delta\epsilon(x)/\Delta\epsilon(0)$ ratio, 0.70, represents chromatin that is supercoiled, but not supersupercoiled, the depression in c.d. arising

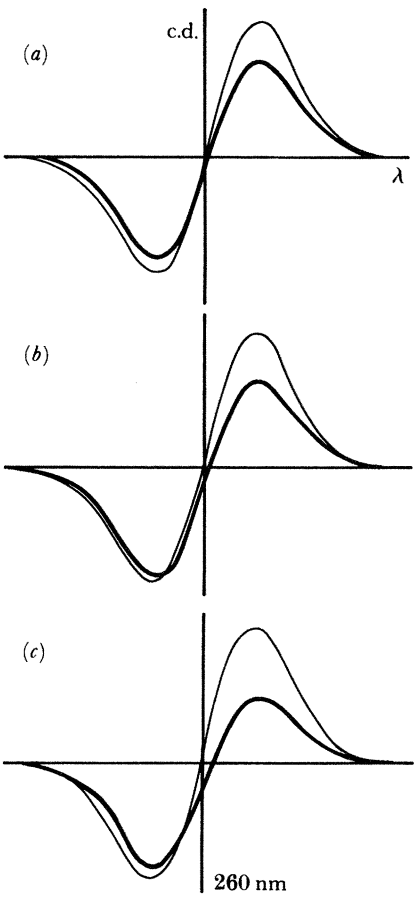

FIGURE 10. Computed superhelix c.d. curves (thick line) with (*a*) base-tipping only, giving $\Delta\epsilon(x)/\Delta\epsilon(0) = 0.71$, (*b*) left handed supersupercoiling only, giving $\Delta\epsilon(x)/\Delta\epsilon(0) = 0.64$, (*c*) base-tipping and supersupercoiling, giving $\Delta\epsilon(x)/\Delta\epsilon(0) = 0.48$; the spectrum of straight B-DNA (thin line) is shown for comparison.

from curvature-induced base-twisting, while larger depressions probably indicate left-handed supersupercoiling. Note that the computed spectra in figure 10 all show a strong depression in the positive lobe at 280 nm, but much less change in the negative lobe when compared with straight B-DNA. This is in agreement with the experimental spectra, and our computations show that although changes in the positive lobe can be explained largely by trends in the conservative contribution, it is actually the small non-conservative contribution that accounts for the lack of change in the negative lobe. The magnitude of the (negative) non-conservative contribution is increased relative to that of straight DNA, thus cancelling the effect of the decreased conservative contribution on the negative lobe but enhancing its effect on the positive lobe.

More accurate computations could sharpen our conclusion about the supersuperhelix handedness, and also enable c.d. to be studied as a function of X and R'. Improvements would not only involve summing to higher n, and averaging over more chromophores with different $\Phi(0^M)$: instead of using the Riemann curvature of a supercoiled helix in (60) for the tip angle, one should really derive the metric and Riemann curvature of a supersupercoiled helix cylinder, because the greater curvature on the inside of the superhelix might produce a greater degree of base-tipping.

7. Conclusions

The aim of this study was first, to resolve the 'secondary against tertiary' controversy surrounding the chromatin c.d., and, second, to establish c.d. as a useful quantitative measure of superhelix density. We have shown that contributions to the c.d. from tertiary interaction between adjacent turns of the superhelix cancel out and so cannot, as frequently and plausibly supposed (Fasman & Cowman 1978), account for the depressed c.d. of chromatin which must therefore be attributable to a change in secondary structure. This somewhat unexpected finding complicates the second objective; in the absence of conclusive experimental evidence, one has to guess the nature of the secondary structural distortion and the form of its dependence on superhelix density. Available experimental evidence (Bram 1971; Bram & Ris 1971; Noll 1974; Kornberg 1977; Taillandier *et al.* 1979) constrains the distorted structure to within the B family, and Levitt's (1978) energy calculations suggest an increased base-normal tipping that is especially pronounced on the inside of the bent helix. We take these considerations into account by proposing a secondary structure differing from standard B-form only in the base-normal tip angle, which is increased in proportion to the nth power of the superhelix density and the phase of the Riemann curvature scalar of the supercoiled helix cylinder; in a B structure, such tipping produces out-of-plane base-twisting (as opposed to tilting), which may relieve curvature-induced strain and crowding. The model contains two parameters, the amplitude β' of the additional tipping, and the power n of the superhelix density to which the distortion is proportional. We obtained excellent agreement with experimental chromatin c.d. spectra using the value $\beta' = 15°$ implied by Levitt's results, which produces a reduction in the calculated positive c.d. at 280 nm to about 70% of that of non-supercoiled B-DNA. A plausible value for n is $n = 6$, but this cannot be confirmed until c.d. spectra over a wider range of superhelix densities are available; it would also be desirable to re-examine experimentally the increase in c.d. at low superhelix density, which our model appears to underestimate. Experiments are planned that will test our model of secondary distortion, and determine the best values of n and β', by measuring the c.d. of DNA over the full range of superhelix density.

PHILOSOPHICAL TRANSACTIONS OF THE ROYAL SOCIETY A MATHEMATICAL, PHYSICAL & ENGINEERING SCIENCES

Because our model gives such good agreement with experiment for chromatin, and the parameters β' and n can be checked experimentally, we believe that it represents a substantial first step towards making superhelix c.d. more quantitatively useful in DNA research. The predicted sharp variation in c.d. at high superhelix densities could become a useful indicator of the slight differences in supercoiling to which gene function is believed to be sensitive. Furthermore, the c.d. is a good indicator of the handedness of the superhelix (except at very high superhelix densities) and also of the supersuperhelix (which our calculations predict to be left-handed in chromatin). The encouraging results from our preliminary calculation on the latter suggest that more accurate computations of c.d. as a function of supersuperhelix density could be useful, and experimental confirmation might be possible by preparing nucleoids with and without the histone H1 that holds the supersuperhelix together.

The success of curvature-induced secondary distortion in accounting for the c.d. of the chromatin superhelix is further evidence in favour of smooth supercoiling and against the kinked models. Because kinking does not introduce curvature, no secondary distortion is necessary in such models, except at the kinks, and it seems unlikely that the few bases involved in kinking could substantially alter the c.d.

Our metric approach introduces a novel interpretation of molecular properties in terms of spatial curvature; this could find application elsewhere.

The author thanks Dr P. W. Atkins for useful discussions.

Appendix 1. Coordinate frames for the helix, superhelix, and supersuperhelix

(a) *The helix*

It is convenient to regard a helix as inscribed on the surface of a cylinder, and we define a triad of unit vectors, $\hat{\boldsymbol{i}}^{\mathrm{h}}[\phi]$, $\hat{\boldsymbol{j}}^{\mathrm{h}}[\phi]$, $\hat{\boldsymbol{k}}^{\mathrm{h}}[\phi]$, written $\{\hat{\boldsymbol{i}}^{\mathrm{h}}[\phi]\}$, that are radial, tangential, and longitudinal respectively to the helix cylinder at an angle ϕ round the helix, as shown in figure A1.1. ϕ is measured clockwise, so the helix axes $\{\hat{\boldsymbol{i}}^{\mathrm{h}}[0]\}$ at zero rotation are taken into those at ϕ by the transformation

$$\{\hat{\boldsymbol{i}}^{\mathrm{h}}[\phi]\} = \boldsymbol{M}(\phi)\,\{\hat{\boldsymbol{i}}^{\mathrm{h}}[0]\}, \tag{A 1.1}$$

where $\boldsymbol{M}(\phi)$ is the rotation matrix

$$\boldsymbol{M}(\phi) = \begin{bmatrix} \cos\phi & \sin\phi & 0 \\ -\sin\phi & \cos\phi & 0 \\ 0 & 0 & 1 \end{bmatrix} \tag{A 1.2}$$

and $\{\hat{\boldsymbol{i}}^{\mathrm{h}}[0]\}$ is treated as a column vector. Chromophores are not in general aligned with the helix axes, so we define a local frame, $\{\hat{\boldsymbol{i}}^{\mathrm{loc}}[\phi]\}$, which is the 'proper' frame of a chromophore at phase ϕ, i.e. the frame in which its polarizability tensor is diagonal. This frame is related to the helix frame by

$$\{\hat{\boldsymbol{i}}^{\mathrm{h}}[\phi]\} = \boldsymbol{L}\{\hat{\boldsymbol{i}}^{\mathrm{loc}}[\phi]\}, \tag{A 1.3}$$

where

$$\boldsymbol{L} = \boldsymbol{M}_z^{-1}(\alpha)\,\boldsymbol{M}_y^{-1}(\beta)\,\boldsymbol{M}_z^{-1}(\gamma), \tag{A 1.4}$$

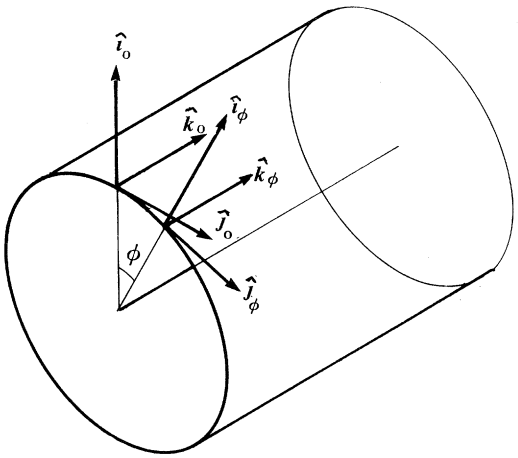

FIGURE A 1.1. The helix axes.

α, β, γ are the Euler angles, and

$$\boldsymbol{M}_z(\alpha) = \begin{bmatrix} \cos\alpha & \sin\alpha & 0 \\ -\sin\alpha & \cos\alpha & 0 \\ 0 & 0 & 1 \end{bmatrix}, \quad \boldsymbol{M}_y(\beta) = \begin{bmatrix} \cos\beta & 0 & -\sin\beta \\ 0 & 1 & 0 \\ \sin\beta & 0 & \cos\beta \end{bmatrix}. \tag{A 1.5}$$

(The helix axes are taken into the local axes by a rotation through α about the z-axis, then through β about the new y-axis, and finally through γ about the new z-axis.)

In DNA, the local axes are oriented as shown in figure A 1.2. Because the polarizability tensor has approximately cylindrical symmetry ($\alpha_{11} = \alpha_{22}$) for the flat aromatic bases, the

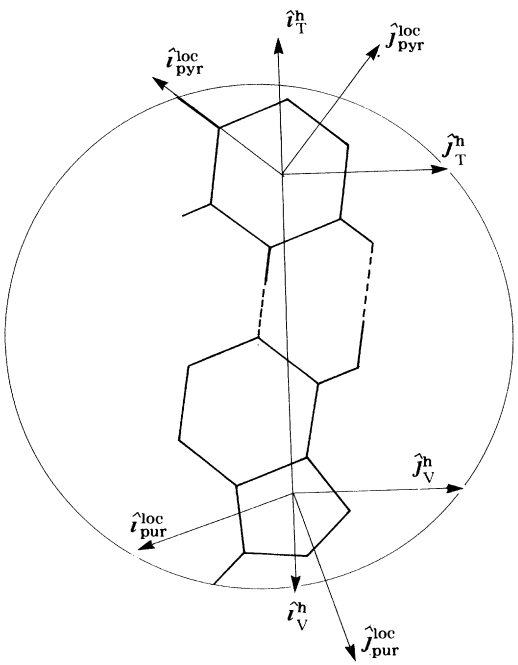

FIGURE A 1.2. The orientation of the local axes.

transformation (A 1.3) is unnecessary if $\beta = 0$, as $\boldsymbol{L}$ is then a simple rotation about $\hat{\boldsymbol{k}}^{\mathrm{loc}}$, leaving the cylindrical polarizability unchanged; in fact β does have a small non-zero value, so the transformation is necessary in B-DNA. However, even for zero β, a transformation is required for the conservative contributions, for which the cylindrical symmetry is broken ($\boldsymbol{B}^{\mathrm{c}}$ has only one component, B^{c}_{11}), and in fact the 'proper' frame (in which $\boldsymbol{B}^{\mathrm{c}}$ is diagonal) is the transition frame $\{\hat{\boldsymbol{\imath}}^{\mathrm{t}}\}$, where $\hat{\boldsymbol{\imath}}^{\mathrm{t}}$ is the direction of the transition moment, defined (figure A 1.3) by its in-plane orientation θ with respect to the local axes:

$$\{\hat{\boldsymbol{\imath}}^{\mathrm{loc}}\} = \boldsymbol{t}\{\hat{\boldsymbol{\imath}}^{\mathrm{t}}\}, \quad \boldsymbol{t} = \boldsymbol{M}^{-1}(\theta). \tag{A 1.6}$$

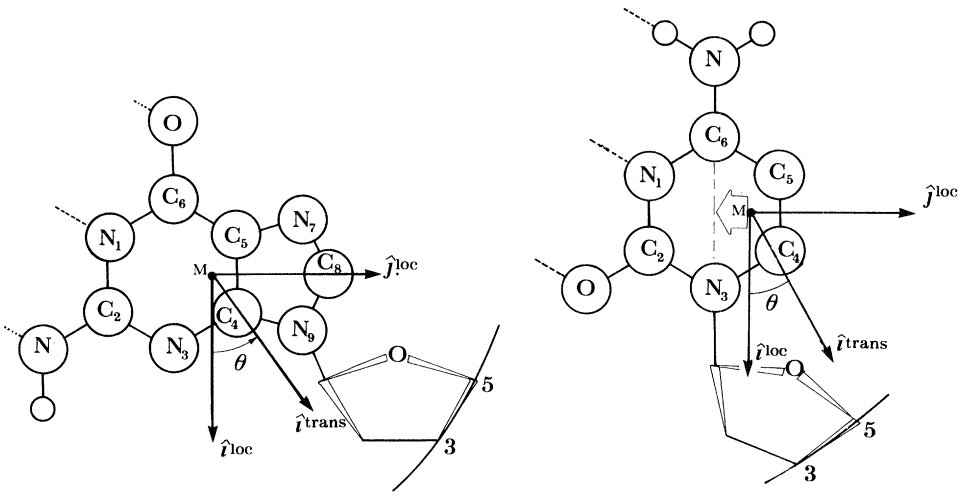

FIGURE A 1.3. The orientation of the transition frame in purine bases (left), and pyrimidine bases (right; arrow indicates position of point transition dipole, M).

The transformation $\boldsymbol{tat}^{-1}$ of course leaves the cylindrical polarizability tensor unchanged, so we can regard $\{\hat{\boldsymbol{\imath}}^{\mathrm{t}}[\phi(n)]\}$ as the proper frame of $\boldsymbol{B}$ in both non-conservative and conservative cases. We evaluate the optical activity in the transition frame $\{\hat{\boldsymbol{\imath}}^{\mathrm{t}}_{\mathrm{T}}[0]\}$ of the zeroth chromophore of the T-helix, and therefore require a matrix $\boldsymbol{P}(0_{\mathrm{T}} \leftarrow n)$ to take the proper frame of the nth group into that of the zeroth group,

$$\{\hat{\boldsymbol{\imath}}^{\mathrm{t}}_{\mathrm{T}}[0]\} = \boldsymbol{P}(0_{\mathrm{T}} \leftarrow n)\,\{\hat{\boldsymbol{\imath}}^{\mathrm{t}}[\phi(n)]\} \tag{A 1.7}$$

and this matrix is used to transform $\{\boldsymbol{B}\}^{\mathrm{t}}_{n}$ (which is just $\boldsymbol{B}$, because $\{\hat{\boldsymbol{\imath}}^{\mathrm{t}}[\phi(n)]\}$ is the proper frame) to its new form $\{\boldsymbol{B}\}^{\mathrm{t}}_{0_{\mathrm{T}}}$ in the new frame $\{\hat{\boldsymbol{\imath}}^{\mathrm{t}}_{\mathrm{T}}[0]\}$:

$$\{\boldsymbol{B}\}^{\mathrm{t}}_{0_{\mathrm{T}}} = \boldsymbol{P}(0_{\mathrm{T}} \leftarrow n)\,\{\boldsymbol{B}\}^{\mathrm{t}}_{n}\,\boldsymbol{P}^{-1}(0_{\mathrm{T}} \leftarrow n). \tag{A 1.8}$$

For interaction with a group n_{T} on the same strand of the double helix, the matrix has the form

$$\boldsymbol{P}(0_{\mathrm{T}} \leftarrow n_{\mathrm{T}}) = \boldsymbol{A}^{-1}\boldsymbol{M}^{-1}(\Delta\phi(0_{\mathrm{T}} \rightarrow n_{\mathrm{T}}))\,\boldsymbol{A}, \tag{A 1.9}$$

where

$$\{\hat{\boldsymbol{\imath}}^{\mathrm{h}}[\phi]\} = \boldsymbol{A}\{\hat{\boldsymbol{\imath}}^{\mathrm{t}}[\phi]\}, \quad \boldsymbol{A} = \boldsymbol{Lt}. \tag{A 1.10}$$

Because the T- and V-helices are identical, this equation applies to both, but as they are anti-parallel, their helix frames are oppositely directed;

$$\{\hat{\boldsymbol{i}}^{\mathrm{h}}_{\mathrm{T}}[\phi]\} = \boldsymbol{S}^{\mathrm{V}}\{\hat{\boldsymbol{i}}^{\mathrm{h}}_{\mathrm{V}}[\phi]\}, \quad \boldsymbol{S}^{\mathrm{V}} = \begin{bmatrix} 1 & 0 & 0 \\ 0 & -1 & 0 \\ 0 & 0 & -1 \end{bmatrix}, \tag{A 1.11}$$

so, for inter-strand interactions, (A 1.9) becomes

$$\boldsymbol{P}(0_{\mathrm{T}} \leftarrow n_{\mathrm{V}}) = \boldsymbol{A}^{-1}\boldsymbol{M}^{-1}(\Delta\phi(0_{\mathrm{T}} \rightarrow n_{\mathrm{V}}))\, \boldsymbol{S}^{\mathrm{V}}\boldsymbol{A}. \tag{A 1.12}$$

Equations (A 1.9) and (A 1.12) can be combined to give

$$\boldsymbol{P}(0_{\mathrm{T}} \leftarrow n) = \boldsymbol{A}^{-1}\boldsymbol{M}^{-1}(\Delta\phi)\, \boldsymbol{S}\boldsymbol{A}, \tag{A 1.13}$$

where

$$\left.\begin{matrix} \boldsymbol{S}^{\mathrm{T}} \\ \\ \boldsymbol{S}^{\mathrm{V}} \end{matrix}\right\} = \begin{bmatrix} 1 & 0 & 0 \\ 0 & \pm 1 & 0 \\ 0 & 0 & \pm 1 \end{bmatrix}. \tag{A 1.14}$$

(*b*) *The superhelix*

For a supercoiled helix, we define a superhelix cylinder on the surface of which the axis of the small helix (called the z direction) itself forms a helix (figure A 1.4). The superhelix axes $\{\hat{\boldsymbol{I}}[\Phi]\}$ are radial, tangential, and longitudinal to the superhelix cylinder at an angle Φ round the superhelix axis. Φ is the angle subtended by the centre ω of the helix cylinder at the centre Ω of the circular cross section of the superhelix cylinder at that point. The helix axes at a point $P(\Phi, \phi)$ on the helix are now written $\{\hat{\boldsymbol{i}}^{\mathrm{h}}[\Phi, \phi]\}$, and P subtends an angle ϕ at ω (the centre of the circular cross-section of the helix cylinder), which subtends an angle Φ at Ω.

The superhelix axes at different superhelical phases are related by

$$\{\hat{\boldsymbol{I}}[\Phi]\} = \boldsymbol{M}(\Phi)\,\{\hat{\boldsymbol{I}}[0]\} \tag{A 1.15}$$

(with $\boldsymbol{M}(\Phi)$ defined in (A 1.2)) and the helix and superhelix axes by

$$\{\hat{\boldsymbol{I}}[\Phi]\} = \boldsymbol{h}\{\hat{\boldsymbol{i}}^{\mathrm{h}}[\Phi, 0]\} \tag{A 1.16}$$

or

$$\{\hat{\boldsymbol{I}}[\Phi]\} = \boldsymbol{h}\boldsymbol{M}^{-1}(\phi)\,\{\hat{\boldsymbol{i}}^{\mathrm{h}}[\Phi, \phi]\}, \tag{A 1.17}$$

where

$$\boldsymbol{h} = \begin{bmatrix} 1 & 0 & 0 \\ 0 & S & C \\ 0 & -C & S \end{bmatrix}, \quad C = \cos\alpha_{\mathrm{sh}}, \quad S = \sin\alpha_{\mathrm{sh}}. \tag{A 1.18}$$

Note that $\boldsymbol{h}$ can only be applied to a triad $\{\hat{\boldsymbol{i}}^{\mathrm{h}}[\Phi, 0]\}$ with zero helical phase ϕ (ϕ being measured from the 'top' of the helix cylinder, i.e. the point farthest from the centre of the superhelix cylinder), so a non-zero helical phase must first be removed with $\boldsymbol{M}^{-1}(\phi)$, as in (A 1.17).

Although $\boldsymbol{M}(\Phi)$ and $\boldsymbol{h}$ are defined above for a right-handed superhelix, left-handed supercoiling is automatically accommodated because both

$$\Phi = \Delta z C/R \tag{A 1.19}$$

and

$$C = \cos\alpha_{\mathrm{sh}} = 2\pi R x/p \tag{A 1.20}$$

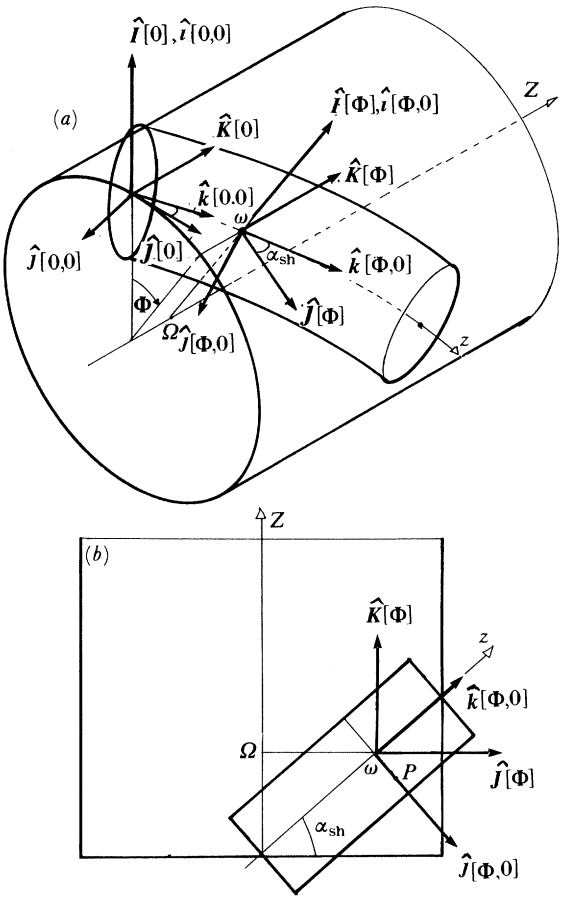

FIGURE A 1.4. Definition of the superhelix axes; the superhelix and helix cylinders seen (*a*) in three dimensions, (*b*) in plan, looking down $\hat{I}[0]$.

change sign for $x < 0$, and we define

$$S = \sin \alpha_{sh} = (1 - C^2)^{\frac{1}{2}}, \tag{A 1.21}$$

taking the positive root.

In the superhelix, therefore, the transformation matrix of (A 1.13) becomes

$$\boldsymbol{P}(0_T^m \leftarrow n) = \boldsymbol{A}^{-1}\boldsymbol{W}^{-1}(0_T^m \rightarrow n)\,\boldsymbol{SA} \tag{A 1.22}$$

where $\boldsymbol{M}(\Delta\phi)$, which takes $\{\hat{\boldsymbol{i}}_T^h[0]\}$ into $\{\hat{\boldsymbol{i}}_T^h[\phi(n)]\}$ in the straight helix, has been replaced by

$$\boldsymbol{W}(0_T^m \rightarrow n) = \boldsymbol{M}(\phi_o + \Delta\phi)\,\boldsymbol{h}^{-1}\boldsymbol{M}(\Phi)\,\boldsymbol{h}\boldsymbol{M}^{-1}(\phi_o), \tag{A 1.23}$$

which takes $\{\hat{\boldsymbol{i}}_T^h[0, \phi_o]\}$ into $\{\hat{\boldsymbol{i}}_T^h[\Phi, \phi_o + \Delta\phi]\}$ (ϕ_o is the phase of the 0_T^m group, given by (20)).

(*c*) *The supersuperhelix*

The supersuperhelix frame $\{\hat{\boldsymbol{I}}'[\Phi']\}$ has axes radial, tangential and longitudinal to the supersuperhelix cylinder at phase Φ'. It is related to the superhelix frame at supersuperhelical phase Φ' and superhelical phase zero by

$$\{\hat{\boldsymbol{I}}'[\Phi']\} = \boldsymbol{H}\{\hat{\boldsymbol{I}}[\Phi', 0]\}, \tag{A 1.24}$$

where

$$\boldsymbol{H} = \begin{bmatrix} 1 & 0 & 0 \\ 0 & S' & C' \\ 0 & -C' & S' \end{bmatrix} \quad \begin{matrix} C' = \cos\alpha_{\mathrm{ssh}} \\ \\ S' = \sin\alpha_{\mathrm{ssh}} \end{matrix} \tag{A 1.25}$$

and α_{ssh} is the supersuperhelix angle. A non-zero superhelical phase must be removed before applying $\boldsymbol{H}$:

$$\{\hat{\boldsymbol{I}}'[\boldsymbol{\Phi}']\} = \boldsymbol{H}\boldsymbol{M}^{-1}(\boldsymbol{\Phi})\,\{\hat{\boldsymbol{I}}[\boldsymbol{\Phi}', \boldsymbol{\Phi}]\}. \tag{A 1.26}$$

In the supersuperhelix, therefore, the matrix

$$\boldsymbol{W}(0_{\mathrm{T}}^{mM} \to n) = \boldsymbol{M}(\phi_{\mathrm{o}} + \Delta\phi)\,\boldsymbol{h}^{-1}\boldsymbol{M}(\boldsymbol{\Phi}_{\mathrm{o}} + \Delta\boldsymbol{\Phi})\,\boldsymbol{H}^{-1}\boldsymbol{M}(\boldsymbol{\Phi}')\,\boldsymbol{H}\boldsymbol{M}(\boldsymbol{\Phi}_{\mathrm{o}})^{-1}\,\boldsymbol{h}\boldsymbol{M}(\phi_{\mathrm{o}})^{-1}, \tag{A 1.27}$$

in the analogue of (A 1.22), takes $\{\hat{\boldsymbol{i}}^{\mathrm{h}}_{\mathrm{T}}[0, \boldsymbol{\Phi}_{\mathrm{o}}, \phi_{\mathrm{o}}]\}$ into $\{\hat{\boldsymbol{i}}^{\mathrm{h}}_{\mathrm{T}}[\boldsymbol{\Phi}', \boldsymbol{\Phi}_{\mathrm{o}} + \Delta\boldsymbol{\Phi}, \phi_{\mathrm{o}} + \Delta\phi]\}$. ($\boldsymbol{\Phi}_{\mathrm{o}}$ is the superhelix phase of the 0_{T}^{mM} group, given by (63).)

Appendix 2. The distance vector

(a) *The helix*

From figure A 2.1, it is clear that the distance vector between chromophores differing in phase by $\Delta\phi$, and in longitudinal displacement by Δz, is

$$\boldsymbol{R} = \hat{\boldsymbol{i}}^{\mathrm{h}}[0]\, r(\cos\Delta\phi - 1) + \hat{\boldsymbol{j}}^{\mathrm{h}}[0]\, r\sin\Delta\phi + \hat{\boldsymbol{k}}^{\mathrm{h}}[0]\,\Delta z, \tag{A 2.1}$$

expressed in the helix frame of the zeroth group.

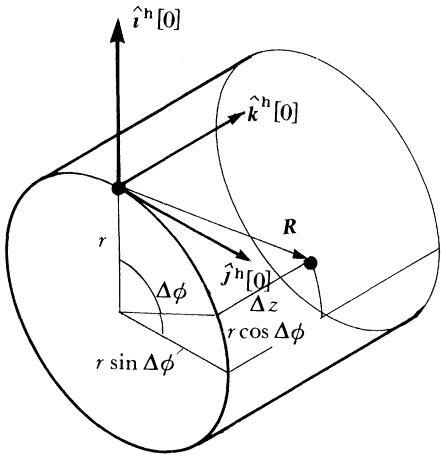

Figure A 2.1. The distance vector in the straight helix.

(b) *The superhelix*

In the superhelix, the distance vector joins points $Q(0, \phi_{\mathrm{o}})$ and $Q'(\boldsymbol{\Phi}, \phi_{\mathrm{o}} + \Delta\phi)$ (figure A 2.2) and is obtained from

$$\omega Q + \boldsymbol{R} = \omega\omega' + \omega' Q'. \tag{A 2.2}$$

Now clearly the vector from the centre ω of the helix to the point Q is

$$\omega Q = \hat{\boldsymbol{i}}^{\mathrm{h}}[0, 0]\, r\cos\phi_{\mathrm{o}} + \hat{\boldsymbol{j}}^{\mathrm{h}}[0, 0]\, r\sin\phi_{\mathrm{o}}, \tag{A 2.3}$$

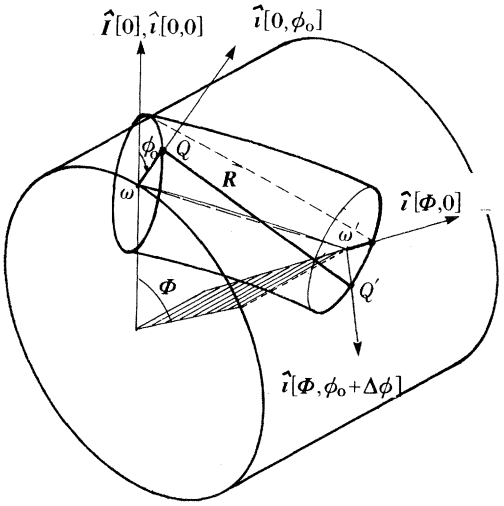

FIGURE A 2.2. The superhelix distance vector. (The broken line depicts the line $\phi = 0$.)

while that between the centres ω and ω' of the helix cylinder at Q and Q' is

$$\omega\omega' = \hat{\boldsymbol{I}}[0]\, R(\cos\Delta\Phi - 1) + \hat{\boldsymbol{J}}[0]\, R \sin\Delta\Phi + \hat{\boldsymbol{K}}[0]\, \Delta z S \tag{A 2.4}$$

by analogy with (A 2.1), and this can be transformed to the $\{\hat{\boldsymbol{i}}^{\mathrm{h}}[0,0]\}$ frame by the matrix $\boldsymbol{h}^{-1}$,

$$\omega\omega' = \hat{\boldsymbol{i}}^{\mathrm{h}}[0,0]\, R(\cos\Delta\Phi - 1) + \hat{\boldsymbol{j}}^{\mathrm{h}}[0,0]\, (RS \sin\Delta\Phi - \Delta z S C) + \hat{\boldsymbol{k}}^{\mathrm{h}}[0,0]\, (RC \sin\Delta\Phi + \Delta z S^2). \tag{A 2.5}$$

Finally,

$$\omega' Q' = \hat{\boldsymbol{i}}^{\mathrm{h}}[\Phi, 0]\, r \cos(\phi_0 + \Delta\phi) + \hat{\boldsymbol{j}}^{\mathrm{h}}[\Phi, 0]\, r \sin(\phi_0 + \Delta\phi), \tag{A 2.6}$$

and this must be transformed into the $\{\hat{\boldsymbol{i}}^{\mathrm{h}}[0,0]\}$ frame, using $\boldsymbol{h}^{-1}\boldsymbol{M}^{-1}(\Delta\Phi)\,\boldsymbol{h}$, before being substituted into (A 2.2), together with (A 2.3) and (A 2.5), to give

$$\begin{aligned}
\boldsymbol{R} = {} & \hat{\boldsymbol{i}}^{\mathrm{h}}[0,0]\, \{R\,[\cos\Delta\Phi - 1] - r\cos\phi_0 + r\cos(\phi_0 + \Delta\phi)\cos\Delta\Phi \\
& \quad - r\sin(\phi_0 + \Delta\phi)\, S \sin\Delta\Phi\} \\
& + \hat{\boldsymbol{j}}^{\mathrm{h}}[0,0]\, \{RS\sin\Delta\Phi - \Delta z S C - r\sin\phi_0 \\
& \quad + r\cos(\phi_0 + \Delta\phi)\, S\sin\Delta\Phi \\
& \quad + r\sin(\phi_0 + \Delta\phi)\, [S^2\cos\Delta\Phi + C^2]\} \\
& + \hat{\boldsymbol{k}}^{\mathrm{h}}[0,0]\, \{RC\sin\Delta\Phi + \Delta z S^2 + r\cos(\phi_0 + \Delta\phi)\, C\sin\Delta\Phi \\
& \quad + r\sin(\phi_0 + \Delta\phi)\, [\cos\Delta\Phi - 1]\, SC\}.
\end{aligned} \tag{A 2.7}$$

This is then transformed, by using $\boldsymbol{A}^{-1}\boldsymbol{M}(\phi_0)$ (39), to the proper frame $\{\hat{\boldsymbol{i}}^{\mathrm{t}}[0, \phi_0]\}$ of the zeroth chromophore, in which we evaluate the optical activity.

(*c*) *The supersuperhelix*

In the supersuperhelix, the distance vector joins points $Q(0, \Phi_0, \phi_0)$ and $Q'(\Phi', \Phi_0 + \Delta\Phi, \phi_0 + \Delta\phi)$ (figure A 2.3) and is obtained from

$$\Omega\omega + \omega Q + \boldsymbol{R} = \Omega\Omega' + \Omega'\omega' + \omega' Q', \tag{A 2.8}$$

PHILOSOPHICAL TRANSACTIONS OF THE ROYAL SOCIETY A MATHEMATICAL, PHYSICAL & ENGINEERING SCIENCES

where

$$\omega Q = \hat{\boldsymbol{i}}^{\mathrm{h}}[0, \Phi_{\mathrm{o}}, 0]\, r \cos\phi_{\mathrm{o}} + \hat{\boldsymbol{j}}^{\mathrm{h}}[0, \Phi_{\mathrm{o}}, 0]\, r \sin\phi_{\mathrm{o}}, \tag{A 2.9}$$

$$\Omega\omega = \hat{\boldsymbol{I}}[0, 0]\, R \cos\Phi_{\mathrm{o}} + \hat{\boldsymbol{J}}[0, 0]\, R \sin\Phi_{\mathrm{o}}, \tag{A 2.10}$$

$$\Omega\Omega' = \hat{\boldsymbol{I}}'[0]\, R'(\cos\Phi' - 1) + \hat{\boldsymbol{J}}'[0]\, R' \sin\Phi' + \hat{\boldsymbol{K}}'[0]\Phi' P'/2\pi, \tag{A 2.11}$$

$$\Omega'\omega' = \hat{\boldsymbol{I}}[\Phi', 0]\, R \cos(\Phi_{\mathrm{o}} + \Delta\Phi) + \hat{\boldsymbol{J}}[\Phi', 0]\, R \sin(\Phi_{\mathrm{o}} + \Delta\Phi), \tag{A 2.12}$$

$$\omega'\Omega' = \hat{\boldsymbol{i}}^{\mathrm{h}}[\Phi', \Phi_{\mathrm{o}} + \Delta\Phi, 0]\, r \cos(\phi_{\mathrm{o}} + \Delta\phi) + \hat{\boldsymbol{j}}^{\mathrm{h}}[\Phi', \Phi_{\mathrm{o}} + \Delta\Phi, 0]\, r \sin(\phi_{\mathrm{o}} + \Delta\phi). \tag{A 2.13}$$

(Ω and Ω' are the centres of the superhelix cylinder at Q and Q'.) Vectors (A 2.10)–(A 2.13) are transformed with the use of appropriate matrices, and substituted into (A 2.8) to give $\boldsymbol{R}$ in the helix frame $\{\hat{\boldsymbol{i}}^{\mathrm{h}}[0, \Phi_{\mathrm{o}}, 0]\}$. This is then transformed to the proper frame $\{\hat{\boldsymbol{i}}^{\mathrm{t}}[0, \Phi_{\mathrm{o}}, \phi_{\mathrm{o}}]$ of the zeroth chromophore.

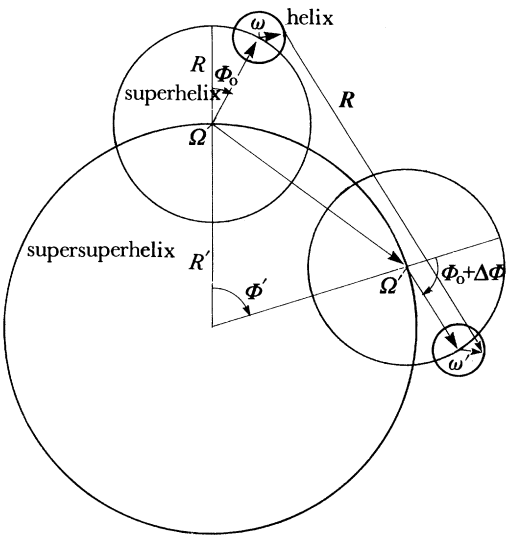

FIGURE A 2.3. The supersuperhelix distance vector (schematic).

APPENDIX 3. METRIC ANALYSIS OF THE SUPERCOILED HELIX CYLINDER

(a) *Derivation of the curved cylinder metric*

For a straight helix, the (flat) metric of the surface of the circumscribed cylinder is

$$\mathrm{d}s^2 = r^2\mathrm{d}\phi^2 + \mathrm{d}z^2, \tag{A 3.1}$$

where z is the displacement measured along the central axis of the helix cylinder, and $\mathrm{d}s$ is the displacement, measured on the surface of the cylinder, produced by coordinate changes $\mathrm{d}\phi$ and $\mathrm{d}z$. The metric coefficients are $g_{\phi\phi} = r^2$, $g_{zz} = 1$.

For the supercoiled helix, the corresponding (curved) metric is

$$\mathrm{d}s^2 = r^2\mathrm{d}\phi^2 + g_{zz}(\phi)\,\mathrm{d}z^2 \tag{A 3.2}$$

where g_{zz} is now ϕ-dependent, being larger on the stretched outside of the cylinder (where displacements along z make a larger contribution to the total distance $\mathrm{d}s$), and smaller on the

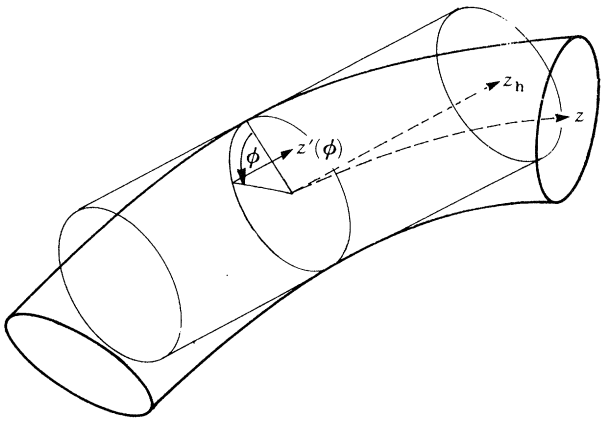

FIGURE A 3.1. The supercoiled helix cylinder, showing the axes z at its centre and $z'(\phi)$ at its surface, and the straight helix cylinder (with axis z_h), whose surface is the tangent flat space to the curved surface of the supercoiled helix cylinder.

compressed underside (where displacements along z make a smaller contribution to ds); the contribution of dϕ to ds is unaffected because the cylinder cross section remains circular and so $g_{\phi\phi} = r^2$ as before.

The curved surface of the bent cylinder can be made to appear (locally) Euclidean by transformation from z to z', which is the *local* longitudinal axis, parallel to z but on the surface of the helix cylinder instead of at its centre (figure A 3.1). The metric of this tangent flat space is

$$\mathrm{d}s^2 = r^2\mathrm{d}\phi^2 + \mathrm{d}z'^2, \tag{A 3.3}$$

which is the same as that of the straight helix cylinder.

A general Riemannian metric $\bar{g}_{\mu\nu}$ is related to the local Euclidean metric $g_{\alpha\beta}$ by

$$\bar{g}_{\mu\nu} = \frac{\partial x^\alpha}{\partial \bar{x}^\mu}\frac{\partial x^\beta}{\partial \bar{x}^\nu} g_{\alpha\beta} \tag{A 3.4}$$

(Atwater 1974), giving in this case (at constant ϕ, for the one-dimensional metric $\mathrm{d}s^2 = g_{zz}\,\mathrm{d}z^2$ and its Euclidean counterpart $\mathrm{d}s^2 = \mathrm{d}z'^2$),

$$g_{zz}(\phi) = \left(\frac{\mathrm{d}z'}{\mathrm{d}z}\right)^2. \tag{A 3.5}$$

The transformation relating z and z' must therefore be found.

Just as the central z-axis of the helix cylinder itself forms a helix on the surface of the superhelix cylinder (radius R, angular coordinate $\boldsymbol{\Phi}$, central axis Z), so the local z' axis, at a given ϕ, also forms a helix but on a different (co-axial) cylinder of radius Q, angular coordinate $\boldsymbol{\Psi}$ (figure A 3.2). This z' cylinder has

$$\mathrm{d}z'^2 = Q^2\mathrm{d}\boldsymbol{\Psi}^2 + \mathrm{d}Z^2, \tag{A 3.6}$$

where all differentials are evaluated at constant ϕ.

The radius vector of a point $P(\boldsymbol{\Phi}, \phi)$ with respect to the centre W of the z' cylinder (figure A 3.2) is clearly

$$\boldsymbol{Q} = (R + r\cos\phi)\,\hat{\boldsymbol{I}}[\boldsymbol{\Phi}] + rS\sin\phi\,\hat{\boldsymbol{J}}[\boldsymbol{\Phi}], \tag{A 3.7}$$

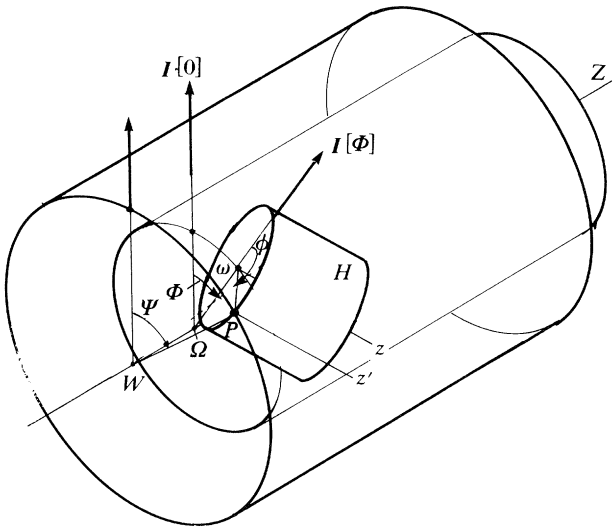

FIGURE A 3.2. The superhelix cylinder (angular coordinate Φ) on which the helix axis z forms a helix, and the larger, co-axial, cylinder (angular coordinate Ψ) on which z' forms a helix.

so the magnitude of the radius is

$$Q = [(R+r\cos\phi)^2+(rS\sin\phi)^2]^{\frac{1}{2}}. \tag{A 3.8}$$

The coordinates of $P(\Phi,\phi)$ on the z' cylinder are seen to be

$$Z = zS-rC\sin\phi, \tag{A 3.9}$$

$$\Psi = \Phi+\cos^{-1}[\hat{\boldsymbol{I}}(\Phi)\cdot\boldsymbol{Q}/Q] = \Phi+\cos^{-1}[(R+r\cos\phi)/Q]. \tag{A 3.10}$$

But at constant ϕ

$$\mathrm{d}Z = S\mathrm{d}z, \quad \mathrm{d}\Psi = \mathrm{d}\Phi = (C/R)\,\mathrm{d}z, \tag{A 3.11}$$

so, from (A 3.6),

$$\mathrm{d}z'^2 = \mathrm{d}z^2\{(QC/R)^2+S^2\}, \tag{A 3.12}$$

and from (A 3.5)

$$\begin{aligned} g_{zz} &= (QC/R)^2+S^2 \\ &= 1+2(r/R)\,C^2\cos\phi+(r/R)^2\,C^2(\cos^2\phi+S^2\sin^2\phi). \end{aligned} \tag{A 3.13}$$

This gives, to first order in r/R, the metric

$$\mathrm{d}s^2 = r^2\,\mathrm{d}\phi^2+[1+2(r/R)\,C^2\cos\phi]\,\mathrm{d}z^2 \tag{A 3.14}$$

for the surface of the supercoiled helix cylinder. The helix follows a straight path on the surface of the cylinder, and for a straight helix this path is defined by the constancy of the helix angle,

$$\tan\alpha_{\mathrm{h}} = \mathrm{d}z/r\mathrm{d}\phi = p/2\pi r. \tag{A 3.15}$$

In the supercoiled helix the local helix angle

$$\tan\alpha_{\mathrm{h}}^{\mathrm{loc}} = g_{zz}^{\frac{1}{2}}\,\mathrm{d}z/r\mathrm{d}\phi = [1+2(r/R)\,C^2\cos\phi]^{\frac{1}{2}}\tan\alpha_{\mathrm{h}}, \tag{A 3.16}$$

varies with ϕ, being larger on the stretched outside of the cylinder, and smaller on the compressed inside. This is because of the curvature of the cylinder, which we now calculate.

(b) The Riemann curvature of the supercoiled helix cylinder

The Riemann curvature tensor is defined (Atwater 1974) by

$$R^{\mu}_{\rho\sigma\lambda} = \{^{\mu}_{\nu\sigma}\}\{^{\nu}_{\rho\lambda}\} - \{^{\mu}_{\nu\lambda}\}\{^{\nu}_{\rho\sigma}\} + \partial_{\sigma}\{^{\mu}_{\rho\lambda}\} - \partial_{\lambda}\{^{\mu}_{\rho\sigma}\}, \tag{A 3.17}$$

where

$$\{^{\alpha}_{\beta\gamma}\} = \tfrac{1}{2}g^{\alpha\nu}\,(g_{\beta\nu,\gamma} + g_{\nu\gamma,\beta} - g_{\beta\gamma,\nu}); \tag{A 3.18}$$

these are the Christoffel symbols. It can be contracted to give the Ricci tensor

$$R_{\alpha\beta} = -R^{\lambda}_{\alpha\beta\lambda} = R^{\lambda}_{\alpha\lambda\beta} \tag{A 3.19}$$

(sign convention as in Misner *et al.* 1973) and the Riemann curvature scalar

$$R^{\mathrm{curv}} = g^{\alpha\beta}R_{\alpha\beta}. \tag{A 3.20}$$

In this case we have

$$g_{\mu\nu} = \begin{bmatrix} r^2 & 0 \\ 0 & [1+2(r/R)\,C^2\cos\phi] \end{bmatrix}, \quad g^{\mu\nu} = \begin{bmatrix} 1/r^2 & 0 \\ 0 & [1+2(r/R)\,C^2\cos\phi]^{-1} \end{bmatrix} \tag{A 3.21}$$

so the only non-zero Christoffel symbol is

$$\begin{Bmatrix} z \\ z\phi \end{Bmatrix} = \tfrac{1}{2}g^{zz}g_{zz,\phi} = -(r/R)\,C^2\sin\phi\,[1+2(r/R)\,C^2\cos\phi]^{-1} \tag{A 3.22}$$

and the Riemann curvature scalar is therefore

$$R^{\mathrm{curv}}(\phi) = (C^2/rR)\cos\phi\,[1+2(r/R)\,C^2\cos\phi]^{-1}, \tag{A 3.23}$$

to first-order in (r/R).

The curvature is positive on the stretched outside ($|\phi| < \frac{1}{2}\pi$), negative on the compressed underside ($\frac{1}{2}\pi < |\phi| < \pi$) that forms a saddle-point at $\phi = 180°$, and zero at $|\phi| = \frac{1}{2}\pi$, where the cylinder is Euclidean; also, it is stronger on the underside ($\cos\phi < 0$), and is independent of the superhelix handedness ($C = \cos\alpha_{\mathrm{sh}}$ is proportional to x, but appears squared).

Appendix 4. Variation of DNA c.d. with secondary structure and transition moment orientation

Because the optical activity (and its variation with superhelix density) is dependent, in the exciton model, on the orientation of the transition dipoles as well as on the helicity of the DNA helix, and because we invoke a change in secondary structure to explain the c.d. of supercoiled DNA, it is important to understand the physical reasons for the variation of c.d. with secondary structure.

The most widely discussed secondary structures are of course the A- and B-forms. The difference between the conservative B spectrum and the non-conservative A spectrum was originally attributed, by Johnson & Tinoco (1969) and others (Tinoco 1962; Fasman & Cowman 1978), to strong base tilting in the A-form, but Moore & Wagner (1973) showed that the major factor is actually the displacement, D, of the base-pair from the helix axis, which is very different in the two forms (figures A 4.1*a*, *b*). We believe, however, that this is better expressed in terms of the inter-helix phase difference, ϕ_{bp}, which determines D, and is related

to the orientation Θ of the average transition moment $\hat{\boldsymbol{i}}^{\mathrm{t}}$ with respect to $\hat{\boldsymbol{i}}^{\mathrm{h}}$ (figure A 4.1*c*); consideration of ϕ_{bp} and Θ greatly facilitates physical explanation of the trends noted by Moore and Wagner. Moreover, these authors do not show the conservative and non-conservative contributions separately, although this is important here because of their very different variation with superhelix density (table 3).

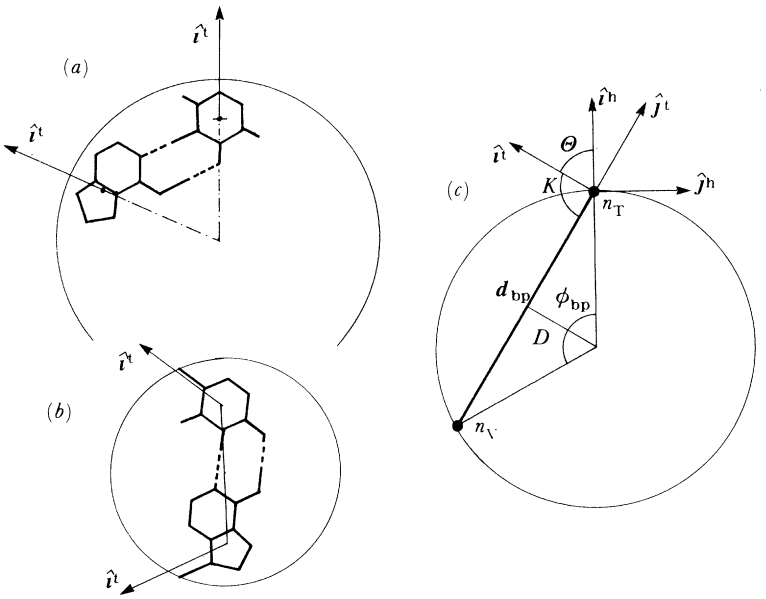

FIGURE A 4.1. (*a*) Cross section of A-DNA. (*b*) Cross section of B-DNA. (*c*) The base orientation Θ, and the inter-strand phase difference ϕ_{bp}.

Figure A 4.2 shows the computed conservative and non-conservative contributions (thin lines) to the total spectrum (thick line) for various secondary structures. (The spectra extend to three standard deviations w on either side of the absorption wavelength (see 12)), which corresponds to the 210–310 nm region around the 260 nm absorption. C.d. units are arbitrary, serving only to indicate relative magnitudes and shapes.) The vertical axis shows c.d. spectra as a function of Θ for 'planar' forms (zero Euler angle β), in which

$$\Theta = \alpha + \gamma + \theta. \tag{A 4.1}$$

The line $\boldsymbol{d}_{\mathrm{bp}}$ joining the paired bases n_{T} and n_{V} is clearly at a fixed angle to the local axis $\hat{\boldsymbol{i}}^{\mathrm{loc}}$, regardless of the orientation of the base-pair. The angle θ between the transition moment, $\hat{\boldsymbol{i}}^{\mathrm{t}}$, and $\hat{\boldsymbol{i}}^{\mathrm{loc}}$, is fixed by the percentage of A–T, so the angle K between $\hat{\boldsymbol{i}}^{\mathrm{t}}$ and $\boldsymbol{d}_{\mathrm{bp}}$ (figure A 4.1*c*) is also constant for all Θ at a given base composition, and can be shown (MacDermott 1981) from atomic coordinates (Arnott *et al.* 1969) to be 113.6° for 50% A–T ($\theta = -4.08°$). The phase difference and radius for a given transition moment orientation Θ are then obtained from

$$|\phi_{\mathrm{bp}}| = 2(K - 90° + |\Theta|) \tag{A 4.2}$$

$$r = \mathrm{d}_{\mathrm{bp}}/2 \sin(\tfrac{1}{2}|\phi_{\mathrm{bp}}|) \tag{A 4.3}$$

(in DNA the V-helix lags behind the T-helix, so Θ and ϕ_{bp} are always negative). Figure A 4.2 also shows the c.d. as a function of β at constant Θ for the Θ values characteristic of A- and B-DNA.

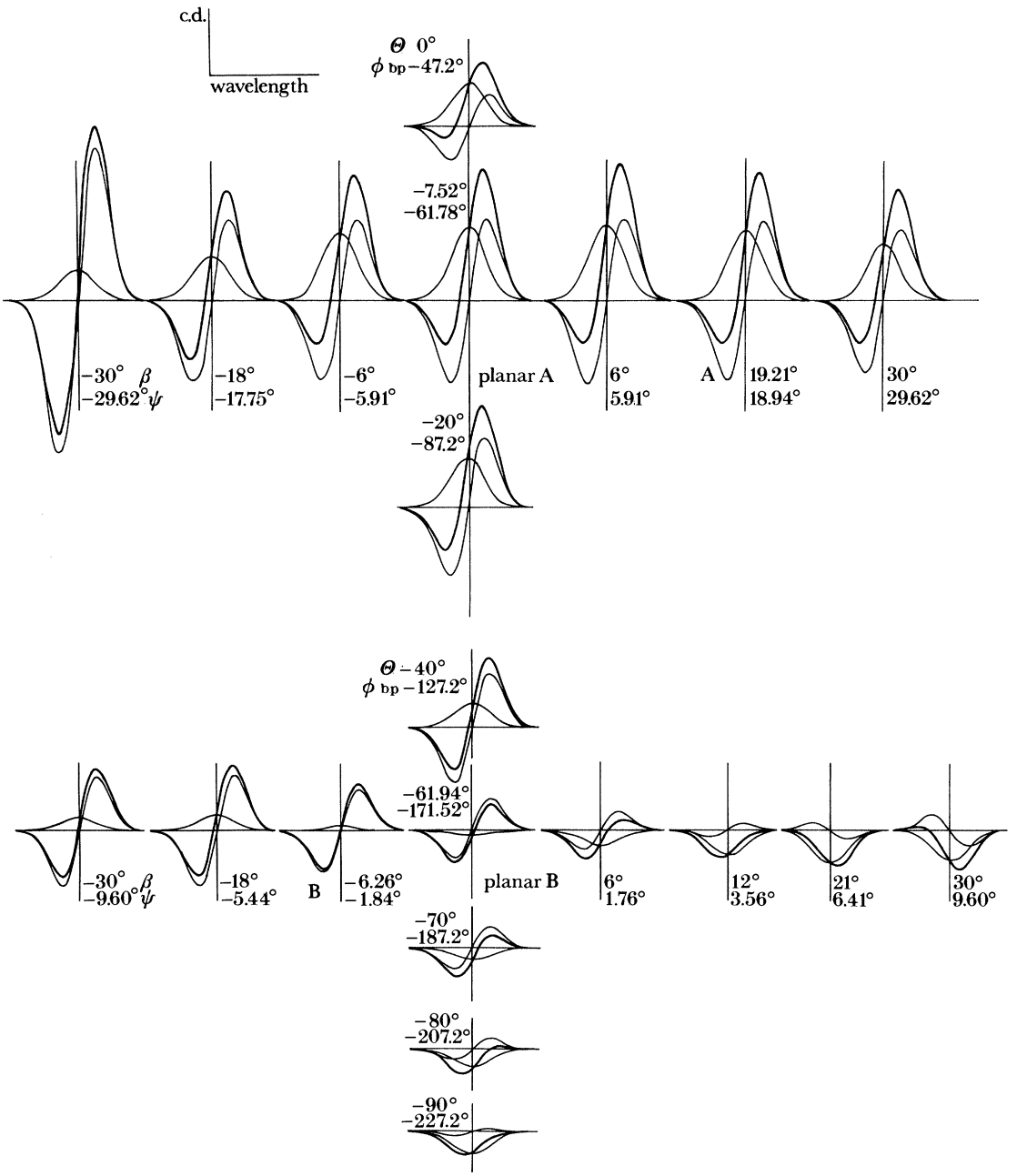

FIGURE A 4.2. Calculated c.d. spectra as a function of in-plane base orientation Θ, and out-of-plane tilt ψ.

(*a*) *The role of in-plane orientation,* Θ, *and inter-helix phase difference* ϕ_{bp}

Three main features are apparent in figure A 4.2.

First, spectra at small $|\Theta|$ (A-like structures) not only show a larger non-conservative component, but are also generally stronger than at larger $|\Theta|$ (B-like structures). This is because in B-DNA the c.d. from interaction with group 2 enhances the effect of interaction with group 1, but is cancelled by that from groups 3 and 4, giving an overall c.d. that reflects mainly interaction with group 1; but in A-DNA, the contributions from $n = 3$ and 4 augment those

from $n = 1$ and 2, resulting in a much larger overall c.d. The explanation (MacDermott 1981) is that the component R_2^t of the distance vector in the transition frame (and hence the helicity of the interaction) changes sign after $n = 2$ for large $|\Theta|$, but not until after $n = 4$ for smaller $|\Theta|$.

Second, B-DNA has only a very small non-conservative component. Table A 4.1 shows that this is because of near-cancellation of the (actually quite sizeable) intrastrand (TT) and interstrand (TV) contributions at this particular ϕ_{bp}. Their signs are the same for lower $|\phi_{bp}|$ (A-like forms) but opposed for larger $|\phi_{bp}|$. Thus, for A-DNA ($\Theta = -7.52°$, $\phi_{bp} = -61.78°$), exciton jump from 0_T to groups n_V and n_T will usually have the same helicity because the phase difference of these groups is small. In B-DNA, however ($\Theta = -61.94°$, $\phi_{bp} = -171.52°$), the near 180° phase difference of n_V and n_T leads to interactions of opposite helicity, and hence the observed TT–TV cancellation for non-conservative interactions (MacDermott 1981). Also, it is only when $\phi_{bp} \approx 180°$ that the TT and TV contributions are even comparable in magnitude; TV interactions are generally much smaller than TT interactions. This is because the phase lag of the V-helix means that TV interactions tend to have less helicity (MacDermott 1981). Thus, for the leading interactions (with $n = 1$ and 2) one finds, for most values of $|\phi_{bp}|$, a rather small $0_T \rightarrow n_V$ phase separation, so that the path of exciton jump is almost directly forward, with little helicity; similarly, the $0_T \rightarrow -n_V$ phase separation is too large for a significant chiral effect; but the $0_T \rightarrow \pm 1_T$ and $0_T \rightarrow \pm 2_T$ phase separations give exciton jumps with helicity angles near the optimum (for high chiral effects) of 45°. Only when $\phi_{bp} \approx 180°$ do the $0_T \rightarrow n_T$ and $0_T \rightarrow n_V$ phase differences become similar in magnitude, producing TT and TV interactions of comparable chirality.

The third feature is that the non-conservative contribution is positive at small $|\Theta|$, and negative at very large $|\Theta|$, apparently undergoing a sign change near the region of B-like forms. This can be accounted for (MacDermott 1981) by the dominant TT interactions, in particular the differing interactions with the $+n_T$ and $-n_T$ groups. The conservative c.d. arises from interactions between the same transition $\boldsymbol{\mu}_{oa}$ on different bases, so the cylindrical symmetry of the helix ensures that transition dipoles on the $+n_T$ and $-n_T$ groups have an identical relationship with the dipole on the 0_T group, and so make equal contributions to the c.d. The non-conservative c.d. arises from interactions between $\boldsymbol{\mu}_{oa}$ on group 0_T and many different transitions $\boldsymbol{\mu}_{ob}$, constituting overall a cylindrical polarizability, on another chromophore. If $\boldsymbol{\mu}_{oa}$ is radial ($\Theta = 0$), it bears the same relationship to the polarizability cylinders on $+n_T$ and $-n_T$, so these give equal contributions to the c.d. But for small, non-zero $|\Theta|$, this symmetry between $+n_T$ and $-n_T$ is broken, so that their c.d. contributions become slightly different. This

Table A 4.1. Intrastrand (TT) and interstrand (TV) contributions to the c.d. of A- and B-DNA

		$\sum_n \Omega_1(0_T \rightarrow n)$ (conservative)	$F^{nc} \sum_n \Omega_3(0_T \rightarrow n)$ (non-conservative)
A	TT	−0.4747	0.2757
	TV	−0.2901	0.1335
	total	−0.7648	0.4092
B	TT	−0.2865	−0.0791
	TV	−0.1252	0.1079
	total	−0.4117	0.0288

difference increases with $|\Theta|$, until, at $|\Theta| = 45°$, $\boldsymbol{\mu}_{oa}$ again has a symmetrical relationship with the two polarizability cylinders, this time producing equal and opposite c.d. contributions from $+n_T$ and $-n_T$ (because the distance vector component $R_1^t(n)$ of the $+n_T$ group is equal to the component $R_2^t(-n)$ of the $-n_T$ group, and also $R_2^t(n) = R_1^t(-n)$). The non-conservative (TT) c.d. is therefore zero at $|\Theta| = 45°$, and becomes negative as $|\Theta|$ is increased further.

It is clear that most base orientations give a non-conservative c.d. spectrum, and that the conservative c.d. of B-DNA is the result of rather unusual geometric circumstances. The medium value of Θ makes the non-conservative TT contribution unusually small because of near-cancellation between $+n_T$ and $-n_T$, and the near 180° phase difference ϕ_{bp} not only gives the TT and TV interactions opposite sign, but also makes them closer in magnitude than usual, producing very effective cancellation. Finally, the value of Θ is also responsible (through cancellation of contributions from groups in the first and second quadrants) for the relatively small magnitude of the conservative contribution that remains after near-cancellation of the non-conservative part. In A-DNA by contrast, the much smaller Θ means that the non-conservative TT interactions are larger (because of reinforcement of first and second quadrant contributions), and augmented (because of the concomitant small ϕ_{bp}), rather than cancelled, by the TV interactions, thus producing a large non-conservative spectrum.

(*b*) *The role of out-of-plane tipping: twisting against tilting*

Figure A 4.2 shows the c.d. of A- and B-family DNA as a function of the Euler angle, β, between the base-normal $\hat{\boldsymbol{k}}^{loc}$ and the helix axis $\hat{\boldsymbol{k}}^{h}$, which we term the tip angle. The tipping of $\hat{\boldsymbol{k}}^{loc}$ away from $\hat{\boldsymbol{k}}^{h}$ can be partitioned into tilting (ψ) and twisting (τ), such that the component of $\hat{\boldsymbol{k}}^{loc}$ along $\hat{\boldsymbol{k}}^{h}$ is given by

$$\cos\beta = \cos\psi\,\cos\tau \tag{A 4.4}$$

where (MacDermott 1981)

$$\psi = \arccos\{\cos\beta\,[\cos^2\beta + \sin^2\beta\,\sin^2(\alpha - \tfrac{1}{2}\phi_{bp})]^{-\frac{1}{2}}\} \tag{A 4.5}$$

$$\tau = \arccos[\cos^2\beta + \sin^2\beta\,\sin^2(\alpha - \tfrac{1}{2}\phi_{bp})]^{\frac{1}{2}}. \tag{A 4.6}$$

Tilt and twist are very different properties, corresponding to rotation about mutually perpendicular axes. This is illustrated in figure A 4.3*a*, which shows the planar form, in which the line $\boldsymbol{d}_{bp}$ joining paired bases on the T- and V-helices is in a plane perpendicular to the helix axis, as are the aromatic ring planes of the bases themselves. Tilting (ψ) is a rotation of $\boldsymbol{d}_{bp}$ out of this plane, so that $\boldsymbol{d}_{bp}$ is no longer perpendicular to the helix axis (and $\hat{\boldsymbol{k}}^{loc}$ is no longer coincident with $\hat{\boldsymbol{k}}^{h}$, although it remains in the $\hat{\boldsymbol{k}}^{h}/\boldsymbol{d}_{bp}$ plane if no twist is present) (see also figure 2). Twisting (τ), however, is simply a rotation of the aromatic ring planes about $\boldsymbol{d}_{bp}$, which itself remains in the plane perpendicular to the helix axis (in the absence of tilt), although the aromatic rings move out of this plane ($\hat{\boldsymbol{k}}^{loc}$ moves out of the $\hat{\boldsymbol{k}}^{h}/\boldsymbol{d}_{bp}$ plane).

The sign convention for ψ and τ has led to much confusion. We regard ψ or τ as negative if it makes β more negative (for $\beta < 0$, $\hat{\boldsymbol{k}}^{loc}$ tips into the helix cylinder), and as positive if it makes β more positive (for $\beta > 0$, $\hat{\boldsymbol{k}}^{loc}$ tips out of the helix cylinder). The negative ψ for B-DNA is illustrated in figure 2 ($\hat{\boldsymbol{k}}^{loc}$ is not shown, but it is perpendicular to $\boldsymbol{d}_{bp}$ in a direction determined by τ). In figure A 4.2, therefore, we have taken both ψ and τ as negative for negative β, and positive for positive β (although it would, of course, be possible for ψ and τ to have opposite signs if they affected β in opposite directions).

PHILOSOPHICAL TRANSACTIONS OF THE ROYAL SOCIETY A MATHEMATICAL, PHYSICAL & ENGINEERING SCIENCES

Our sign convention is the same as that of Arnott (1970), Arnott & Selsing (1975) and Studdert & Davis (1974), but is opposite to that of Moore & Wagner (1973) and Johnson *et al.* (1981), the latter authors having apparently taken data from Arnott & Selsing (1975) but changed the sign. We consider that our convention is the least confusing because the signs of ψ and τ follow that of the Euler angle β which is unambiguously fixed ($\beta > 0$ if $\hat{\boldsymbol{k}}$ moves towards $\hat{\boldsymbol{\imath}}$).

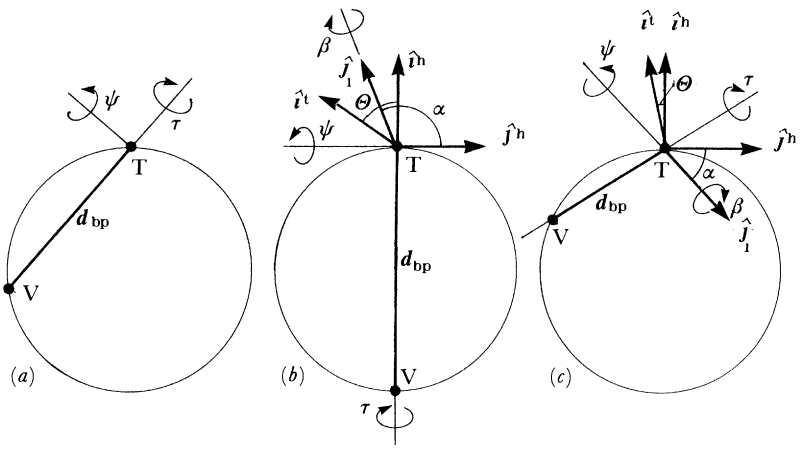

FIGURE A 4.3. Partition of β between ψ and τ; (*a*) ψ and τ correspond to rotations about perpendicular axes, (*b*) β is a ψ-type rotation in B-DNA, (*c*) β is a τ-type rotation in A-DNA.

The Euler angle β is a rotation about $\hat{\boldsymbol{\jmath}}_1$, which is the $\hat{\boldsymbol{\jmath}}^{\mathrm{h}}$ axis rotated through the Euler angle α about $\hat{\boldsymbol{k}}^{\mathrm{h}}$, so that partition of β into ψ and τ depends on whether $\hat{\boldsymbol{\jmath}}_1$ is more nearly perpendicular or parallel to $\boldsymbol{d}_{\mathrm{bp}}$, which in turn depends on the values of α and ϕ_{bp}. This explains the crucial role of $\alpha - \frac{1}{2}\phi_{\mathrm{bp}}$ in (A 4.5) and (A 4.6). We see from figures A 4.3*b*,*c* that the values of α and $\frac{1}{2}\phi_{\mathrm{bp}}$ are such that, for B-DNA, rotation about $\hat{\boldsymbol{\jmath}}_1$ is a τ-type rotation ($\hat{\boldsymbol{\jmath}}_1$ being almost parallel to $\boldsymbol{d}_{\mathrm{bp}}$) while for A-DNA, this rotation is of ψ-type ($\hat{\boldsymbol{\jmath}}_1$ being almost perpendicular to $\boldsymbol{d}_{\mathrm{bp}}$). In quantitative terms, for A-DNA ($\alpha = 49.14°$, $\frac{1}{2}\phi_{\mathrm{bp}} = -30.89°$) we have $(\alpha - \frac{1}{2}\phi_{\mathrm{bp}}) \approx 90°$, i.e. $\tau \approx 0$ (from (A 4.6)); so $\beta \approx \psi$ (from (A 4.4) or (A 4.5)). For B-DNA ($\alpha = -102.89°$, $\frac{1}{2}\phi_{\mathrm{bp}} = -89.76°$) we have $(\alpha - \frac{1}{2}\phi_{\mathrm{bp}}) \approx 0$ (actually 16°), so ψ is very small and $\beta \approx \tau$.

The strong β-sensitivity of the B-family c.d. in figure A 4.2 is thus a sensitivity to changes in τ, while the β-insensitivity of the A-family c.d. indicates that ψ has almost no effect on DNA c.d. (Note that the spectra of 'real' and 'planar' A-DNA are almost identical, despite the huge tilt, $\psi = 19.21°$, of the former). The much stronger influence of twisting is in agreement with the conclusion of Johnson *et al.* (1981) (although their results indicate a depressed c.d. for negative instead of positive τ owing to their opposite sign convention), but in disagreement with Studdert & Davis (1974), who suggest that tilting is more important. However, consideration of the geometry of the Watson–Crick base-pair shows beyond doubt that twisting has more affect. The c.d. is determined by the orientation of the transition dipoles, i.e. by the direction of $\hat{\boldsymbol{\imath}}^{\mathrm{t}}$, which is at a fixed angle K to $\boldsymbol{d}_{\mathrm{bp}}$ in a Watson–Crick base-pair (figure A 4.1*c*). If $\hat{\boldsymbol{\imath}}^{\mathrm{t}}$ were parallel to $\boldsymbol{d}_{\mathrm{bp}}$, its direction would not be affected at all by a τ-type rotation about $\boldsymbol{d}_{\mathrm{bp}}$, but would be affected dramatically by the perpendicular ψ-type rotation. Similarly, if $\hat{\boldsymbol{\imath}}^{\mathrm{t}}$

were perpendicular to $\boldsymbol{d}_{\mathrm{bp}}$, it would be affected only by τ-type rotations. Because $K = 113.6°$, $\hat{\boldsymbol{\imath}}^{\mathrm{t}}$ is nearly perpendicular to $\boldsymbol{d}_{\mathrm{bp}}$, and so its direction is altered very much more by τ-type than by ψ-type rotations (figure A 4.4), this being equally true at all values of ϕ_{bp}.

With increasing τ, the transition dipoles on the T- and V-helices point in increasingly opposite directions, thereby affecting the balance between the TT and TV interactions. At small or zero τ, the non-conservative TT and TV interactions in B-DNA cancel, but at large τ of either sign,

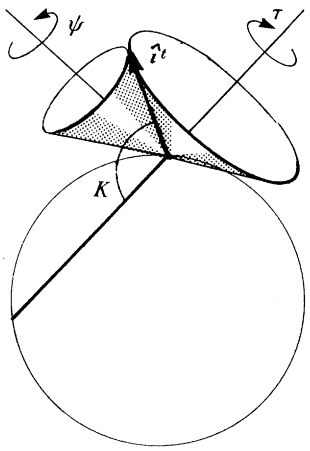

FIGURE A 4.4. The transition moment direction (and hence the c.d.) is more affected by τ than by ψ because it processes through a much wider cone as τ is varied.

they no longer do so, thus giving rise to a much larger non-conservative contribution. But the overall effect (figure A 4.2) is for the c.d. of B-DNA to remain conservative at negative τ, while becoming strongly non-conservative at positive τ. This is explained by the dominant conservative TT interactions. For negative τ, the transition dipole on the 0_{T} group tips forward towards the other T dipoles, producing a large conservative TT interaction; for positive τ, the dipoles tip backward, away from the other T dipoles, so that the conservative contribution gets smaller (eventually going through a sign change), thus allowing the non-conservative part to become dominant.

(*c*) *The effect of supercoiling on different secondary structures*

Table A 4.2 shows the variation in $\Delta\epsilon(x)/\Delta\epsilon(0)$ with negative superhelix density (similar variations, but in the opposite direction, occur for positive x) for some of the secondary structures whose c.d. at zero superhelix density appears in figure A 4.2. The x-dependence follows a more conservative pattern (increased c.d. for left supercoiling, see table 3) or a more non-conservative pattern (slight increase, followed by large decrease in c.d. for left supercoiling) according to whether the spectrum of the non-supercoiled form (A 4.2) is conservative (as for large $|\boldsymbol{\Theta}|$ and $|\phi_{\mathrm{bp}}|$) or non-conservative (small $|\boldsymbol{\Theta}|$ and $|\phi_{\mathrm{bp}}|$).

The amplitude of variation appears greater for large $|\boldsymbol{\Theta}|$ and for positive β. But the ratio $\Delta\epsilon(x)/\Delta\epsilon(0)$ is perhaps misleading in this respect, because in the B-family (table A 4.2*b*) the actual numerical variations in c.d. are roughly the same for all β (maximum increase in conservative component *ca.* 0.04, maximum decrease in non-conservative component *ca.* 0.013).

TABLE A 4.2 (*a*). $\Delta\epsilon(x)/\Delta\epsilon(0)$ AS A FUNCTION OF x FOR STRUCTURES WITH $\beta = 0$ AND VARYING Θ

	x	−0.1337	−0.12	−0.10	−0.08	−0.06	−0.04	−0.02
planar A	$\Theta = -7.52°$	1.006	0.993	0.986	0.995	1.006	1.010	1.007
	$\Theta = -20°$	1.001	0.982	0.974	0.985	0.997	1.003	1.004
	$\Theta = -40°$	0.995	0.985	0.983	0.999	1.014	1.018	1.012
planar B	$\Theta = -62°$	1.007	1.068	1.097	1.133	1.144	1.121	1.068
	$\Theta = -70°$	1.026	1.180	1.247	1.307	1.312	1.252	1.139

TABLE A 4.2 (*b*). $\Delta\epsilon(x)/\Delta\epsilon(0)$ AS A FUNCTION OF x FOR B-LIKE STRUCTURES ($\Theta = -62°$) WITH VARYING β

	x	−0.1337	−0.12	−0.10	−0.08	−0.06	−0.04	−0.02
standard B	$\beta = -6.21°$	0.996	1.028	1.046	1.072	1.082	1.076	1.040
planar B	$\beta = 0°$	1.007	1.068	1.097	1.133	1.144	1.121	1.068
	$\beta = +6°$	1.042	1.120	1.260	1.330	1.343	1.279	1.154

This is because the c.d. changes arise from chiral torsion of the helix frame and changes in the distance vector, which are independent of dipole orientation and depend only on superhelix density; these changes are proportionately large if the original c.d. is small (as for positive β or large $|\Theta|$), leading to a large variation in $\Delta\epsilon(x)/\Delta\epsilon(0)$. In the case of large $|\Theta|$, however, an additional effect operates; larger $|\Theta|$ and $|\phi_{bp}|$ imply a smaller helix radius r (see (A 4.3)), which implies stronger Riemann curvature (see (A 3.21)) and hence greater distortion on supercoiling. Thus the maximum change in conservative c.d. is 0.04 for B-like forms ($r = 325$ pm), but only 0.01 for A-like forms, which are less distorted by supercoiling because of their larger radius ($r = 595$ pm).

The c.d. spectrum of chromatin, with its depressed positive lobe, which in §5 we attributed to increased base-tipping, clearly has considerable non-conservative character; it might therefore be thought that the computed variation with negative superhelix density in the curvature-induced base-tipping model (equation (60) and figure 9: an increase at small x, followed by a large decrease at large x) represents the typical non-conservative pattern. However, the sharp decrease at large x does not represent the effect of supercoiling on the increasing non-conservative element in the altered secondary structure: the decrease reflects mainly the altered secondary structure itself (as β becomes positive, the dipoles tip backwards, away from their T neighbours, giving a smaller c.d.).

(*d*) *Varying transition moment orientation within a given secondary structure*

Throughout this work we have taken the angle between $\hat{\boldsymbol{i}}^{t}$ and $\hat{\boldsymbol{i}}^{loc}$ to be $\theta = -4.08°$, calculated for the 'average base' at 50% A–T by using one transition on A, T, G and C in the 260–280 nm region (table 1). If more transitions were included in the averaging process, a different θ would be obtained, so in this section we examine the x-dependence of the c.d. of B-DNA at varying θ.

We saw in §4 (*c*) that the x-dependence of $\Delta\epsilon(x)/\Delta\epsilon(0)$ depends on the c.d. at $x = 0$: it follows a conservative (increased c.d. for left supercoiling) or non-conservative (slight increase followed by large decrease for left supercoiling) pattern according to whether the original c.d. is predominantly conservative or non-conservative, and the amplitude of variation appears

proportionately larger if the original c.d. is smaller. Further, we saw in §4(*a*) that the c.d. at $x = 0$ is determined by Θ (small $|\Theta|$ means large c.d. because of intra-turn augmentation rather than cancellation), ϕ_{bp} (spectrum conservative near $\phi_{bp} = 180°$, because of non-conservative TT–TV cancellation) and r (small r means large distortion on supercoiling). Variation of θ within a B structure corresponds to variation of Θ at constant ϕ_{bp} and r, so one expects the $x = 0$ c.d. spectra for different θ to follow a similar trend to that for varying Θ in figure A 4.2, except that they should deviate less from the B-type spectrum since only Θ, and not ϕ_{bp} or r, is changed. Thus, planar B-DNA ($\Theta = -61.94°$, $\phi_{bp} = -171.52°$, $\beta = 0$) with $\theta = -4.08°$ has conservative and non-conservative contributions $O^c = -0.30$, $O^{nc} = -0.03$, which for planar A-DNA ($\Theta = -7.52°$, $\phi_{bp} = -61.78°$, $\beta = 0$, $\theta = -4.08°$) change to $O^c = -0.58$, $O^{nc} = 0.32$. But for planar B-DNA with $\theta = +50.34°$, corresponding to the A-like $\Theta = -7.52°$ (but still with $\phi_{bp} = -171.52°$), one obtains $O^c = -0.43$, $O^{nc} = -0.09$, representing a much smaller change, especially in O^{nc}, which cannot become as large as in true A-DNA so long as ϕ_{bp} remains in the TT–TV cancellation region around 180°. Nevertheless, O^{nc} has at least become large enough, compared to O^c, to produce a 'non-conservative' x-dependence in $\Delta\epsilon(x)/\Delta\epsilon(0)$ for planar B with A-like Θ; but because the radius retains its small B-like value, the amplitude of variation is greater (minimum $\Delta\epsilon(x)/\Delta\epsilon(0) = 0.94$) than in true A-DNA (minimum $\Delta\epsilon(x)/\Delta\epsilon(0) = 0.98$).

Because the transitions in table 1 are the most important contributors to the c.d. at 260–280 nm, any additional transitions from neighbouring regions (e.g. the 240–250 nm transitions in A and G) would be given less weight in the averaging process, so a more accurate θ would be unlikely to produce an A-like Θ, and it is more pertinent to consider smaller θ values. As expected, the trends in the computed $\Delta\epsilon(x)/\Delta\epsilon(0)$ for varying θ are similar to those in table A 4.2, but less pronounced, because only Θ, and not ϕ_{bp} or r, is varied. Thus, if additional transitions make θ(and hence Θ) more negative, one expects a smaller c.d. at $x = 0$, and hence a larger amplitude for the (conservative-type) variation in $\Delta\epsilon(x)/\Delta\epsilon(0)$. For example, at $\theta = -25°$, corresponding to $\Theta = -83°$ (cf. $\Theta = -62°$ for $\theta = -4.08°$), one obtains a maximum increase of 15% (cf. only 8% for $\theta = -4.08°$), but no decrease at high x; when base-tipping is introduced according to (60), a decrease to $\Delta\epsilon(x)/\Delta\epsilon(0) = 0.51$ is obtained, suggesting that for more negative θ a smaller degree of supercoiling-induced base-tipping, β', will suffice to reproduce the observed $\Delta\epsilon(x)/\Delta\epsilon(0) = 0.70$. If additional transitions make θ more positive (e.g. the 240–250 nm transitions on A and G at $\theta \approx +90°$), a more non-conservative pattern is expected, i.e. decreased $\Delta\epsilon(x)/\Delta\epsilon(0)$ at high x. Thus, for $\theta = +25°$ ($\Theta = -33°$), the maximum reduction in $\Delta\epsilon(x)/\Delta\epsilon(0)$ is 0.96, which base-tipping further reduces only to 0.94 (a positive θ increases K, so that base-twisting has less effect) indicating that a larger β' might be necessary. However, these computations employ $F^{nc} = 0.6777$, calculated for the table 1 transitions; additional transitions would, from (48), reduce $P(c)$ and hence increase F^{nc}. This could result in a much larger non-conservative component, and hence a larger decrease in $\Delta\epsilon(x)/\Delta\epsilon(0)$ at high x, thus reducing the need for a larger β'.

Inclusion of other transitions should thus improve agreement with experiment (giving a larger increase at small negative x, and a sharper decrease at large x) if θ becomes more negative, and probably maintain agreement at large x (with perhaps a larger β', depending on how the transitions are weighted) for small positive θ, although the increase at low x may be lost. Taking just one transition on each base (table 1) is therefore a reasonable approximation, especially because it is not immediately obvious how other transitions should be weighted in calculating $P(c)$.

PHILOSOPHICAL TRANSACTIONS OF THE ROYAL SOCIETY A MATHEMATICAL, PHYSICAL & ENGINEERING SCIENCES

Glossary of symbols

σ	conventional superhelix density (number of superhelical turns per 10 base-pairs)
x	geometrical superhelix density (number of superhelical turns per helical turn)
X	supersuperhelix density (number of supersuperhelical turns per superhelical turn)
k	number of base-pairs per turn of double helix
$\Delta\epsilon$	circular dichroism (c.d.)
$\Delta\epsilon(x)$	c.d. of DNA of superhelix density x
$\Delta\epsilon(0)$	c.d. of straight, non-supercoiled DNA
ν_{OA}	frequency of polymer transition $\mathrm{O}\rightarrow\mathrm{A}$
$\nu_{\mathrm{OA}K}$	frequency of polymer transition $\mathrm{O}\rightarrow\mathrm{A}_K$ (state A is split into exciton levels A_K)
R_{OA}	rotational strength of polymer transition $\mathrm{O}\rightarrow\mathrm{A}$
$R_{\mathrm{OA}K}$	rotational strength of polymer transition $\mathrm{O}\rightarrow\mathrm{A}_K$
σ_ν	standard deviation in frequency units
u	frequency in units of standard deviations, σ_ν, from the absorption frequency ν_{OA}
σ_λ	standard deviation in wavelengths
w	wavelength in units of standard deviations
$f(u)$ or $f(w)$	non-conservative line-shape (Gaussian) as a function of frequency or wavelength
$f'(u)$ or $f'(w)$	conservative line-shape (first derivative of Gaussian) as a function of frequency or wavelength
ν_{a}	frequency of transition $\mathrm{o}\rightarrow\mathrm{a}$ on individual monomers
$\boldsymbol{\mu}_{i\mathrm{oa}}$	electric dipole transition moment for transition $\mathrm{o}\rightarrow\mathrm{a}$ on monomer i
μ	magnitude of $\boldsymbol{\mu}_{i\mathrm{oa}}$
$V_{i\mathrm{oa};j\mathrm{ob}}$	interaction potential between electric dipole transition moments $\boldsymbol{\mu}_{i\mathrm{oa}}$ and $\boldsymbol{\mu}_{j\mathrm{ob}}$ for transition $\mathrm{o}\rightarrow\mathrm{a}$ on monomer i and transition $\mathrm{o}\rightarrow\mathrm{b}$ on monomer j
$\boldsymbol{R}^{ij}$	distance vector between monomers i and j
$(\boldsymbol{B}^j)^{\mathrm{nc}}$	polarizability tensor of monomer j that appears in expression for non-conservative c.d. contribution
$(\boldsymbol{B}^j)^{\mathrm{c}}$	conservative analogue of polarizability of monomer j
O^{nc}, O^{c}	total non-conservative and conservative contributions to the c.d.
Ω^j	geometric factor in c.d. contribution from interaction of transition moment on zeroth group with transition moment on jth group; summation over j and multiplication by a numerical factor gives O^{nc} and O^{c}
$\hat{\boldsymbol{a}}(0)$	unit vector in direction of transition moment on zeroth group

$\boldsymbol{P}^j$	matrix relating proper frame of jth group to proper frame of zeroth group
$\boldsymbol{R}^j$	distance vector from zeroth group to jth group
$\Omega(0_{\mathrm{T}} \rightarrow n_{\mathrm{T}})$	geometric factor in contribution to c.d. from interaction between zeroth group and its nth neighbour on the same (i.e. T-) strand of the double helix
$\Omega(0_{\mathrm{T}} \rightarrow n_{\mathrm{V}})$	geometric factor in contribution to c.d. from interaction between zeroth group and its nth neighbour on the other (i.e. V-) strand of the double helix (the two identical and equivalent helices are arbitrarily named T and V)
$\Omega(0_{\mathrm{T}}^m \rightarrow n_{\mathrm{T}})$	geometric factor in c.d. from interaction of zeroth group of m-type and its nth neighbour (in the superhelix, the zeroth group may assume one of 10 different helical phases, denoted by the index m)
Ω	geometric factor in contribution to c.d. from an arbitrary pair of interacting groups
Ω_q	qth component of Ω divided by the polarizability component B_{qq} (see (22))
$\Omega^{\mathrm{nc}}, \Omega^{\mathrm{c}}$	geometric factors in non-conservative and conservative c.d. contributions from an arbitrary pair of interacting groups
$\alpha_\perp = B_{11} = B_{22}$	in-plane polarizability (perpendicular to $\hat{\boldsymbol{k}}^{\mathrm{t}}$)
$\alpha_\parallel = B_{33}$	out-of-plane polarizability (in direction of $\hat{\boldsymbol{k}}^{\mathrm{t}}$)
F^{nc}	ratio of numerical factors multiplying total non-conservative and conservative geometric factors to give total c.d. contributions O^{nc} and O^{c} (equations (47) and (48)). Because only relative values of non-conservative and conservative contributions required, total non-conservative geometric factor $\Sigma\Omega_3$ is multiplied by F^{nc} to give O^{nc}, and total conservative geometric factor $\Sigma\Omega_1$ is put equal to O^{c} (equation 51))
ϕ	phase round helix cylinder
$\hat{\boldsymbol{i}}^{\mathrm{h}}$	unit vector radial to helix cylinder
$\hat{\boldsymbol{j}}^{\mathrm{h}}$	unit vector tangential to helix cylinder
$\hat{\boldsymbol{k}}^{\mathrm{h}}$	unit vector longitudinal to helix cylinder
$\{\hat{\boldsymbol{i}}^{\mathrm{h}}[\phi]\}$	triad of unit vectors radial, tangential, and longitudinal to helix cylinder at phase ϕ
$\boldsymbol{M}(\phi)$	matrix that rotates $\{\hat{\boldsymbol{i}}^{\mathrm{h}}[0]\}$ through ϕ, about $\hat{\boldsymbol{k}}^{\mathrm{h}}$, into $\{\hat{\boldsymbol{i}}^{\mathrm{h}}[\phi]\}$
$\{\hat{\boldsymbol{i}}^{\mathrm{loc}}[\phi]\}$	local frame in which $\boldsymbol{B}^{\mathrm{nc}}$ is diagonal
$\boldsymbol{L}$	matrix that rotates local frame $\{\hat{\boldsymbol{i}}^{\mathrm{loc}}[\phi]\}$ into helix frame $\{\hat{\boldsymbol{i}}^{\mathrm{h}}[\phi]\}$
α, β, γ	Euler angles relating helix axes to local axes
$\hat{\boldsymbol{i}}^{\mathrm{t}}$	direction of electric dipole transition moment for monomer transition o$\rightarrow$a.
θ	angle between $\hat{\boldsymbol{i}}^{\mathrm{loc}}$ and $\hat{\boldsymbol{i}}^{\mathrm{t}}$
$\boldsymbol{t}$	matrix that rotates transition frame $\{\hat{\boldsymbol{i}}^{\mathrm{t}}[\phi]\}$ into local frame $\{\hat{\boldsymbol{i}}^{\mathrm{loc}}[\phi]\}$
$\boldsymbol{A} = \boldsymbol{L}\boldsymbol{t}$	matrix that rotates transition frame $\{\hat{\boldsymbol{i}}^{\mathrm{t}}[\phi]\}$ into helix frame $\{\hat{\boldsymbol{i}}^{\mathrm{h}}[\phi]\}$
$\{\hat{\boldsymbol{i}}_{\mathrm{T}}^{\mathrm{t}}[0]\}$	transition frame (in which $\boldsymbol{B}^{\mathrm{c}}$ is diagonal) of zeroth group of T-helix

$\boldsymbol{B}$	polarizability of a group in the frame in which it is diagonal, i.e. its proper frame (its transition frame)
$\{\boldsymbol{B}\}^{\mathrm{t}}_{n} = \boldsymbol{B}$	polarizability of the nth group in its own transition frame
$\{\boldsymbol{B}\}^{\mathrm{t}}_{0_{\mathrm{T}}}$	polarizability of the nth group in transition frame of zeroth group on T-helix, i.e. in the frame in which c.d. is evaluated
$\boldsymbol{P}(0_{\mathrm{T}} \leftarrow n)$	matrix that transforms $\{\boldsymbol{B}\}^{\mathrm{t}}_{n}$ into $\{\boldsymbol{B}\}^{\mathrm{t}}_{0_{\mathrm{T}}}$, i.e. rotates proper frame of nth group into that of 0_{T} group
$\boldsymbol{S}^{\mathrm{V}}$	matrix that reverses y and z axes of $\{\hat{\boldsymbol{i}}^{\mathrm{h}}_{\mathrm{V}}[\phi]\}$ to give $\{\hat{\boldsymbol{i}}^{\mathrm{h}}_{\mathrm{T}}[\phi]\}$; used for inter-strand interactions (the T- and V-helices are anti-parallel)
$\boldsymbol{\Phi}$	phase round superhelix cylinder
$\{\hat{\boldsymbol{i}}^{\mathrm{h}}[\boldsymbol{\Phi}, \phi]\}$	helix frame at superhelical phase $\boldsymbol{\Phi}$ and helical phase ϕ
$\hat{\boldsymbol{I}}$	unit vector radial to superhelix cylinder
$\hat{\boldsymbol{J}}$	unit vector tangential to superhelix cylinder
$\hat{\boldsymbol{K}}$	unit vector longitudinal to superhelix cylinder
$\{\hat{\boldsymbol{I}}[\boldsymbol{\Phi}]\}$	triad of unit vectors radial, tangential, and longitudinal to superhelix cylinder at superhelical phase $\boldsymbol{\Phi}$
$\boldsymbol{h}$	matrix that rotates helix frame $\{\hat{\boldsymbol{i}}^{\mathrm{h}}[\boldsymbol{\Phi}, 0]\}$ into superhelix frame $\{\hat{\boldsymbol{I}}[\boldsymbol{\Phi}]\}$
r	radius of helix
p	pitch of helix
$\alpha_{\mathrm{h}} = \tan^{-1}(p/2\pi r)$	helix angle
R	superhelix radius
P	superhelix pitch
$\alpha_{\mathrm{sh}} = \tan^{-1}(P/2\pi R)$	superhelix angle
$C = \cos\alpha_{\mathrm{sh}} = 2\pi Rx/p$	
$S = \sin\alpha_{\mathrm{sh}}$	
ϕ_{o}	helical phase of zeroth group
$\phi(0^{m}_{\mathrm{T}})$	helical phase of zeroth group of type m on T-helix (in the superhelix there are 10 types of chromophore site, distinguished by the index m)
$\boldsymbol{\Phi}'$	phase round supersuperhelix cylinder
$\{\hat{\boldsymbol{I}}[\boldsymbol{\Phi}', \boldsymbol{\Phi}]\}$	superhelix frame at supersuperhelical phase $\boldsymbol{\Phi}'$ and superhelical phase $\boldsymbol{\Phi}$
$\hat{\boldsymbol{I}}'$	unit vector radial to supersuperhelix cylinder
$\{\hat{\boldsymbol{I}}'[\boldsymbol{\Phi}']\}$	triad of unit vectors radial, tangential and longitudinal to supersuperhelix cylinder at supersuperhelical phase $\boldsymbol{\Phi}'$
$\boldsymbol{H}$	matrix that rotates superhelix frame $\{\hat{\boldsymbol{I}}[\boldsymbol{\Phi}', 0]$ into supersuperhelix frame $\{\hat{\boldsymbol{I}}'[\boldsymbol{\Phi}']\}$
R'	supersuperhelix radius
P'	supersuperhelix pitch
$\alpha_{\mathrm{ssh}} = \tan^{-1}(P'/2\pi R')$	supersuperhelix angle
$C' = \cos\alpha_{\mathrm{ssh}}$	
$S' = \sin\alpha_{\mathrm{ssh}}$	
$\boldsymbol{\Phi}_{\mathrm{o}}$	superhelical phase of zeroth group
$\boldsymbol{\Phi}(0^{M})$	superhelical phase of zeroth group of type M

PHILOSOPHICAL TRANSACTIONS OF THE ROYAL SOCIETY A MATHEMATICAL, PHYSICAL & ENGINEERING SCIENCES

$\{\hat{\boldsymbol{i}}^{\mathrm{t}}[0]\}$	proper frame of zeroth group (transition frame at zero helical phase), in which helix c.d. is evaluated
$\{\hat{\boldsymbol{i}}^{\mathrm{t}}[0, \phi_{\mathrm{o}}]\}$	proper frame of zeroth group (transition frame at zero superhelical phase and helical phase ϕ_{o}), in which superhelix c.d. is evaluated
$\{\hat{\boldsymbol{i}}^{\mathrm{t}}[0, \boldsymbol{\Phi}_{\mathrm{o}}, \phi_{\mathrm{o}}]$	proper frame of zeroth group (transition frame at zero supersuperhelical phase, superhelical phase $\boldsymbol{\Phi}_{\mathrm{o}}$, and helical phase ϕ_{o}), in which supersuperhelix c.d. is evaluated
$\Delta\phi$	difference in helical phase between a pair of interacting chromophores (zeroth and nth groups)
Δz	difference in longitudinal displacement (along helix axis) between a pair of interacting chromophores
$\Delta\boldsymbol{\Phi}$	difference in superhelical phase between interacting groups
$\Delta\boldsymbol{\Phi}' = X\Delta\boldsymbol{\Phi}$	difference in supersuperhelical phase between interacting groups
$\Delta\phi(0_{\mathrm{T}} \rightarrow n_{\mathrm{T}})$	difference in phase between groups 0_{T} and n_{T} on same strand of double helix
$\Delta\phi(0_{\mathrm{T}} \rightarrow n_{\mathrm{V}})$	difference in phase between groups 0_{T} and n_{V} on opposite strands of double helix
$\phi_{\mathrm{bp}} = \Delta\phi(n_{\mathrm{T}} \rightarrow n_{\mathrm{V}})$	phase difference between paired bases
$\boldsymbol{d}_{\mathrm{bp}}$	vector joining paired bases n_{T} and n_{V}
d_{bp}	magnitude of $\boldsymbol{d}_{\mathrm{bp}}$
$\{\boldsymbol{R}\}^{\mathrm{t}}[0]$	distance vector expressed in $\{\hat{\boldsymbol{i}}^{\mathrm{t}}[0]\}$ frame (to evaluate helix c.d.)
$\{\boldsymbol{R}\}^{\mathrm{t}}[0, \phi_{\mathrm{o}}]$	distance vector expressed in $\{\hat{\boldsymbol{i}}^{\mathrm{t}}[0, \phi_{\mathrm{o}}]\}$ frame (to evaluate superhelix c.d.)
β_{h}	Euler angle β ('tip angle' of base-pair) in straight helix
β_{sh}	tip angle in supercoiled helix
β'	maximum additional tipping that occurs when helix is supercoiled
$R^{\mathrm{curv}}(\phi)$	Riemann curvature scalar of surface of supercoiled helix cylinder at helical phase ϕ
θ	angle between $\hat{\boldsymbol{i}}^{\mathrm{loc}}$ and $\hat{\boldsymbol{i}}^{\mathrm{t}}$
$\boldsymbol{\Theta}$	angle between $\hat{\boldsymbol{i}}^{\mathrm{h}}$ and $\hat{\boldsymbol{i}}^{\mathrm{t}}$
K	angle between $\hat{\boldsymbol{i}}^{\mathrm{t}}$ and $\boldsymbol{d}_{\mathrm{bp}}$
β	angle of base-tip (Euler angle between $\hat{\boldsymbol{k}}^{\mathrm{h}}$ and $\hat{\boldsymbol{k}}^{\mathrm{loc}}$)
ψ	angle of base-tilt
τ	angle of base-twist

References

Akrigg, A. & Cook, P. R. 1980 *Nucleic Acids Res.* **8**, 845–853.
Arnott, S. 1970 *Progr. Biophys. molec. Biol.* **21**, 265–319.
Arnott, S., Dover, S. D. & Wonacott, A. J. 1969 *Acta crystallogr.* B **25**, 2129–2206.
Arnott, S. & Selsing, E. 1975 *J. molec. Biol.* **98**, 265–269.
Atwater, H. A. 1974 *Introduction to general relativity*. Oxford: Pergamon.
Bauer, W. & Vinograd, J. 1968 *J. molec. Biol.* **33**, 141–171.

PHILOSOPHICAL TRANSACTIONS OF THE ROYAL SOCIETY A MATHEMATICAL, PHYSICAL & ENGINEERING SCIENCES

Bloomfield, V. A., Crothers, D. M. & Tinoco, I. Jr 1971 *Physical chemistry of the nucleic acids*. London: Harper & Row.
Bradbury, E. M 1978 *Recherche* **9**, 644–653.
Brahms, J. 1979 *Biopolymers* **18**, 1877–1888.
Bram, S. 1971 *J. molec. Biol.* **58**, 277–288.
Bram, S., Butler-Browne, G., Baudy, P. & Ibel, K. 1975 *Proc. natn. Acad. Sci. U.S.A.* **72**, 1043–1045.
Bram, S. & Ris, H. 1971 *J. molec. Biol.* **55**, 325–336.
Bush, C. A. & Brahms, J. 1967 *J. chem. Phys.* **46**, 79–88.
Campbell, A. M. 1978 *Trends biochem. Sci.* **3**, 104–108.
Campbell, A. M., Cotter, R. I. & Pardon, J. F. 1978 *Nucleic Acids Res.* **5**, 1571–1580.
Colman, A. & Cook, P. R. 1977 *Eur. J. Biochem.* **76**, 63–78.
Cook, P. R. 1974 *Biol. Rev.* **49**, 51–84.
Cook, P. R. & Brazell, I. A. 1975 *J. Cell Sci.* **19**, 261–279.
Cook, P. R. & Brazell, I. A. 1976 *J. Cell Sci.* **22**, 303–324.
Cook, P. R. & Brazell, I. A. 1980 *Nucleic Acids Res.* **8**, 2895–2905.
Cook, P. R., McGready, S. J., Godwin, J., Mason, D. W. & Brazell, I. A. 1980 *J. Cell Sci.* **46**, 365–386.
Cowman, M. K. & Fasman, G. D. 1978 *Proc. natn. Acad. Sci. U.S.A.* **75**, 4759–4763.
Crick, F. H. C. & Klug, A. 1975 *Nature, Lond.* **255**, 530–533.
Denhardt, D. T. 1979 *Nature, Lond.* **280**, 196–198.
Ehrlich, M. & Wang, R. Y.-H. 1981 *Science, Wash.* **212**, 1250–1257.
Fasman, G. D. & Cowman, M. K. 1978 *Cell Nucleus* **5**, 55–97.
Feinberg, A. P. & Vogelstein, B. 1983*a* *Nature, Lond.* **301**, 89–91.
Feinberg, A. P. & Vogelstein, B. 1983*b* *Biochem. biophys. Res. Commun.* **111**, 47–54.
Finch, J. T. & Klug, A. 1976 *Proc. natn. Acad. Sci. U.S.A.* **73**, 1897–1901.
Finch, J. T., Lutter, L. C., Rhodes, D., Brown, R. S., Rushton, B., Levitt, M. & Klug, A. 1977 *Nature, Lond.* **269**, 29–36.
Gama-Soza, M. A., Midgett, R. M., Slagel, V. A., Githens, S., Kuo, K. C., Gehrk, C. W. & Ehrlich, M. 1983 *Biochim. biophys. Acta* **740**, 212–216.
Georgiev, G. P., Nedospasov, S. A. & Bakayev, V. V. 1978 *Cell Nucleus* **6**, 3–34.
Gray, D. M., Taylor, T. N. & Lang, D. 1978 *Biopolymers* **17**, 145–157.
Hanlon, S., Johnson, R. S., Wolf, B. & Chan, A. 1972 *Proc. natn. Acad. Sci. U.S.A.* **69**, 3263–3267.
Hartwig, M. 1980 *Stud. Biophys.* **80**, 149–155.
Hartwig, M. & Matthes, F. 1979 *Stud. Biophys.* **77**, 141–148.
Henson, P. & Walker, I. O. 1970 *Eur. J. Biochem.* **16**, 524–531.
Ivanov, V. I., Minchenkova, L. E., Schyolkina, A. K. & Poletayev, A. I. 1973 *Biopolymers* **12**, 89–110.
Johnson, B. B., Dahl, K. S., Tinoco, I. Jr, Ivanov, V. I. & Zhurkin, V. B. 1981 *Biochemistry* **20**, 73–78.
Johnson, W. C. & Tinoco, I. Jr 1969 *Biopolymers* **7**, 727–749.
Kallenbach, N. R., Appleby, D. W. & Bradley, C. H. 1978 *Nature, Lond.* **272**, 134–138.
Klevan, L., Armitage, E. M. & Crothers, D. M. 1979 *Nucleic Acids Res.* **6**, 1607–1616.
Kornberg, R. D. 1977 *A. Rev. Biochem.* **46**, 931–954.
Lefevre, C. G. & Lefevre, R. J. W. 1955 *Rev. Pure appl. Chem.* **5**, 261–318.
Levitt, M. 1978 *Proc. natn. Acad. Sci. U.S.A.* **75**, 640–644.
Levitt, M. & Warshel, A. 1978 *J. Am. chem. Soc.* **100**, 2607–2613.
Lilley, D. M. J. 1983 *Nature, Lond.* **305**, 276–277.
Lindahl, T. 1981 *Nature, Lond.* **290**, 363–364.
Lu, L.-J. W., Randerath, E. & Randerath, K. 1983 *Cancer Lett.* **19**, 231–235.
Luchnik, A. N. 1980 *Molec. Biol. Rep.* **6**, 3–9.
Luchnik, A. N., Bakayev, V. V. & Glaser, V. M. 1982 *Cold Spring Harb. Symp. Quant. Biol.* **47**, 793–801.
Luchnik, A. N. & Glaser, V. M. 1981 *Molec. gen. Genet.* **183**, 553–556.
Maestre, M. F. & Wang, J. C. 1971 *Biopolymers* **10**, 1021–1030.
MacDermott, A. J. 1981 D.Phil. thesis, University of Oxford.
MacDermott, A. J. 1982 *New Scient.* **95**, 228–237.
MacDermott, A. J. 1985 *Molec. Phys.* (In the press.)
Matsuyama, A., Tagashira, Y. & Nagata, C. 1971 *Biochim. biophys. Acta* **240**, 184–190.
Miller, U., Zentgraf, H., Eicken, I. & Keller, W. 1978 *Science, Wash.* **201**, 406–415.
Mirkin, S. M., Bogdanova, E. S., Gorlenko, Zh. M., Gragerov, A. I. & Larionov, O. A. 1979 *Molec. gen. Genet.* **177**, 169–175.
Misner, C. W., Thorne, K. S. & Wheeler, J. A. 1973 *Gravitation*. San Francisco: Freeman.
Moffitt, W. 1956 *Proc. natn. Acad. Sci. U.S.A.* **42**, 736–746.
Moore, D. S. & Wagner, T. E. 1973 *Biopolymers* **12**, 201–221.
Nicolini, C. 1979 *NATO ASI Series* A **21***b*, 613–666.
Nicolini, C. 1980 *J. Submicrosc. Cytol.* **12**, 475–490.
Nicolini, C., Ajiro, K., Borun, T. W. & Baserga, R. 1975 *J. biol. Chem.* **250**, 3381–3385.

PHILOSOPHICAL TRANSACTIONS OF THE ROYAL SOCIETY A MATHEMATICAL, PHYSICAL & ENGINEERING SCIENCES

Noll, M. 1974 *Nucleic Acids Res.* **1**, 1573–1578.
Nordheim, A., Pardue, M. L., Lafer, E. M., Möller, A., Stollar, B. D. & Rich, A. 1981 *Nature, Lond.* **294**, 417–422.
Pauling, L. 1960 *The nature of the chemical bond.* Ithaca: Cornell University Press.
Permogorov, V. I., Debabov, V. G., Sladkova, I. A. & Rebentish, B. A. 1970 *Biochim. biophys. Acta* **199**, 556–558.
Preumont, A. M., Stoffels, G. L. & De Reuck, M. 1981 *Cancer Res.* **41**, 2529–2533.
Pulleyblank, D. E., Shure, M., Tang, D., Vinograd, J. & Vosberg, H.-P. 1975 *Proc. natn. Acad. Sci. U.S.A.* **72**, 4280–4284.
Razin, A. & Riggs, A. D. 1980 *Science, Wash.* **210**, 604–610.
Redmann, S. M. Jr & Rhodes, W. 1979 *Biopolymers* **18**, 393–409.
Rhodes, W. & Redmann, S. M. Jr 1977 *J. chem. Phys.* **22**, 215–220.
Rhodes, W. 1961 *J. Amer. chem. Soc.* **83**, 3609–3617.
Shih, T. Y. & Fasman, G. D. 1970 *J. molec. Biol.* **52**, 125–129.
Shindo, H. & McGhee, J. D. 1980 *Biopolymers* **19**, 523–537.
Simpson, R. T. & Sober, H. A. 1970 *Biochemistry* **9**, 3103–3109.
Smith, G. R. 1981 *Cell* **24**, 599–600.
Sobell, H. M., Tsai, C.-C., Gilbert, S. G., Jain, S. C. & Sakore, T. D. 1976 *Proc. natn. Acad. Sci. U.S.A.* **73**, 3068–3072.
Sobell, H. M., Tsai, C.-C., Jain, S. C. & Sakore, T. D. 1978 *Phil. Trans. R. Soc. Lond.* B **283**, 295–298.
Studdert, D. S. & Davis, R. C. 1974 *Biopolymers* **13**, 1377–1389.
Taillandier, E., Taboury, J., Liquier, J., Gadenne, M. C., Champagne, M. & Brahms, J. 1979 *Biopolymers* **18**, 1877–1888.
Thoma, F., Koller, Th. & Klug, A. 1979 *J. Cell Biol.* **83**, 403–427.
Tinoco, I. Jr 1962 *Adv. chem. Phys.* **4**, 113–160.

PHILOSOPHICAL TRANSACTIONS OF THE ROYAL SOCIETY A MATHEMATICAL, PHYSICAL & ENGINEERING SCIENCES